Design and Testing of a Novel Fusion Construct for Atlantoaxial Instability

by

Timothy Lasswell

A thesis

presented to the University of Waterloo

in fulfillment of the

thesis requirement for the degree of

Master of Applied Science

in

Mechanical and Mechatronics Engineering

Waterloo, Ontario, Canada, 2017

Author's Declaration

I hereby declare that I am the sole author of this thesis. This is a true copy of the thesis, including any required final revisions, as accepted by my examiners.

I understand that my thesis may be made electronically available to the public.

Abstract

The atlantoaxial joint of the upper cervical spine is unique in its anatomy due to the absence of an intervertebral disc. Instead, the atlantoaxial joint is comprised of the odontoid process and associated ligaments that together create a pin joint that allows the large range of motion present at the C1-C2 segment. Atlantoaxial instability occurs when there is excessive motion at the C1-C2 segment and is most commonly caused by traumatic fracture of the odontoid process. The conventional surgical treatment for atlantoaxial instability in the geriatric patient population is posterior fusion, which consists of implanting a screw/rod construct to stabilize the C1-C2 segment of the upper cervical spine and promote long term fusion. However, controversy exists regarding the existing fusion procedures due to high intraoperative risks, extended operating times and invasiveness of the surgery that results in a large portion of the patient population being unfit for surgical treatment and instead are treated conservatively with poor outcomes.

The purpose of the present thesis is to design a less invasive implant for the surgical treatment of atlantoaxial instability that uses the posterior arch of C1 as a fixation site. This novel implant could then be used with existing C2 fixation methods such as translaminar screws to create a C1-C2 fusion construct that presents less intraoperative risks, shorter operating times and a less invasive surgery with the result of being able to treat more geriatric patients surgically.

An optimization study based on minimizing the mean squared difference between experimental load rotation curves and computed load-rotation curves was done to determine ligament laxity values which improved the physiological motion response of an upper cervical spine finite element model. Atlantoaxial instability was simulated and simplified fusion constructs were then implemented in the finite element model for the purpose of predicting the stability of novel constructs that used the C1 posterior arch as a fixation site and comparing these values to the predicted stability of clinically available fusion constructs. The stability predictions of the finite element model suggested that a fusion construct that used the C1 posterior arch as a fixation site was feasible if fixation in C2 was achieved at either the pedicle or lamina. The finite element model was also used to calculate the loads in each construct.

Through a series of iterations in the design phase, the novel implant was embodied as a clamp that grasped the posterior arch of C1 and could be connected to C2 translaminar or C2 pedicle screws through the use of rods, thus creating the full fusion construct. Several prototypes

were manufactured using a 3D printing technique (selective laser melting) and benchtop test methods were performed to ensure that the implant could withstand the loads predicted by the FE model.

The stability of the novel constructs relative to existing, clinically successful constructs was examined through biomechanical cadaveric testing. The results of this study showed that constructs that used C2 translaminar screws were significantly more stable than existing constructs that used C2 translaminar screws. Additionally, novel constructs that used C2 pedicles screws were significantly more stable than existing constructs that used C2 pedicle screws. These results present a strong clinical promise for the novel C1 posterior arch clamp in terms of high fusion rates, reduced operating times, less intraoperative risks and less invasive surgeries.

Acknowledgements

Dedication

The present thesis is dedicated to my Father, Lawrence Lasswell, who instilled in me a drive to achieve more and to my Mother, Anya Lasswell, who kept me humble and taught me to be thankful with less.

Table of Contents

List of Figures

xiii

List of Tables

List of Abbreviations

AAI: Atlantoaxial instability

UCS: Upper cervical spine

FE: Finite element

ROM: Range of motion

NZ: Neutral zone

SD: Standard deviation

Avg: Average

MIS: Minimally invasive surgery

TAS+H: Transarticular screw with integrated C1 hook construct

C2PS+H: C2 pedicle screw with integrated C1 hook construct

C1LM/C2TL: C1 lateral mass and C2 translaminar

C1PA/C2TL: C1 posterior arch and C2 translaminar

C1PA/C2P: C1 posterior arch and C2 pedicle

1.0 Introduction

Atlantoaxial instability (AAI) occurs when there is excessive motion at the C1-C2 segment (Figure 1) of the cervical spine and can be caused by inflammatory diseases, degenerative osteoarthritis or traumatic fracture of the odontoid[1]. If left untreated, AAI causes chronic pain, myelopathy (compression of the spinal cord impairing nerve signal transmission) and even death, if additional trauma occurs to the destabilized C1-C2 segment[2].
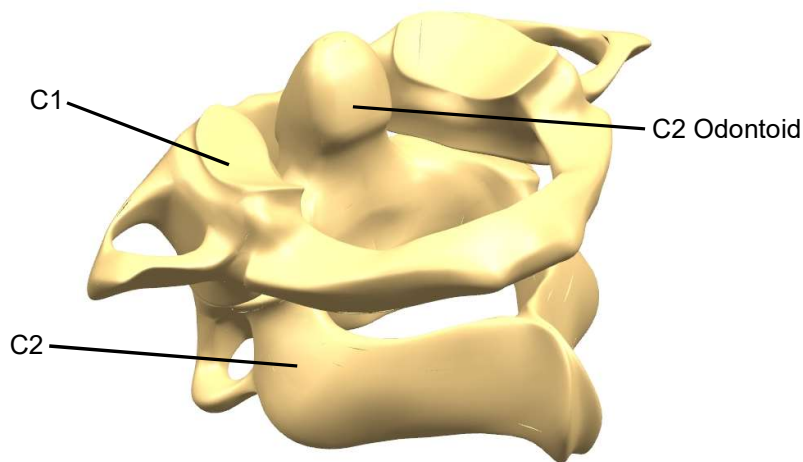
Figure 1: Bony anatomy of the C1-C2 segment

The leading cause of AAI is traumatic fracture of the odontoid, which accounts for 20% of all cervical spine fractures[3]. Three types of odontoid fractures have been classified by Anderson and D'Alonzo[4] depending on the location of the fracture line in the C2 vertebra (Figure 2). It is generally accepted that type I and type III odontoid fractures can be treated conservatively with hard collar immobilization resulting in adequate healing regardless of patient age[5]. For type II odontoid fractures, there is a very high risk of fracture non-union when treated with hard collar immobilization. So, non-geriatric patients are successfully treated with a surgical procedure that uses a compression screw to hold the odontoid in place while healing occurs.
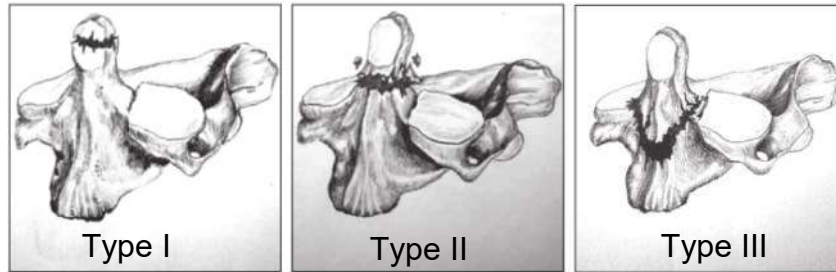
Figure 2: Odontoid fracture classifications[6]

However, for the geriatric patient population there is a high risk of fracture non-union despite holding the odontoid in place with a compression screw. Thus, a different surgical approach is used. Constructs are implanted that immobilize the entire C1-C2 segment until bony fusion occurs[7]. This results in a permanent loss of motion for the patient at the C1-C2 segment but prevents the serious consequences of untreated AAI (pain, myopathy and possible death). There remains concerns related to intraoperative blood loss, long operating times, surgical invasiveness, recovery times and the risk of non-fusion due to construct instability[8]. With these concerns in mind, only about half of the current geriatric patient population is healthy enough to undergo surgery for AAI[8]. The remaining half of the geriatric patient population does not have an effective treatment and their prognosis is poor. Even when surgical treatment is possible for the geriatric patient, choosing both the optimal construct and the optimal surgical procedure are quite difficult and a common consensus has not yet been reached in the literature.

Commercially available fusion constructs for the C1-C2 segment include all of the following techniques: transarticular screw fixation[9], posterior wiring[10], interlaminar clamping[11] and the Harms[12]. Since being introduced in 2001, the Harms procedure (Figure 3) has become the gold standard in fusion for the C1-C2 segment due to better surgical safety and better stability compared with the other constructs[13].
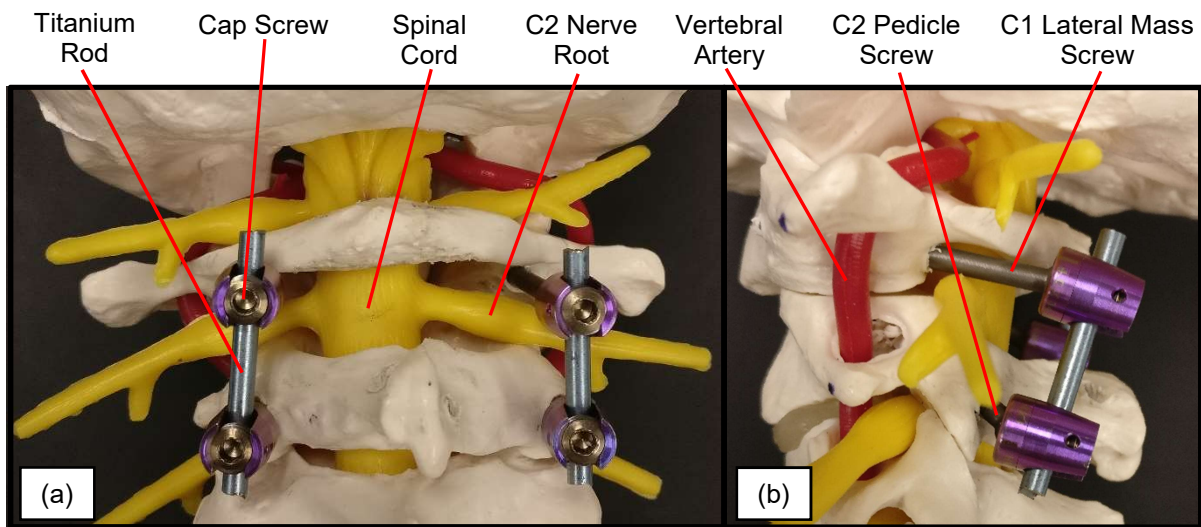
Figure 3: Upper cervical spine anatomical model showing: a) posterior view and b) lateral view of Harms construct used in C1-C2 fusion

Although there are many commercially available fusion constructs to treat AAI, none cater to the unique anatomy of the C1-C2 segment. For example, the Harm's procedure utilizes polyaxial screws and rods that have been designed for general use in the entire cervical spine. However, placing screws in C1 and C2 presents additional challenges that are not found in the rest of the cervical spine. These challenges include an increased risk of injuring the vertebral artery and potentially sacrificing the C2 nerve roots in order to achieve better screw trajectories[14]. Therefore, it is believed that there is an opportunity to develop an implant which has been specifically designed to treat AAI and take into consideration the unique needs and constraints of the C1-C2 segment.

Attempts have been made both clinically and experimentally to develop new constructs and surgical techniques that better suit the needs of the C1-C2 segment. Most notably, C2 translaminar screws have been used with excellent clinical success to replace C2 pedicle screws in the Harms construct and thus eliminate the risk of a C2 screw injuring the vertebral artery[15,16]. Although C2 translaminar screws have allowed posterior fusion procedures to be safer, the surgery remains as invasive as the Harms procedure with regards to blood loss and operating time because of the continued use of C1 lateral mass screws.

The purpose of the present thesis is to determine the feasibility of a less invasive fusion construct that should allow more geriatric patients suffering from AAI (predominantly due to type II odontoid fracture) to be treated surgically. The development will be focused on the C1

portion of the construct since C2 translaminar screws already provide a less invasive alternative to C2 pedicle screws. Furthermore, the fixation location of the C1 implant will be restricted to the posterior arch of C1 so that, when used in conjunction with C2 translaminar screws, the construct provides a less invasive solution for C1-C2 fusion. The ultimate goal is to show that the proposed construct is as effective at reducing motion at C1-C2 as the Harms construct through a cadaveric study. Future work can then be carried out clinically with the goal of proving that the proposed construct reduces blood loss, operating time, recovery time and in turn can treat a larger patient population than existing surgical solutions.

This thesis has been organized to start with a literature review in Chapter 2 in order to give the reader a better understanding of the anatomy and biomechanics of the upper cervical spine (UCS). AAI is also discussed in more detail along with clinically available treatment techniques as well as novel treatment techniques that have been experimentally tested in cadaveric studies or computationally modeled through finite element (FE) modeling. Chapter 3 discusses the FE model that was used to help in the design process of the novel C1 posterior arch implant. Chapter 4 highlights the design process that was used to develop this implant. Chapter 5 discusses the procedures and methods that were used for the experimental bench top testing and for the cadaveric study. The results of the cadaveric study are discussed in Chapter 6 followed by a discussion of these results in Chapter 7. Conclusions regarding the feasibility of the C1 posterior arch implant have been made in Chapter 8 and references have been presented in Chapter 9. Appendices have also been included that contain supplemental data and material that provide further support for some aspects of the present thesis. An investigation, that includes the design and testing of a novel implant for the posterior arch of C1, has been done with the intent of improving AAI surgical procedures and patient outcomes.

2.0 Literature Review

The present thesis proposes a novel implant design for posterior instrumented fusion of the C1-C2 segment to treat AAI. Background knowledge of spinal anatomy, function, degenerative disorders and existing treatment options is required to give the reader a better context in which the novel design can be assessed. It is also helpful to establish a coordinate system consisting of three planes that is commonly used when describing anatomy (Figure 4).
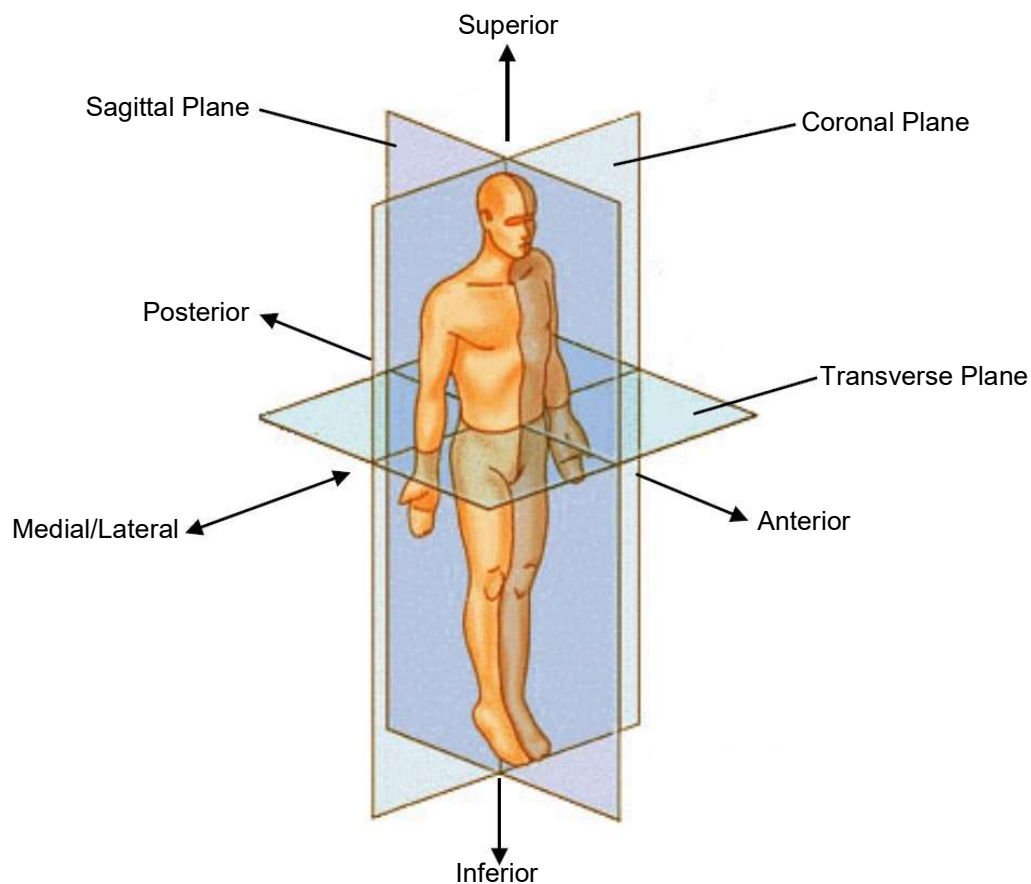
Figure 4: Anatomical coordinate system for the human body (Obtained from United States public domain)

Along with the coronal plane, sagittal plane and transverse plane, six directions of motion are also defined. In the head to toe axis, up is defined as the superior direction and down is defined as the inferior direction. In the coronal plane, the medial direction describes moving towards the midline of the body and the lateral direction describes moving away from the

midline. Finally, in the transverse plane forward is defined as the anterior direction and backward is defined as the posterior direction.

2.1 General Anatomy of the Spine

The spinal column is a flexible structure consisting of a series of bones, called vertebrae, that are surrounded by soft tissues such as ligaments, musculature and intervertebral discs. In total, there are 33 vertebrae in the spine spread throughout five regions[17]. The regions, ordered from superior to inferior are cervical, thoracic, lumbar, sacral and coccygeal (Figure 5). With the exception of the coccygeal region of the spine, individual vertebrae are often referenced by the first letter of the spinal region they belong to and the number of the vertebra within that region (numbered from top to bottom, starting from 1). For example, the seventh vertebra in the cervical spine is referred to as C7. Additionally, the base of the skull (formally named the occipital) shares an articulating surface with C1 and as a result is often referred to as C0.

In a mature spine, the anatomy of vertebrae C3 through to L5 is similar (Figure 6). Each vertebra within this range consists of a vertebral body on the anterior side that connects to an inferior and superior intervertebral disc. These discs then connect to the adjacent spinal vertebrae and give the spinal column flexibility. The posterior region of a vertebra creates a structure that protects the spinal cord and consists of transverse processes, pedicles, laminae and the spinous process. In addition to protecting the spinal cord, the posterior portion of a vertebra also contains synovial facet joints which are responsible for providing some constraint to motion under torque, compression and shear loading. Apart from these commonalities, there are specific details about each region that are unique. Vertebrae in the cervical spine are the smallest and can be easily distinguished by the presence of two foramina (passageways) on the transverse processes which encase the vertebral artery that supplies oxygenated blood to the brain. The thoracic vertebrae gradually increase in size from the end of the cervical spine to the start of the lumbar spine. They are distinguished by the presence of additional facet joints that articulate with the rib cage. The lumbar spine contains the largest vertebrae and can be identified by the lack of foramina on their traverse processes as well as no facet joints for rib cage articulation. Additionally, the pedicles in the lumbar spine extend posteriorly and have little or no lateral angulation[17].

Cervical Spine
(C1-C7)

Thoracic Spine
(T1-T12)

Lumbar Spine
(L1-L5)

Sacral Spine
(S1-S5)

Coccygeal Spine
(Tail Bone)
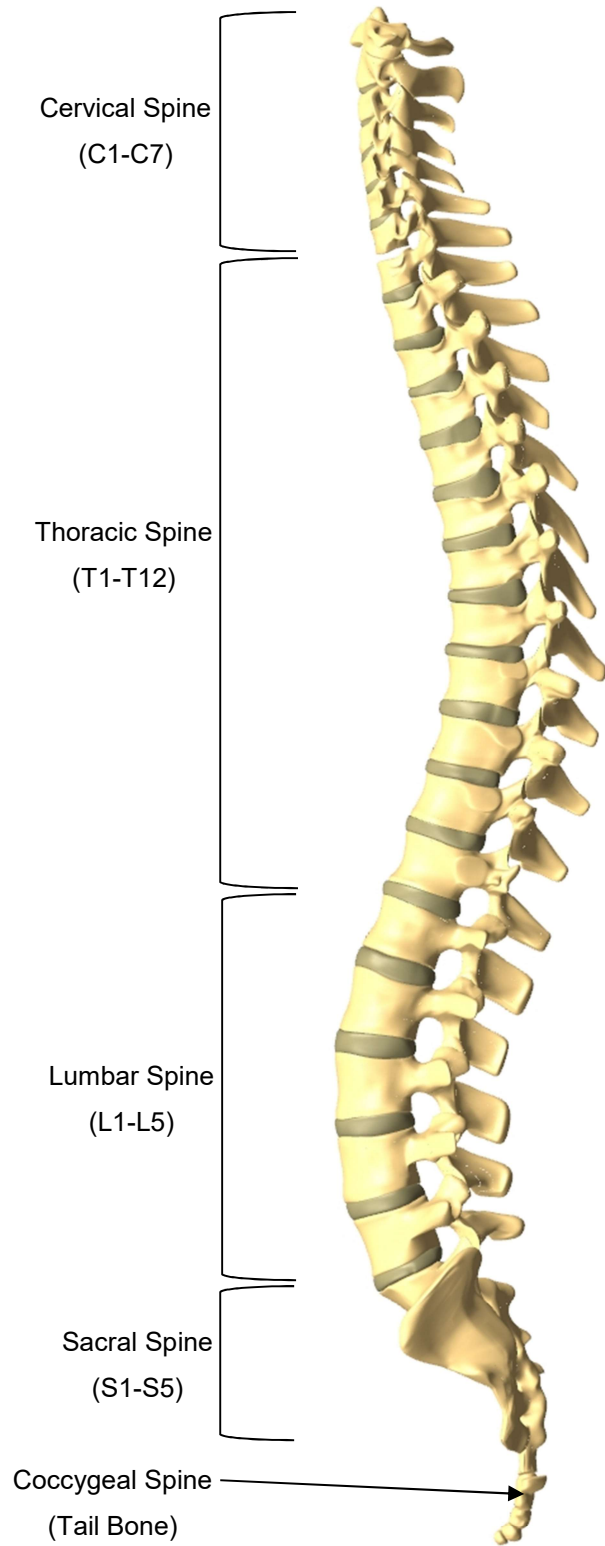
Figure 5: Complete Spinal Column (C0 omitted)
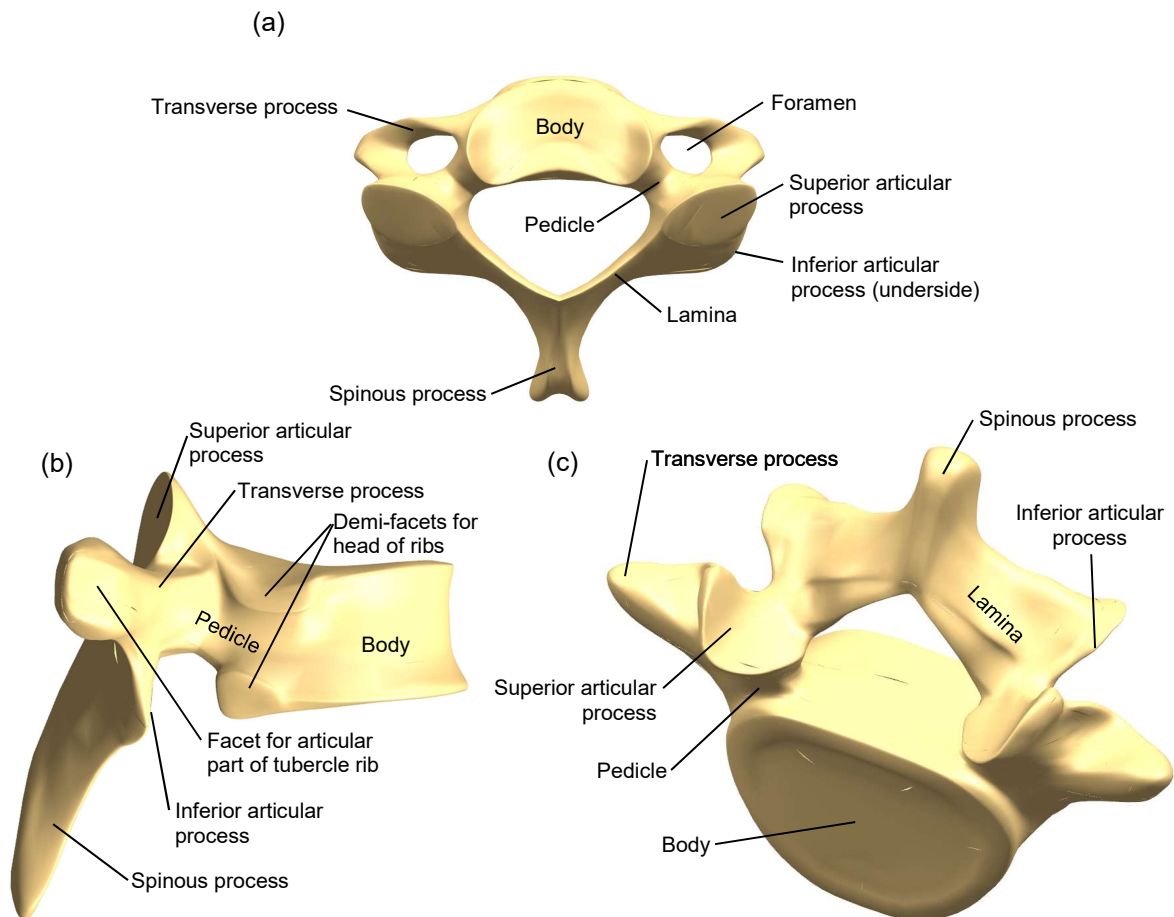
Figure 6: a) Transverse view of a cervical vertebra, b) lateral view of a thoracic vertebra and c) isometric view of lumbar vertebra[17]

The sacral vertebrae and the coccygeal vertebrae differ from segments C3 to L5 because they lack an intervertebral disc due to a natural fusion that occurs early in life. The S1-S5 vertebrae fuse to form the sacrum and the four vertebrae in the coccygeal fuse to form the coccyx, also known as the tail bone. The C1-C2 segment also lacks an intervertebral disc and instead contains the atlantoaxial joint that is sometimes described as a pivot joint.

2.1.1 Anatomy of the Upper Cervical Spine

The UCS includes the C1 and C2 vertebrae (Figure 7) that must be described separately from the rest of the cervical spine due to the unique features that are present.

C1 Superior View

Superior articular surface for occipital condyle
Anterior tubercle
Anterior arch
Articular facet for odontoid
Transverse process
Lateral mass
Transverse foramen
Groove for vertebral artery
Posterior arch
Posterior tubercle

C2 Anterior View

Odontoid
Anterior articular facet for anterior arch of atlas
Superior articular facet for atlas
Transverse process
Anterior articular facet for C3
Body

C1 Inferior View

Inferior articular facet for axis
Posterior arch
Anterior arch

C2 Posterior View

Posterior articular facet for cruciate ligament
Pedicle
Spinous process
Lamina

Figure 7: Anatomy of UCS vertebrae

As previously mentioned, a notable feature about the C1-C2 segment is the lack of an intervertebral disc. C1 is also unique because instead of a vertebral body there are two lateral masses that are connected by anterior and posterior arches. The posterior arch of C1 has a groove which carries the vertebral artery out laterally from the base of the skull to the transverse foramen. Motion at C1-C2 is facilitated by a complex atlantoaxial joint that is itself composed of three synovial joints which allow approximately 50% of cervical spine rotation[18]. Two of these three joints are located laterally (being analogous to facet joints but horizontally oriented) and consist of the C2 superior articular facets contacting with the inferior articular facets of the C1 lateral masses. The third joint consists of contact between the articular facet of the C1 anterior arch and the anterior articular facet of the C2 odontoid.

In addition to the boney anatomy of the UCS, the ligamentous structures are also very complex (Figure 8). The internal (within the spinal canal) cruciate ligament and alar ligaments

restrain the odontoid to ensure that contact is maintained with the C1 anterior arch. The external ligaments include the capsular ligaments which enclose the lateral articulating surfaces, the membrane ligaments which enclose the spinal canal and the interspinous ligament which connects the spinous processes (Images generated by AnatomyTV, Informa UK).
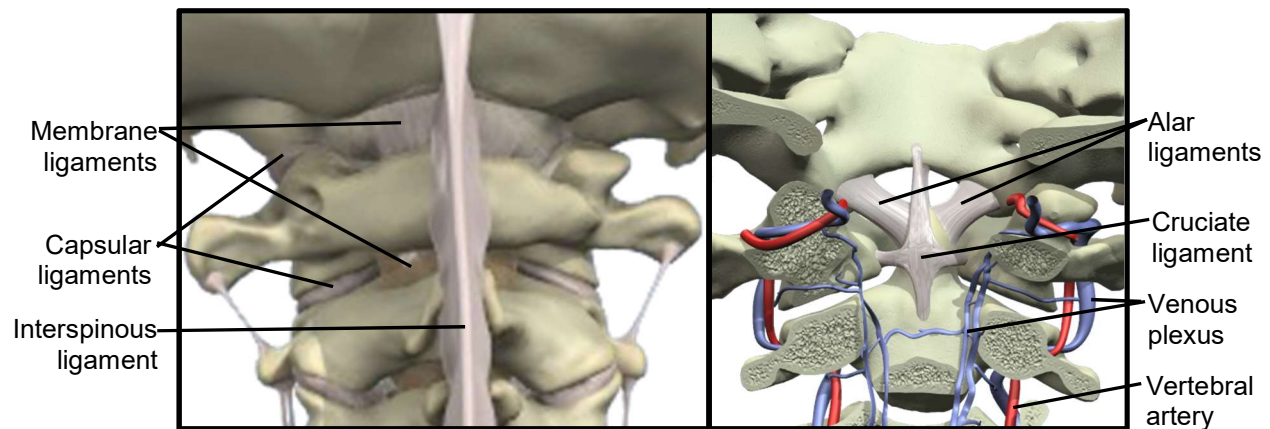
Figure 8: Significant ligaments in the UCS: a) external ligaments and b) internal ligaments

2.1.2 Anatomical Anomalies of the Upper Cervical Spine

Two anatomical anomalies can be present on the posterior arch of C1. The first anomaly is the presence of a posterior ponticle which is a small "bridge" that occurs on the superior side of the groove for the vertebral artery and develops by the calcification of the oblique atlanto-occipital ligaments (Figure 9). This can develop unilaterally or bilaterally and is more common in females with an 8% overall incidence rate[19]. Another, less common, anatomical anomaly is congenital hypoplasia of the posterior arch of C1. This results in the presence of a gap in the posterior arch due to failed ossification in the first 5 years of life and has a less than 3% incidence rate[20] (Figure 9).
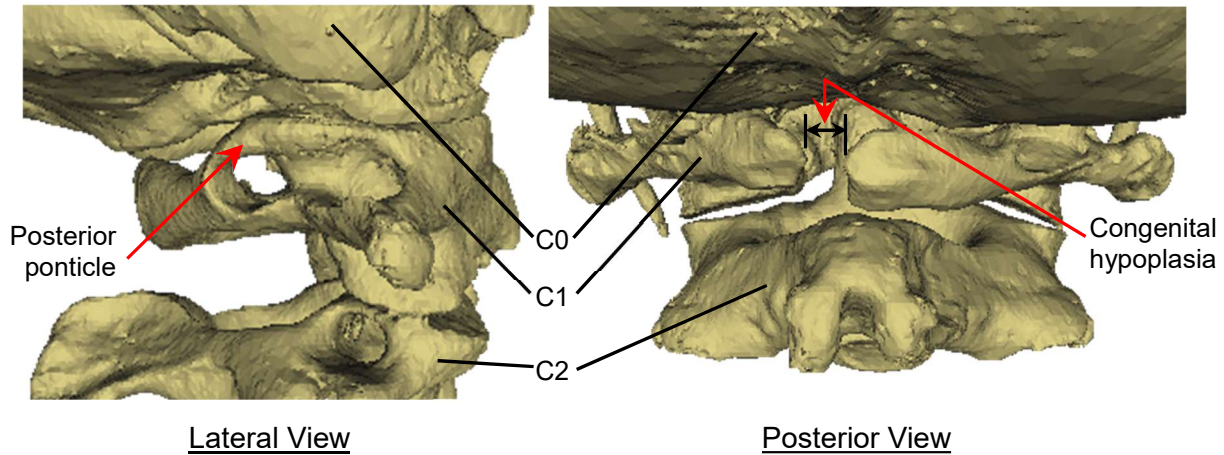
Figure 9: 3D models created from CT scans showing anomalies: unilateral posterior ponticle (left) and congenital hypoplasia of C1 arch (right)

2.2 Loads and Motions of the Upper Cervical Spine

Prior to 1988, only the kinematics of physiological motion of the UCS had been studied through patient radiographs and cadaveric dissections; the most detailed quantitative investigation was provided by Werne[21]. In 1988, moment-rotation relationships for physiological motion of the UCS were first presented in two separate studies by Goel et al[22] and Panjabi et al[23] In these studies, pure bending moments were applied to cadaveric specimens and vertebral motion was recorded using an LED based optical tracking system. In the Panjabi et al study, it was found that external moments up to 1.5 Nm applied in flexion, extension, axial rotation and lateral bending resulted in physiological range of motion (ROM) across the C0-C2 complex. Since these initial studies, several other studies have presented ROM data for the UCS obtained from cadaveric specimens using a similar testing protocol (Table 1).

Table 1: Experimental ROM data for the UCS (Avg = average, SD = standard deviation)

Study Details	C0/C1 ROM: Avg ± SD	C1-C2 ROM: Avg ± SD
Goel et al[22] Cadavers: 10 C0-C5 specimens Max. applied load: 0.3 Nm	Flexion: 6.5º ± 2.5º Extension: 16.5º ± 7.6º Lateral bending: 3.4º ± 2.8º Axial rotation: 2.4º ± 1.2º	Flexion: 4.9º ± 2.0º Extension: 5.2º ± 2.9º Lateral bending: 4.2º ± 2.8º Axial rotation: 23.3º ± 11.2º

Panjabi et al[23] Cadavers: 10 C0-C7 specimens Max. applied load: 1.5 Nm	Flexion*: 3.5º Extension*: 21.0º Lateral bending*: 5.3º Axial rotation*: 7.2º	Flexion*: 11.5º Extension*: 10.9º Lateral bending*: 6.7º Axial rotation*: 38.9º
Panjabi et al[24] Cadavers: 10 C0-C3 specimens Max. applied load: 1.5 Nm	Flexion: 14.4º ± 3.2º Extension: 14.4º ± 3.2º Lateral bending: 5.4º ± 2.8º	Flexion: 12.7º ± 3.2º Extension: 10.5º ± 3.2º Lateral bending: 10.5º ± 5.9º
Panjabi et al[25] Cadavers: 10 C0-C3 specimens Max. applied load: 1.5 Nm	Axial Rotation: 4.7º ± 3.6º	Axial Rotation: 35.7º ± 9.4º
Panjabi et al[26] Cadavers: 1 C0-C5, 5 C0-C6, 2 C0-C7, 8 C2-C7 specimens Max. applied load: 1.0 Nm	Flexion: 7.2 ± 2.5º Extension: 20.2 ± 4.6º Lateral bending: 9.1 ± 1.5º Axial Rotation: 9.9 ± 3.0º	Flexion: 12.3 ± 2.0º Extension: 12.1 ± 6.5º Lateral bending: 6.5 ± 2.3º Axial Rotation: 56.7 ± 4.8º

*Surprisingly, SD was not presented for this data set

All studies showed large standard deviations in the specimen sample population and even more variation was found when comparing results between studies, however some general observations have been made. The majority of motion in flexion/extension occurred at C0-C1 in all studies, over 80% of motion in axial rotation occurred at C1-C2 and motion in lateral bending was roughly equal at C0-C1 and C1-C2. When compared to the ROM of the rest of the cervical spine, the UCS exhibits more motion in flexion/extension and axial rotation[26]. To accommodate and facilitate these larger motions, it has been proposed that the UCS is held together by ligaments that have a large amount of laxity[27]. These ligament laxities were the main contributor to the large neutral zones (NZ) that were present in the moment-rotation curves. The NZ was defined as the amount of rotation that occurs at negligible load. The studies in Table 1 that also reported NZ data have been presented below (Table 2).

Table 2: Experimental data for neutral zone motions of the UCS

Study Details	C0/C1 NZ: Avg ± SD	C1-C2 NZ: Avg ± SD
Panjabi et al[23] Cadavers: 10 C0-C7 specimens NZ load definition: 0.0 Nm	Flexion*: 1.1º Extension*: 1.1º Lateral bending*: 1.5º Axial rotation*: 1.6º	Flexion*: 3.2º Extension*: 3.2º Lateral bending*: 1.2º Axial rotation*: 29.6º
Panjabi et al[24] Cadavers: 10 C0-C3 specimens NZ load definition: 0.0 Nm	Flexion: 10.5º ± 3.0º Extension: 10.4º ± 3.0º Lateral bending: 3.6º ± 2.8º	Flexion: 7.6º ± 3.1º Extension: 8.1º ± 3.5º Lateral bending: 7.4º ± 5.0º
Panjabi et al[25] Cadavers: 10 C0-C3 specimens NZ load definition: 0.0 Nm	Axial rotation: 0.9º ± 2.3º	Axial rotation: 27.5º ± 10.0º
Panjabi et al[26] Cadavers: 1 C0-C5, 5 C0-C6, 2 C0-C7, 8 C2-C7 specimens NZ load definition: 0.0 Nm	Flexion: 3.3º ± 1.8º Extension: 13.9º ± 4.1º Lateral bending: 3.6º ± 1.5º Axial rotation: 2.5º ± 1.6º	Flexion: 4.6º ± 2.4º Extension: 8.7º ± 6.7º Lateral bending: 2.4º ± 1.2º Axial rotation: 39.6º ± 7.5º

*Surprisingly, SD was not presented for this data set

The NZ data from these studies exhibited large amounts of within and between study variations. However, some observations were made when analyzing the NZ as a percentage of the ROM. Variations in NZ as a percentage of ROM were large for all motions except axial rotation and as a result general conclusions could not be made for flexion, extension and lateral bending. The NZ of axial rotation as a percentage of ROM showed good agreement between studies and as a result it was concluded that in axial rotation the NZ of C0-C1 motion accounts for approximately 20% of the ROM and the NZ of C1-C2 motion accounts for approximately 75% of the ROM.

In addition to the primary motions, coupled motions were also presented by Panjabi et al[24,25] for the UCS. Primary motion was significantly larger than coupled motion in flexion, extension and axial rotation at both C0-C1 and C1-C2. However, for lateral bending, large

coupled motions in flexion, extension and axial rotation were present (Figure 10). The most significant coupled motion during lateral bending was axial rotation at the C1-C2 level. For this case, the coupled motion of axial rotation was approximately three times larger than the primary motion of lateral bending.
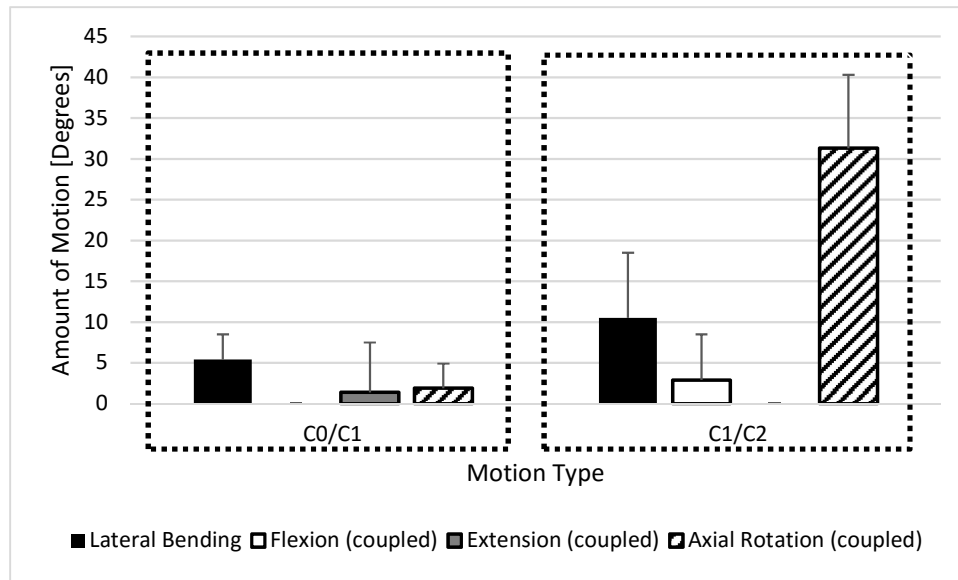
Figure 10: Coupled motion (with SD bars) of the UCS in lateral bending (data digitized from figures)[24,25]

2.3 Atlantoaxial Instability

Atlantoaxial instability (AAI) occurs when there is excessive movement at the C1-C2 junction generally caused by rheumatoid arthritis, degenerative osteoarthritis or cervical spine trauma at the C1-C2 level (which is the most common cause of AAI)[1]. A quantitative analysis of the increase in ROM due to AAI is presented in the next section. AAI caused by traumatic fracture of the odontoid process accounts for approximately 20% of all cervical fractures[3]. Odontoid fractures have been classified into three types by Anderson and D'Alonzo[4] as previously shown in Figure 2. type I fractures occur at the tip of the odontoid process and are the least common. type II fractures are the most common and most unstable, these fractures occur at the junction of the odontoid process and the body of the C2. type III fractures are classified by the fracture line passing through the body of C2 as well as the odontoid process[6].

While odontoid fractures can occur in all age groups, there are two significant age peaks. The first peak represents patients in their 2nd or 3rd decade of life who have sustained a high energy trauma, most commonly caused by motor vehicle accidents. The second peak represents elderly patients that have suffered low energy trauma, most commonly caused by ground level falls[7]. Significantly, odontoid fractures in elderly patients over the age of 70 are the most common spinal column injury[28].

2.4 Existing Clinical Treatment for Atlantoaxial Instability

As discussed in the Introduction, type I and type III odontoid fractures are commonly treated conservatively with hard collar immobilization[5]. Also, it is recommended that younger patients with type II odontoid fractures be treated surgically with a motion conserving anterior odontoid screw technique, provided a good screw trajectory is possible[29].

Controversy arises when it comes to the recommended treatment for elderly patients suffering from type II odontoid fractures. There is no consensus as to whether these patients should be treated conservatively or surgically. Furthermore, if it decided to treat these patients surgically, controversy also remains over the optimal surgical technique[7,8,30–32].

So, overall selection of the optimal treatment for type II odontoid fractures depends on several factors including patient age, comorbidities and fracture characteristics such as fracture displacement and fracture line orientation. The decision to treat type II odontoid fractures conservatively should be made if patients are unfit for conventional surgical techniques because of concerns related to blood loss, anesthetic and/or concurrent injuries (all of which are generally concerns for elderly patients). It is also important to assess the integrity of the transverse ligament in order to select the appropriate treatment. A compromised transverse ligament may lead to AAI regardless of whether bony union is achieved at the fracture line[6].

Type II odontoid fracture non-union rates associated with conservative treatment have been reported by Ochoa[3] to range from 35-80% for all patient demographics. The primary risk factor for non-union with conservative treatment was given as fracture displacement greater than 4mm. Other risk factors included posterior displacement of the odontoid, patients older than 40 years of age, fracture rotation of greater than 10° and a delay in diagnosis of greater than 3 weeks. According to Ochoa, union rates can be improved to nearly 100% by selecting the appropriate surgical technique based on patient indications.

2.4.1 Historical Surgical Treatments

Surgical treatments for AAI can be classified into one of two groups: motion-preserving or fusion. In current clinical practice, the only available motion-preserving surgical technique is anterior odontoid screw fixation, originally proposed by Nakanishi and Böhler[33]. In this technique, an incision is made on the anterior side of the neck and the patient's air passage is displaced laterally to allow for a compression screw to be placed through the body of C2 and into the fractured odontoid (Figure 11).

Figure 11: X-ray of patient treated for a type II odontoid fracture using anterior odontoid screw fixation[34]

According to Reindl et al[35] odontoid union rates of over 90% can be achieved using this technique provided that there are no contraindications present. Contraindications associated with the C2 trauma included the inability to reduce the odontoid fracture, a compromised transverse ligament and an oblique fracture that could cause the odontoid to shear anteriorly during screw lagging. Also anatomical contraindications were reported[35] that might interfere with the ideal trajectory of the odontoid screw such as short neck, thoracic kyphosis and barrel chest. Thoracic kyphosis and barrel chest are more common in the geriatric patient population as well as osteoporosis, which is another significant contraindication. Pre-existing osteoporosis makes odontoid fracture more likely in low energy traumatic incidents[36]. Additionally, geriatric patients may not be healthy enough to tolerate the high risk of post-operative pneumonia due to the

invasiveness of the surgery on the patient's air passage[37]. For these reasons, it is generally accepted that the anterior odontoid screw technique is not ideal for the elderly patient population with non-union rates reported as high as 77% for patients older than 65 years[31].

A more common surgical treatment for elderly patients suffering from type II odontoid fractures is posterior instrumented fusion of C1-C2. Although fusing C1-C2 results in a 50% loss of cervical spine axial rotation, it is necessary to stabilize the joint when conservative techniques have failed or look highly unlikely to succeed or the anterior odontoid screw technique is contraindicated. Posterior wiring techniques were the first constructs proposed to promote fusion at C1-C2. Originally introduced by Gallie[10] in 1939, the technique consisted of passing wires underneath the laminae of C1 and C2 and using them to hold a bone graft in place (Figure 12a). Multiple iterations of the Gallie wiring technique have been reported but all were prone to implant loosening, increased risk of spinal cord injury and poor biomechanical stability under axial rotation and lateral bending[38,39]. For these reasons, posterior wiring techniques have been largely abandoned and have not seen popular clinical use since the 1980's. In 1984, interlaminar clamps were introduced as the Halifax technique by Holness et al[40] for C1-C2 fusion (Figure 12b). These clamps improved upon wiring techniques by eliminating the need for sublaminar passage. However, the Halifax technique did not provide any additional biomechanical stability when compared to wiring techniques which resulted in a high rate of non-fusion and implant failure[41].
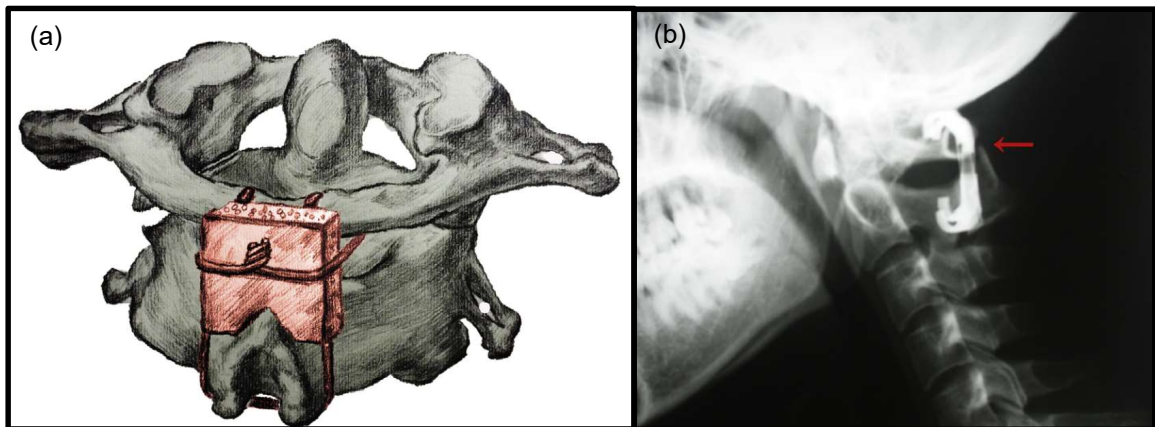
Figure 12: a) Gallie wiring technique and b) Halifax interlaminar clamp for posterior C1-C2 fusion[13]

Screws were first incorporated into C1-C2 fusion by Jeanneret and Magerl[42] with the introduction of the transarticular screw technique. In this technique, two screws are inserted

bilaterally through the articulating surfaces of C1-C2 (Figure 13). Up to the present time, transarticular screws have shown superior biomechanical stability over any other posterior fusion construct and as a result have achieved excellent fusion rates[43]. However, the steep learning curve and technical demands of this technique have resulted in a higher occurrence of injury to the vertebral artery as well as a higher chance of postoperative neurological complications if the C2 nerve root is injured[44]. Additionally, this technique cannot be used on approximately 20% of patients due to anatomical variations in the UCS[45].
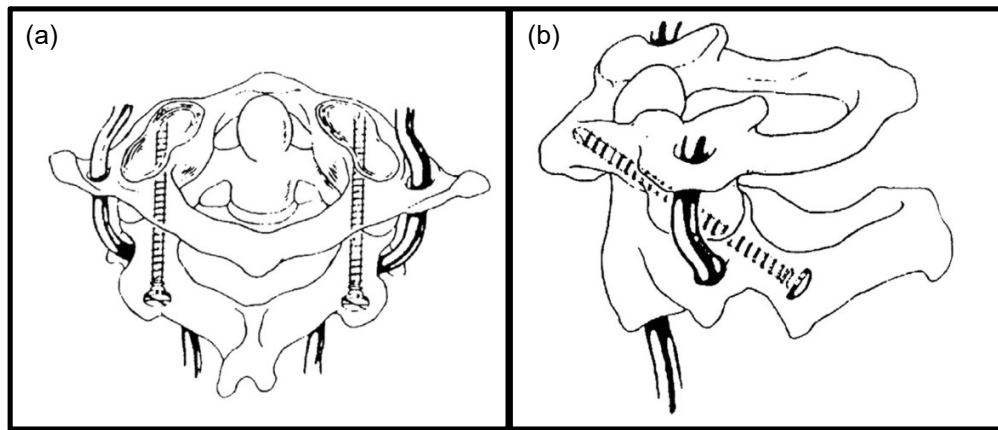
Figure 13: a) Posterior view and b) lateral view of transarticular screw technique for posterior C1-C2 fusion[13]

In recent years, screw/rod constructs have gained popularity in posterior C1-C2 fusion with the Harms construct as introduced by Harms and Melcher[12] being the most widely used. The Harms construct consisted of two polyaxial screws placed bilaterally in each lateral mass of C1 and two polyaxial screws placed bilaterally in the pedicles of C2. Connecting rods were then placed in the head of the polyaxial screws and tightened in place with set screws (Figure 14). Polyaxial screws were designed to allow rotation of the screw head after the screw has been implanted in the bone. This rotational mobility allowed easier alignment with the rod compared to fixed head screws. Once the rods were in place and the set screws were tightened down, the polyaxial screws were locked into place and no longer allowed motion. The Harms procedure has shown good biomechanical stability and clinical fusion rates have commonly been reported over 90%[31]. These high fusion rates and the less technically demanding surgical

procedure compared with the transarticular screw technique have resulted in the Harms construct becoming the "gold standard" in posterior instrumented fusion since its introduction in 2001.
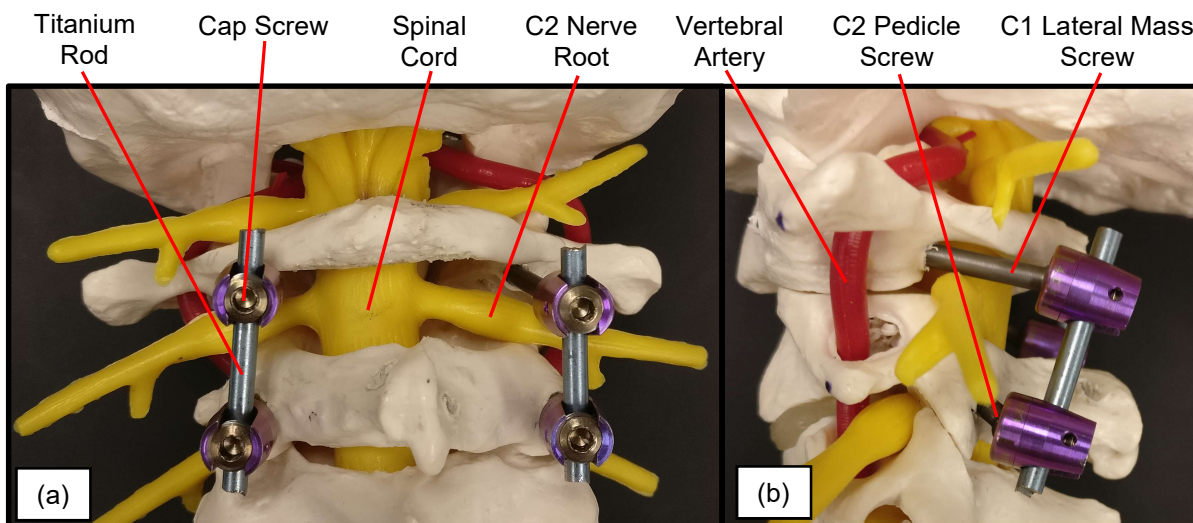
Figure 14: Upper cervical spine anatomical model showing: a) posterior view and b) lateral view of Harms construct used in C1-C2 fusion

Although the Harms procedure has continued to be the surgical treatment of choice for the elderly patient population, there were still several downfalls associated with this procedure. Primarily, there was a risk of injury to the vertebral artery due to initial exposure and placement of the screws into C1 and C2[46]. Additionally, the C2 nerve root was often sacrificed to achieve optimal placement of the C1 lateral mass screw. While this nerve sacrifice had been reported to only cause minor numbing in the patient's shoulders, it was considered better to leave the C2 nerve root intact[14]. The surgery was also very invasive because dissection must be done all the way down to the C1 lateral mass and C2 pedicle. This led to concerns related to blood loss, operating time and patient recovery time. With all of these factors in mind, only approximately half of the geriatric patient population was deemed healthy enough to undergo surgery[8]. Furthermore, operative treatment for geriatric patients with type II odontoid fractures did not significantly improve long term mortality rates when compared to the non-operative treatment because of the various complications associated with current surgical treatment options of which Harms was the most common[8,36].

2.4.2 Less Invasive Procedures

In an attempt to reduce the controversy around surgical treatment of type II odontoid fractures in the elderly, several less invasive surgical procedures were proposed. An alternative to the Harms procedure, where C2 translaminar screws were used in place of C2 pedicle screws, was proposed by Wright[15] in 2004. In this technique, bilateral, crossing screws were placed in the lamina of C2 and then connected to C1 lateral mass screws through the use of rods (Figure 15). Using C2 translaminar screws reduced the risk of injury to the vertebral artery, but constructs incorporating C2 translaminar screws were shown to provide less biomechanical stability under lateral bending and axial rotation when compared with the Harms construct[47]. However, despite the reduced stability, C2 translaminar screws have shown excellent fusion rates clinically[48] and the decision to use them should be based on implantation concerns rather than acute stability issues[49].
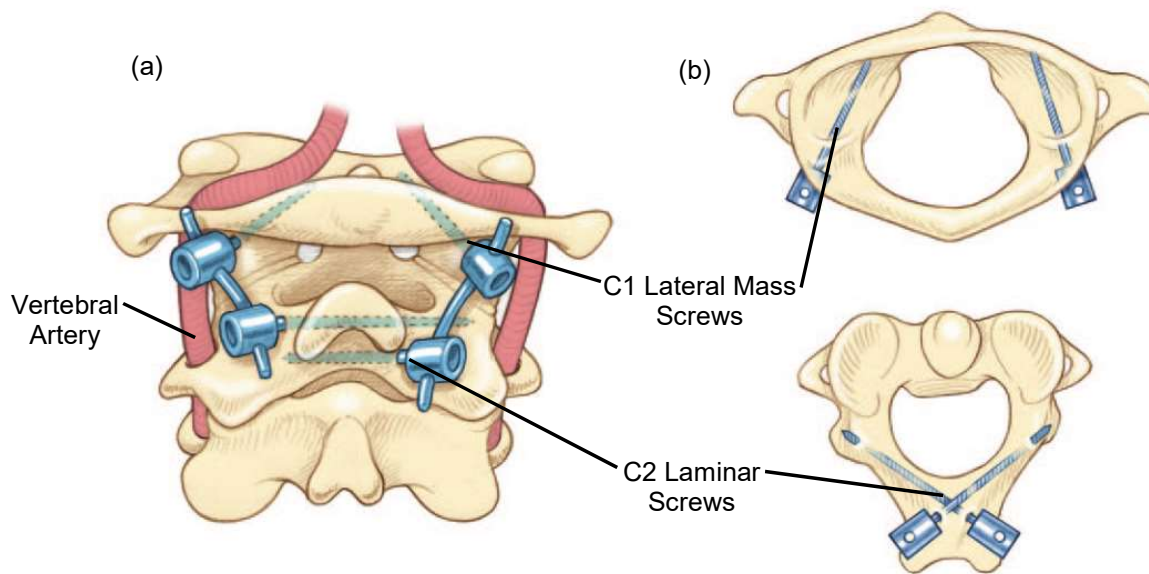
Figure 15: a) Posterior view of screw rod construct using C2 laminar screws and b) axial views to show screw trajectory in C1 and C2[49]

A less invasive surgical technique (as opposed to a less invasive construct) was proposed for the traditional Harms procedure by Taghva et al[50]. This minimally invasive surgery (MIS) was initially tested on five cadaveric specimens for feasibility, and then applied to 2 clinical cases. As noted above, the Harms construct was used in the MIS procedure and it did not differ from that used in a traditional open procedure. What did differ however was the surgical approach, in which two incisions were made bilaterally at the C1-C2 segment as compared to a

central single posterior incision for the open procedure. The incisions were then dilated using K-wire guidance and minimal access X-tube retractors (Medtronic Sofamor Danek, Memphis, TN) to allow for the Harms construct to be implanted.

Radiological observations for the cadaver testing confirmed good screw and implant placement with the C2 nerve being preserved in all cases and there was no evidence of injury to the vertebral arteries. The MIS approach from the cadaver study was then used to treat two patients (age: 71 and 84 years) with type II odontoid fractures. Each case took 3.5 hours and the blood loss was 150 mL for the 84 year old patient and 100 mL for the 71 year old patient. The C2 nerve was sacrificed in one case and preserved in the other. In the case of the 84 year old patient, pneumonia was contracted post operatively and successfully treated with intravenous antibiotics for two weeks in hospital. The 84 year old patient also suffered from vertebral artery compression by the rod construct that required an open revision surgery to successfully correct. At a follow up of four months, both cases demonstrated solid fusion and atlantoaxial stability.

In another clinical study by Kantelhardt et al[51], three patients underwent a MIS Harms procedure to treat type II odontoid fractures. The average patient age was 87.7 years (85-89) and the average blood loss was 390 mL (170-700) with an average operating time of 135 minutes (75-150). Successful fusion and atlantoaxial stability occurred in all three cases at final follow up.

Despite these attempts to create a MIS Harms procedure for atlantoaxial instability, the author of the present thesis believes that the benefits to the patient are minimal. Blood loss and operating time remain similar in the MIS versions of the Harms procedure compared with the traditional open procedure. A potential benefit of the MIS Harms approach is faster recovery times due to smaller incisions. However, it is believed that this marginal benefit of the MIS Harms procedure is outweighed by the increased surgical complexity and higher risk of injury to the vertebral artery due to reduced access and visibility.

2.5 Proposed Novel Treatment for Atlantoaxial Instability

Several implants that are early in their design cycle have been proposed for treating AAI through C1-C2 fusion but they have not yet been used clinically. Mostly, these implants have been evaluated in cadaveric tests by comparing the stability of the novel construct with the stability of the Harms procedure. In other cases (discussed later in this section), FE modeling has

been used to evaluate the potential of novel constructs that are in even earlier stages of the design cycle. Often, in these FE models, boundary conditions are used to mimic experimental conditions and the stability of the novel construct is estimated and compared with experimental data for the Harms procedure.

2.5.1 Evaluation of Novel Implant Constructs in Cadaveric Studies

In a 2008 cadaveric study, Kelly et al[52] proposed a construct consisting of a novel C1 posterior locking plate paired with C2 translaminar screws and connected with 3.5 mm rods (Figure 16). The motivation for the C1 posterior locking plate was to reduce the risk of injury to neurological and vascular structures by replacing C1 lateral mass screws. The C1 plate was designed to be bendable to allow for better conformity to the C1 posterior arch. Additionally, anatomical measurements were performed on radiographs from fifty cadaveric specimens which showed that a plate length of 30 mm, secured with four 2.4 mm diameter x 8 mm long screws was feasible.
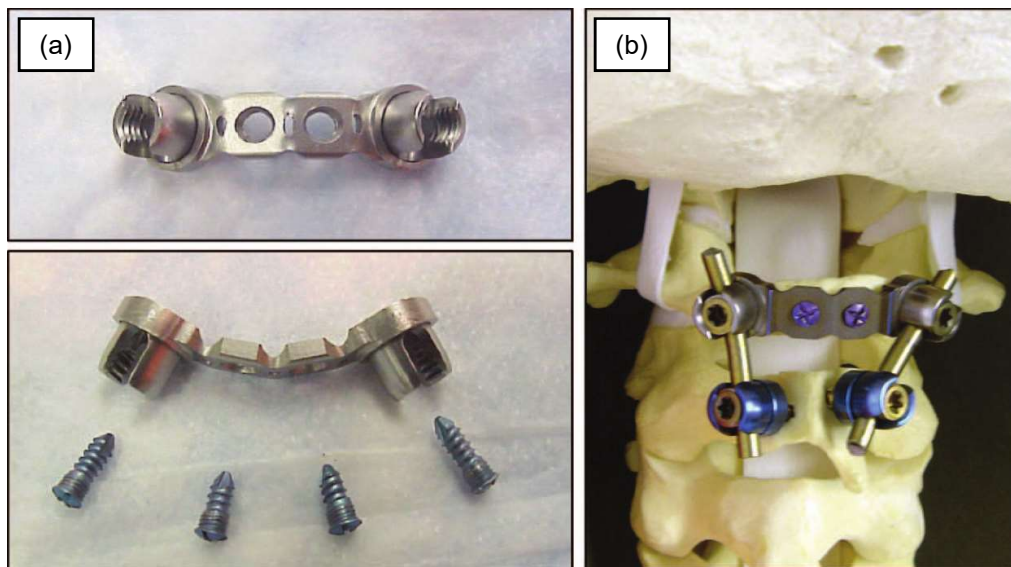
Figure 16: a) Bendable C1 posterior locking plate with 2.4mm by 8mm bone screws and b) anatomical model showing full construct with C2 translaminar screws and 3.5mm rods[52]

To test the biomechanical stability of the novel construct, seven cadaveric spine specimens (C0-C4) were used. The specimens were mounted in a programmable testing apparatus and loaded up to 1.5 Nm under flexion/extension, lateral bending and axial rotation. Motion was collected using optical trackers placed on each vertebra and Euler angles were

calculated to assess stability[53]. Three cases were tested: intact odontoid, destabilized odontoid with Harms construct and destabilized odontoid with novel construct. To destabilize the odontoid, a high speed bur was used to simulate a type II odontoid fracture. However, the destabilized case without instrumentation was not tested in the study. Statistical analysis using a one-way, repeated-measures ANOVA followed by a post-hoc Student-Newman-Keuls test did not detect any significant differences between the stability of the Harms construct and the novel construct in all modes of loading (Table 3).

Table 3: Summary of angular displacement data (Avg ± SD) comparing novel posterior locking plate construct with Harms construct (data obtained from plots)**[52]**

C1-C2 Segment	Intact	Locking Plate Construct	Harms Construct
Flexion/Extension	5.5º ± 3.0º	1.0º ± 0.7º	1.4º ± 1.0º
Lateral Bending	1.7º ± 1.2º	1.1º ± 0.8º	0.7º ± 0.4º
Axial Rotation	24.1º ± 7.8º	1.4º ± 0.8º	1.0º ± 0.7º

Another cadaveric study by Robertson et al[54] proposed a novel "integrated" device for intra-articular stabilization and fusion of C1-C2. The motivation for designing this device (Figure 17) was to develop a construct that provided superior stability to the Harms procedure and was less technically demanding to implant than transarticular screws. The device consisted of an intra-articular blade with roughened surfaces to promote interference, a passage in the blade that allowed for placement of an oblique bicortical fixed angle screw in the C1 lateral mass and a posterior leg that allowed for two bone screws to be placed in the lamina of C2. Information on dimensions of the screws was not given in this study.
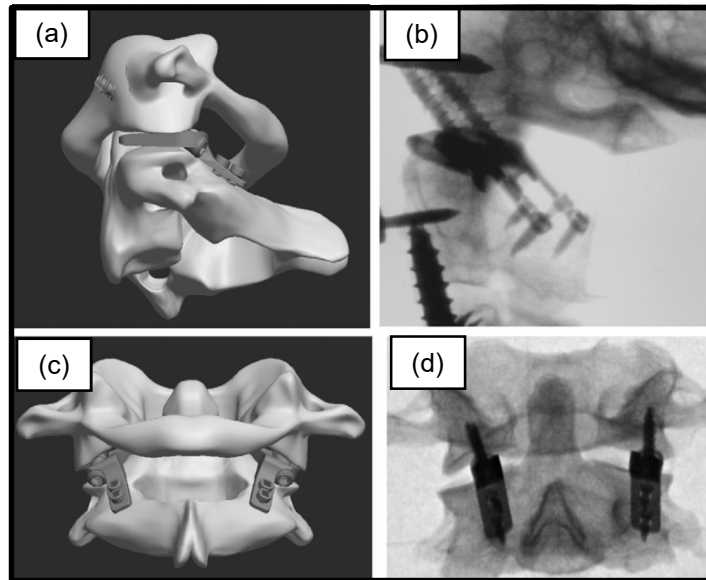
Figure 17: a) lateral schematic diagram of integrated device, b) lateral radiograph of integrated device in cadaveric spine, c) posterior schematic diagram of integrated device and d) posterior radiograph of intergrated device in cadaveric spine[54]

To test the biomechanical stability of the integrated device, six cadaveric spine specimens were used. The specimens were mounted in a device that allowed loading up to 1.5 Nm in flexion/extension, lateral bending and axial rotation. Motion was collected using optical trackers placed on each vertebra and Euler angles were calculated to assess stability[53]. Four cases were tested: intact odontoid, destabilized odontoid (type II fracture created with high speed bur), destabilized odontoid with integrated construct and destabilized odontoid with Harms construct. Statistical analysis performed using repeated-measures ANOVA with a post-hoc Bonferroni correction for comparing the different cases. With the exception of lateral bending (where the integrated construct was more stable), the data failed to detect significant differences for the stability of the Harms construct compared with the integrated construct in all other modes of loading (Table 4).

Table 4: Summary of data comparing novel integrated construct to Harms construct[54]

C1-C2 Segment	Intact	Destabilized	Integrated Construct	Harms Construct
Flexion/Extension	14.1º ± 2.9º	31.6º ± 4.6º	3.6º ± 1.8º	4.0º ± 1.4º
Lateral Bending	1.8º ± 1.1º	14.1º ± 5.8º	0.4º ± 0.3º	1.4º ± 0.7º
Axial Rotation	67.3º ± 13.8º	742º ± 16.1º	0.9º ± 0.7º	1.4º ± 0.7º

Another cadaveric study by Xu et al[55] proposed using a novel C1 hook combined with transarticular screws (TAS+H) or C2 pedicle screws (C2PS+H) for C1-C2 fusion. The motivation for designing this hook was to improve the stability of transarticular screws in flexion/extension without the addition of Gallie wiring. The novel portion of the device consisted of a rod with a hook on the superior end which wrapped around the posterior arch of C1. The inferior end of the rod was connected to a polyaxial transarticular screw.

To test the biomechanical stability of the TAS+H and C2PS+H constructs, Xu et al[55] used seven cadaver spine specimens (C0-C3). The specimens were mounted in a programmable testing apparatus and loaded up to 1.5 Nm under flexion/extension, lateral bending and axial rotation. Motion was collected using optical trackers placed on each vertebra and Euler angles were calculated to assess stability[53]. Six cases were tested: intact odontoid, destabilized odontoid (type II fracture created with high speed burr), destabilized odontoid with transarticular screws plus Gallie wiring (TAS+G) (Figure 18a), destabilized odontoid with TAS+H (Figure 18b), the Harms construct (Figure 18c) and destabilized odontoid with C2PS+H (Figure 18d). Statistical analysis was done using ANOVA techniques but the specific details were not given. The C2PS+H construct was reported to have significantly more motion than the other constructs in axial rotation. No significant differences were detected between the Harms construct and TAS+G and TAS+H constructs for all other modes of loading. Unfortunately, actual values for the ROM of each construct were not provided in the study.
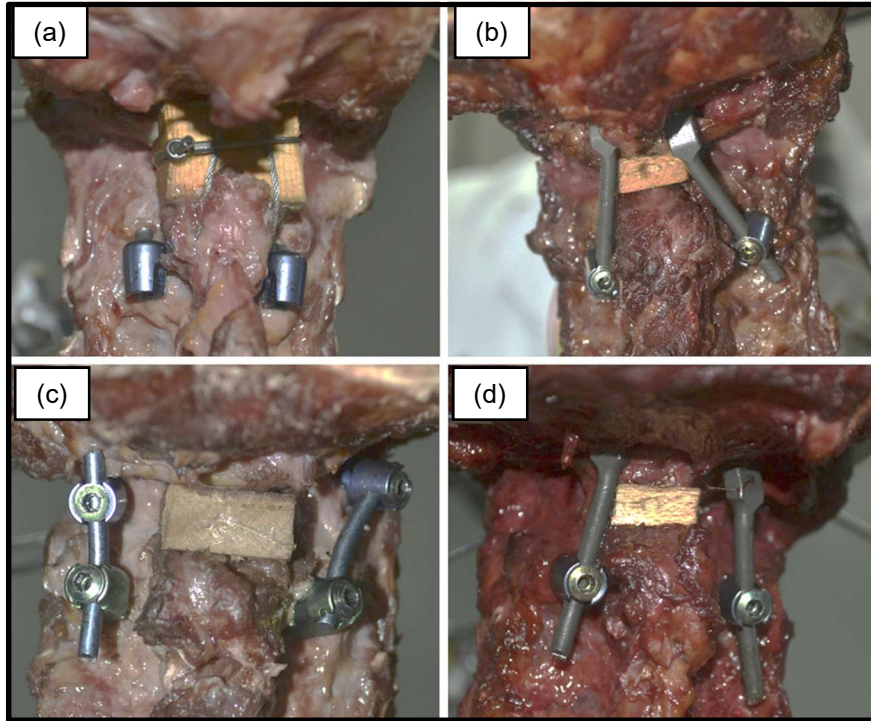
Figure 18: cadaveric models of a) TAS+G construct, b) TAS+H construct, c) Harms construct and d) C2PS+H construct[55]

2.5.2 Evaluation of Novel Implant Constructs in Finite Element Modeling

Since the early 2000's, FE modeling has been used to assess the performance of novel UCS implants prior to cadaveric testing. Provided that the FE model has been compared with experimental data and has shown some agreement (enough to be considered validated), the results of an FE model can be used to guide the implant design process and largely reduce the amount of prototyping and experimental testing required for novel implant designs. As a result, the cost and time of an implant design cycle can be reduced. In general, studies that involved modeling novel implant designs for the UCS consisted of the following components: UCS FE model generation, FE model validation against experimental ROM data, addition of constructs into the FE model, comparing parameters of interest between constructs as shown in Table 5.

Table 5: Summary of published FE studies of novel UCS fusion implants

Study	Study Objective	FE Model Generation	FE Model Validation	Parameter Comparisons	Optimal Construct
Puttlitz et al[56]	Analysis of two different C0-C2 fusion constructs	−anatomy from CT scan −material properties from the literature	− quasi-static moments applied − compared with experimental ROM studies	−joint kinematics −joint stresses −construct stresses	Bilateral hybrid C0 plates/rods with C2 pedicle
Cai et al[57]	Analysis of two different C1-C2 fusion constructs	−Anatomy from CT scan −Material properties from published literature	−Quasi-static moments applied −Results compared with experimental ROM studies	−Joint kinematics, stress at implant/bone interface	C1-C2 transarticular screws with locking plate
Cai et al[58]	Analysis of two different C0-C2 fusion constructs	−Anatomy from CT scan −Material properties from published literature	−Dynamic boundary prescribed motion −Results compared with experimental ROM studies	−Joint kinematics, construct stresses	Novel screw/locking plate design
Zhang et al[59]	Analysis of two different C1-C2 fusion constructs	−Anatomy from CT scan −Material properties from published literature	−Quasi-static moments applied −Results compared with experimental ROM studies	−Joint kinematics, stress at implant/bone interface	Control construct

2.5.2.1 Ligament Properties in Upper Cervical Spine FE Modeling

In addition to the information provided in Table 5, more background is required to develop an understanding of how the non-linear ligament properties of the UCS were implemented into the FE models. Specifically, ligament properties in an UCS FE model must incorporate laxity in order for the generated NZ response to be accurate. However, determining appropriate ligament laxities from experimental data was difficult because ligament laxity was lost once individual ligaments were dissected for force-displacement testing. As a result, the protocol for implementing ligament laxity in FE models was unclear and varied from model to model. The scatter and uncertainty in the experimental data values that were used for validation of these FE models tended to obscure the role of ligament laxity in the accuracy of the FE model predictions.

In an UCS FE model developed by Brolin et al[60], ligament properties were implemented in the model by assuming that the NZ was one third of the failure displacement and that the curve was linear from the end of the NZ to the failure load. The force value and displacement value at which ligament failure occurred was the only point that was checked against experimental values. Additionally, a parameter study which varied the stiffness and NZ length of each ligament was conducted to achieve a better agreement between the ROM of the FE model and the ROM of experimental studies.

In another UCS FE model developed by Zhang et al[61], the ligament force-displacement curves were "reasonably adjusted to improve the segmental motions" and thus achieve better agreement between the ROM and NZ of the FE model and the experimental results. Furthermore, the in-vitro force displacement curves were simplified before being implemented into the model by assuming linearity between the end of the NZ and the failure displacement. This assumption effectively made the FE model response of the ligaments less stiff in the elastic zone than the in-vitro response.

Adjusting the in-vitro ligament force-displacement data is considered by the present author to be beneficial in understanding the effect that each ligament has on the FE model response. However, it is suggested that these adjustments should not be used to calibrate the FE model to agree with the experimental data because this reduces the biofidelity of the model when loading conditions are altered.

2.5.2.2 The Global Human Body Models Consortium Finite Element Model

Commercial explicit finite element software (LS-DYNA, LSTC, Livermore, CA) had been used to generate a seated position full human body FE model for injury prediction and prevention in automotive applications (Figure 19a). This FE model had been developed by an international group of industry, government and academic institutions that work with the Global Human Body Models Consortium (GHMBC, http://www.ghbmc.com/). The FE model was based on the anatomy of a fiftieth percentile male (M50) and was validated both at the body region and full body levels[62].

A UCS FE model similar to the FE models described earlier in this chapter was extracted from the GHMBC M50 FE model and musculature was removed (Figure 19b). The material properties for this UCS FE model were taken from experimental data as described in more detail

by Shateri and Cronin[63]. Individual ligaments were modeled using a series of non-linear tension-only elements, following the approach proposed by Panzer et al[64] and Dewit et al[65] The total ligament force was divided evenly between the elements. The non-linear ligament force-displacement response was incorporated directly from the experimental data of Mattucci et al[66]
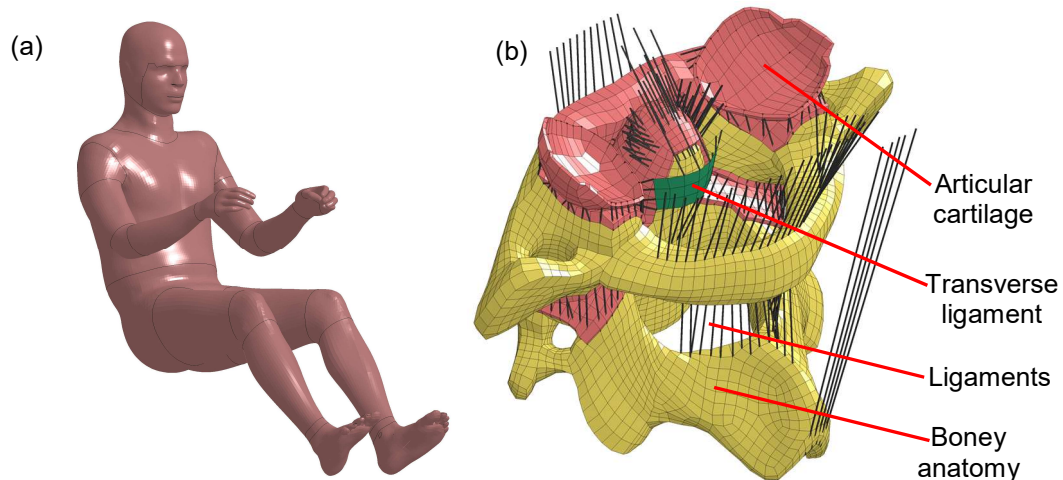
Figure 19: a) GHBMC M50 full body FE model in seated position and b) UCS FE model (base of skull omitted from figure)

Ligament laxity was defined in the FE model as the amount of displacement that a ligament could undergo before a force response was generated. Apart from this laxity definition, the ligament force-displacement curves used in the FE model were the same as the in-vitro data. Ligament laxity values were numerical optimized to achieve a best fit between the segment level moment-rotation response of the FE model and the segment level moment rotation response of experimental data from Goel et al[27] and Nightingale et al[67] under flexion, extension and axial rotation at the load range occurring in automotive trauma scenarios. In the current GHMBC M50 UCS FE model (v4.4), laxity was implemented into 6 ligaments and varied from 0.9mm to 1.4mm (Figure 20).
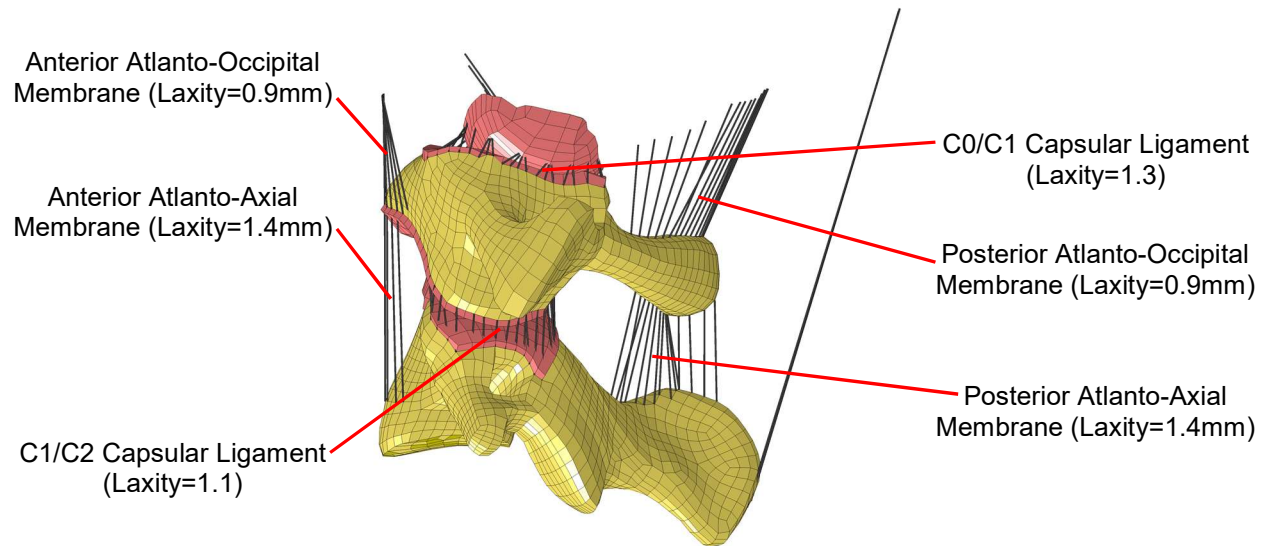
Figure 20: Ligament laxities of selected ligaments in the current GHMBC M50 FE model optimized for traumatic loading

2.6 Objectives and Scope of the Research

Both the objectives and the scope of the present research have been given in the Introduction (Chapter 1). However, they can be re-stated in more detail based on the preceding review of the current literature. It is clear that the ideal surgical management of type II odontoid fractures in the geriatric patient population is not known. The beneficial outcomes of surgical intervention are often cancelled out by the high risk procedures that are available today. Additionally, conservative treatment of type II odontoid fractures using external hard collar immobilization results in very low fracture union rates and high complications (even patient death).

Due to the controversial treatment options currently available for type II odontoid fractures, specifically in the geriatric patient population, it is believed that there is an opportunity to develop a novel construct that addresses the concerns of surgical practitioners. This construct can be designed to promote high fusion rates by applying posterior fixation at C1-C2. A main focus of the new construct is to reduce the invasiveness of the surgery while achieving the fixation required to promote fusion with less intraoperative risk than the Harms construct. The construct adopts C2 translaminar screws because they present a safer alternative than C2 pedicle screws and have already shown good clinical outcomes. However, commercially available fixation methods for C1 rely solely on the use of lateral mass screws. For these reasons, the

30

research presented in this thesis addresses the design of a novel implant construct that attaches to the posterior arch of C1. This new construct which can include C2 translaminar screws, is intended to present a less invasive, safer and effective alternative to the Harms construct. This would allow the successful surgical treatment of more geriatric patients suffering from type II odontoid fractures.

The scope of the current research will first involve the use of FE modeling to assess the feasibility of the posterior arch as a potential fixation location. Simplified constructs will be modeled and the stability of each construct will be compared with that estimated for the Harms procedure in order to determine the ideal configuration of the novel construct. The information gained from FE modeling is to be used in the detailed design phase to generate fully functional prototypes. Harms constructs are also obtained. These prototypes and the Harms constructs are to be tested experimentally in a cadaveric study to compare their ROM performances. The experimental results are compared with the earlier results obtained from the FE model. Based on all of these results, conclusions are made regarding the efficacy of the developed device.

3.0   Finite Element Modeling of the Upper Cervical Spine

The GHMBC M50 UCS FE model was used as the starting point for the FE modeling that was done for the present thesis. Before this FE model could be used to model C1-C2 fusion constructs, it had to first be validated for ROM under physiological loads imposed by activities of daily living (as opposed to the traumatic loading experienced during automobile crashes). When the moment-rotation response of the existing GHMBC FE M50 FE model was run under physiological loading, it was found that the model response was too stiff in all types of motion. To address this problem, a new ligament laxity optimization process was performed to improve the moment-rotation response of the model for physiological loads as opposed to the traumatic load values that had been used in its current validation.

This optimization process was discussed in detail in a paper that was submitted to The Spine Journal. Minor revisions have been completed and the paper is now accepted and "in press"[68]. The findings of the optimization process have been summarized below.

The six ligaments that were selected for laxity optimization in the physiological load range were the same ligaments that had been modeled with laxity for the traumatic load range in the existing GHBMC M50 UCS FE model. However, the new "physiological loading" optimized laxity values were larger, ranging from 1.4 mm to 5.8 mm (Table 6) to better agree with the large ROM of the UCS. After ligament laxity was optimized for ROM, the agreement between the FE model and experimental data was greatly improved for all types of motion compared with assuming zero ligament laxity (Figure 21).

Table 6: Optimized ligament laxity values for ROM

Ligament	Laxity Value
Anterior Atlanto-Occipital Membrane	5.8 mm
Posterior Atlanto-Occipital Membrane	5.8 mm
Anterior Atlanto-Axial Membrane	3.3 mm
Posterior Atlanto-Occipital Membrane	3.3 mm
C0/C1 Capsular Ligament	1.4 mm
C1-C2 Capsular Ligament	5.4 mm
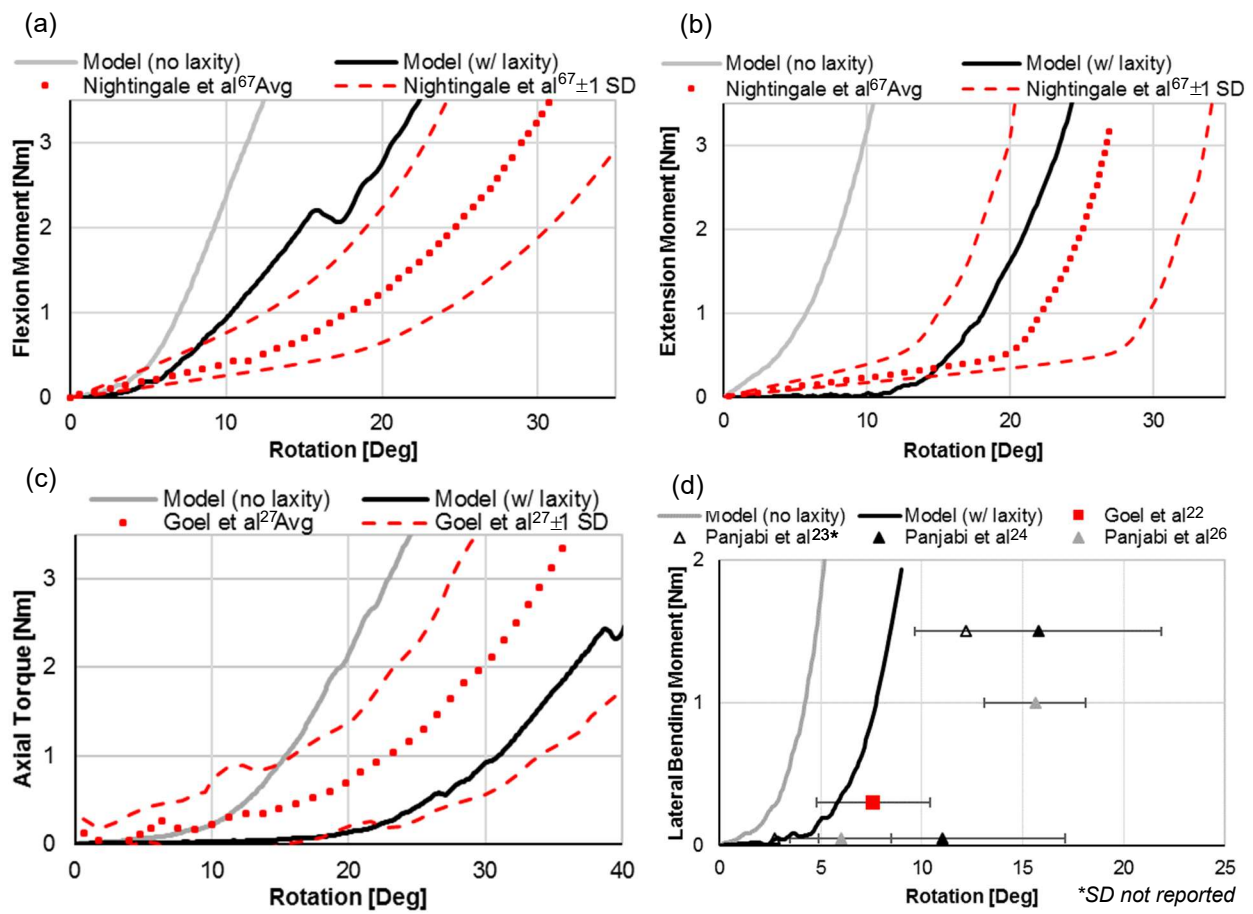
Figure 21: Load rotation curves of UCS FE model for (a) axial rotation, (b) flexion, (c) extension and (d) lateral bending

For the flexion response, the FE model was still slightly out of the ±SD corridor of the experimental data after laxity was optimized. Additionally, the bump in the moment-rotation curve at approximately 2 Nm was due to the onset of motion at C1-C2. When the boundary moment was less than 2 Nm, motion occurred at C0-C1 only. The extension moment-rotation curve fell within the ±SD corridor of the experimental data and had a smooth response over the load range that was simulated. The axial rotation moment-rotation curve fell within the ±SD corridor of the experimental data but predicted motion that was larger than the Avg curve. The different levels of agreement above were, in part, a consequence of using the multi-objective function to optimize all modes of loading with a *single set* of ligament laxity values. This criterion gave laxity values that were physically consistent. However, the ligament force-displacement properties measured and input into the model were the average values from a large number of cadaveric specimens[66] and thus were not the quite same as the ligament properties of the cadavers involved in the ROM experiments that were used for laxity optimization. Thus, the

ROM behaviors of the FE model and the experimental data were likely intrinsically different and so the optimization could only achieve a compromise in the ROM agreements for all motion types. However, it was considered that the ligament properties adopted and their optimized laxities would give the best chance of accurate predictions of spinal ROM for a new patient group. Such predictions would be useful for those doing biomechanical studies of the UCS both with and without fusion constructs in place.

3.1 Type II Odontoid Fracture Modeling

As a check on the chosen ligament properties and the optimized ligament laxities in the FE model, a simulation of AAI was performed by creating a type II odontoid fracture. This was done by deleting the cartilage, cortical bone and cancellous bone elements located at the base of the odontoid (Figure 22). The FE model was then run under the same boundary conditions as the ROM study to determine the increase in motion as a result of the odontoid destabilization (Table 7). The ROM values for flexion and extension were averaged and reported as flexion/extension in order to better compare the results of the FE model to experimental studies which did not usually report flexion and extension separately and instead used this same averaging technique. Contact between the odontoid and vertebral body of C2 would have been modeled using a standard penalty-based contact algorithm, but contact did not occur in any of the loading cases due to the odontoid being distracted away from the vertebral body of C2. Motion has been presented in terms of the relative vertebral rotation of C1-C2 about the axis in which the boundary prescribed motion had been applied to simulate flexion/extension, lateral bending and axial rotation. The motion for both the stabilized and destabilized cases has been reported when the boundary load in the axis of applied motion reached a value of 1.5 Nm.
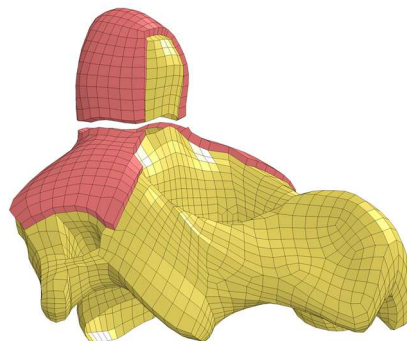
Figure 22: Implementation of a type II odontoid fracture in the FE model to simulate AAI

34

Table 7: Intact vs. destabilized C1-C2 motion at 1.5 Nm

	FE Model - Intact	FE Model - Destabilized	Increase
Flexion/Extension	9.3°	13.9°	49%
Lateral Bending	2.5°	16.3°	546%
Axial Rotation	26.7°	29.6°	11%

When a type II odontoid fracture was simulated in the FE model with ligament laxity, ROM at the C1-C2 level increased in all cases. This increase in ROM was within the range of the experimental data from the literature[49,54,69] (Figure 23). While the scatter in the experimental data was large (both within and between studies), the general trend shows that a type II odontoid fracture caused lateral bending to have the largest relative increase in ROM, followed by flexion/extension and axial rotation respectively. The fact that the FE model predictions were within the range of the average values from the experimental studies provided some support for the robustness of the FE model because the odontoid fracture case had not been used to determine the optimal ligament laxities.
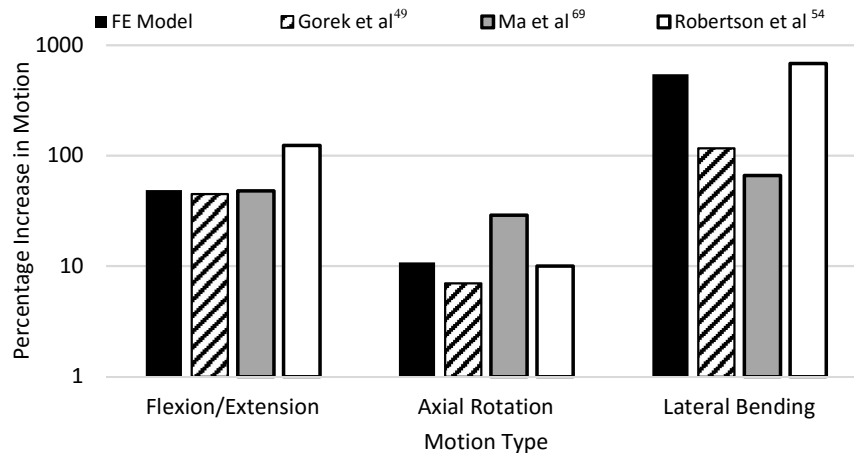
Figure 23: Increase in C1-C2 motion at 1.5 Nm due to a type II odontoid fracture compared to the intact state (log scale used so that the large scatter in the experimental findings of the various studies could be clearly visualized)

3.1.1 Method of Projecting Angles onto Planes

To illustrate how the C1-C2 rotations were calculated for comparison of motion between the intact and destabilized conditions, the procedure will be explained for the case of extension with an intact odontoid (Figure 24). The C1-C2 rotations reported in Table 7 were obtained by

calculating Δβ (change in the angle β shown in Figure 24) in a plane normal to the primary axis of motion. This method was used as an efficient way to quickly analyze changes in motion caused by the odontoid fracture as well as different implant constructs that will be discussed in later chapters. Additionally, the C1 and C2 vertebrae were modeled as deformable solids so angle analyses that rely on rigid body assumptions, such as Euler analysis, could not be used. The same methodology was used to measure the C1-C2 rotation in flexion, lateral bending and axial rotation. However, for the lateral bending different nodes were selected (Table 8).
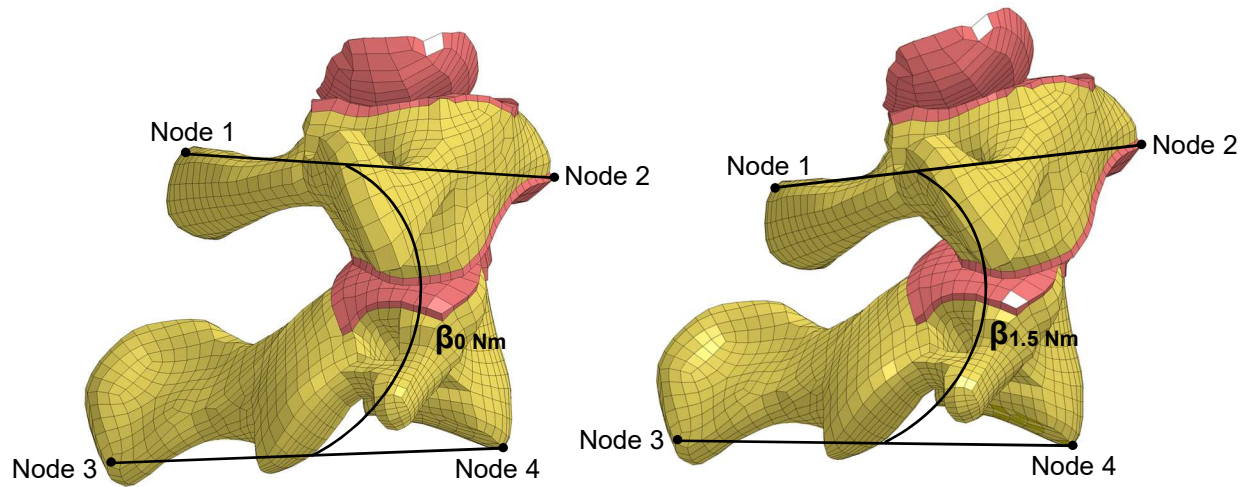
Figure 24: The β angle (angle of intersection of the lines) for C1-C2 at 0 Nm (left) and 1.5 Nm (right)

Table 8: Node selection in FE model for projecting angles onto planes of motion

Motion	Node 1	Node 2	Node 3	Node 4
Flexion	2030306	2210660	2029662	2030015
Extension	2030306	2210660	2029662	2030015
Axial Rotation	2030306	2210660	2029662	2030015
Lateral Bending	2210672	2210660	2029901	2030015

3.1.2 Coupled Motion in Lateral Bending

When running the FE model in flexion, extension and axial rotation, the primary motions dominated in each case and coupled motions were negligible. However, for the case of lateral bending there was a significant amount of coupled motion present in the form of axial rotation and extension. This coupled motion was also reported by Panjabi et al[24] who found that when a moment was applied to induce lateral bending, axial rotation at C1-C2 still dominated and generated motions that were approximately three times larger than the primary lateral bending motion. The coupled motion response in the lateral bending simulation provided some further support for the robustness of the model because it generated a realistic response even though this motion had not been involved in the model validation that was done by optimizing ligament laxities.

3.1.3 Application of the Type II Odontoid Fracture Modeling

It was considered important to note that a consistent representation of AAI in the UCS FE model had been achieved and it was based on independently measured ligament properties and a single set of optimized ligament laxities. This gave a good foundation for accurate predictions of UCS instability after a type II odontoid fracture and the further application of modeling fusion constructs.

3.2 Modeling Simplified C1-C2 Fusion Constructs

As suggested above, the next step was to begin modeling simplified fusion constructs to stabilize the odontoid fracture. The methodology for implementing each construct was the same and only the fixation locations of each construct on C1 and C2 varied. Beam elements were used to create bilateral frame structures, with 16 beam elements in each structure, spanning the fixation locations between C1 and C2. The beam elements were modeled as commercially pure titanium and the material properties were obtained from CES Edupack 2016 (Granta Designs Limited, Cambridge, UK). Although other rod materials are commercially available (such as cobalt-chrome and titanium alloy), commercially pure titanium was specifically chosen because it had the lowest elastic modulus and thus the model generated the worst case scenario when predicting construct stability. Additionally, the cross sectional area summation of the 16 beam elements of each rod was equal to 9.62 mm^2. This was chosen as the total cross sectional area

because it corresponded to a rod with a 3.5 mm diameter, which was very common in cervical spine fusion constructs.

Initially, three construct configurations were modeled (Figure 25): Harms construct, C1 lateral mass screws with C2 translaminar screws (C1LM/C2TL) and a novel construct which assessed the feasibility of using the C1 posterior arch as a fixation location in conjunction with C2 translaminar screws (C1PA/C2TL). To predict the stability of each construct, the FE model was run under the same conditions as the ROM study and the C1-C2 angular motion of each construct was reported at 1.5 Nm (Figure 26). The method of projecting angles onto primary planes of motion was used to measure the C1-C2 angular motion (same as the method discussed in section 3.1.1).
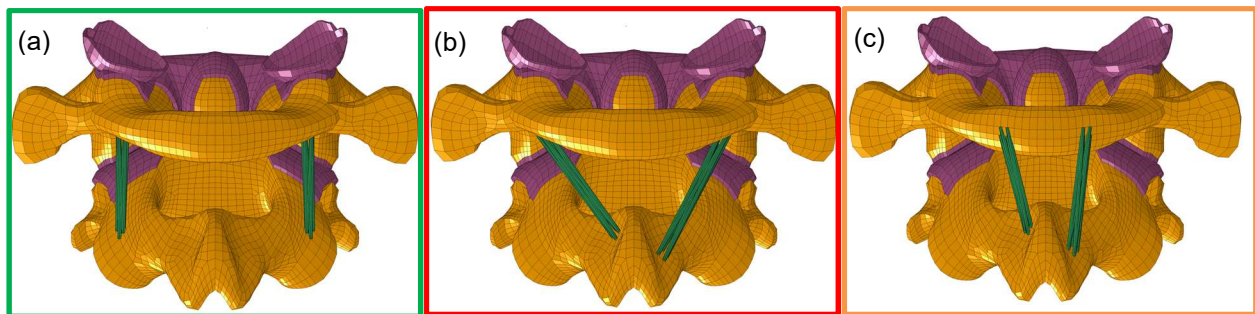
Figure 25: Simplified constructs for FE modeling: a) Harms, b) C1LM/C2TL and c) C1PA/C2TL
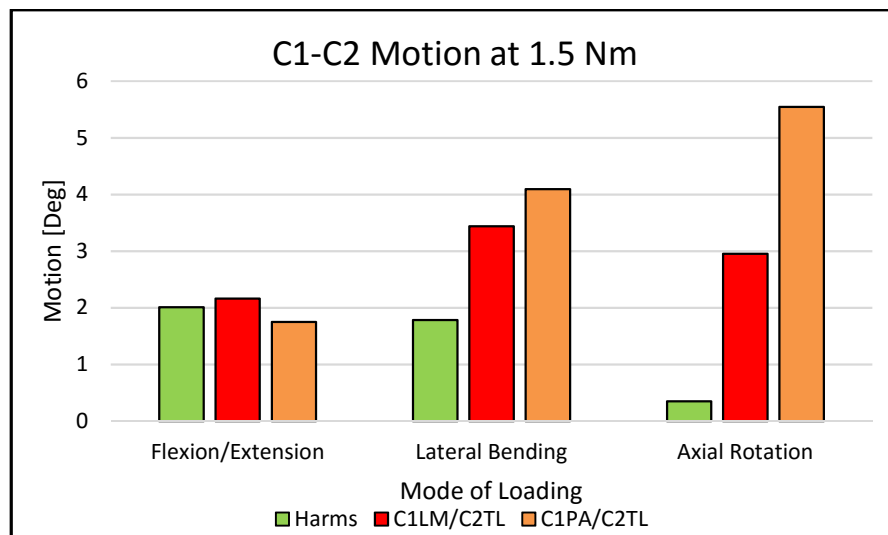
Figure 26: Construct stability predictions from FE model

In flexion/extension, the FE model predicted that all three constructs reduced motion to approximately 2º at 1.5 Nm. In lateral bending and axial rotation, the FE model predicted that the Harms construct was the most stable, followed by the C1LM/C2TL construct then the C1PA/C2TL construct. The difference between construct stability was most pronounced for the axial rotation case. These model predictions made sense since the lateral profiles of the C1LM/C2TL and C1PA/C2TL constructs were not as wide as the Harms procedure. This resulted in the C1LM/C2TL and C1PA/C2TL constructs having a smaller moment arm when resisting lateral bending and axial rotation and thus more motion was present in these constructs. While this might seem like an obvious result, the quantitative effect of this result would not have been easily calculated without the use of FE modeling. Furthermore, the model predictions for the C1LM/C2TL construct was consistent with experimental data which found that replacing the C2 pedicle screws of a Harms construct with C2 translaminar screws resulted in a construct that was significantly less stable in lateral bending and axial rotation[70].

Since the FE model predicted that the novel C1PA/C2TL construct was less stable than the Harms construct, it was decided to model a new construct configuration which consisted of connecting the posterior arch of C1 to the pedicle of C2 (C1PA/C2P). The same methodology was used to model this construct (Figure 27a) as the three previous constructs and construct stability was predicted by running the same boundary conditions as the ROM study (Figure 27b).
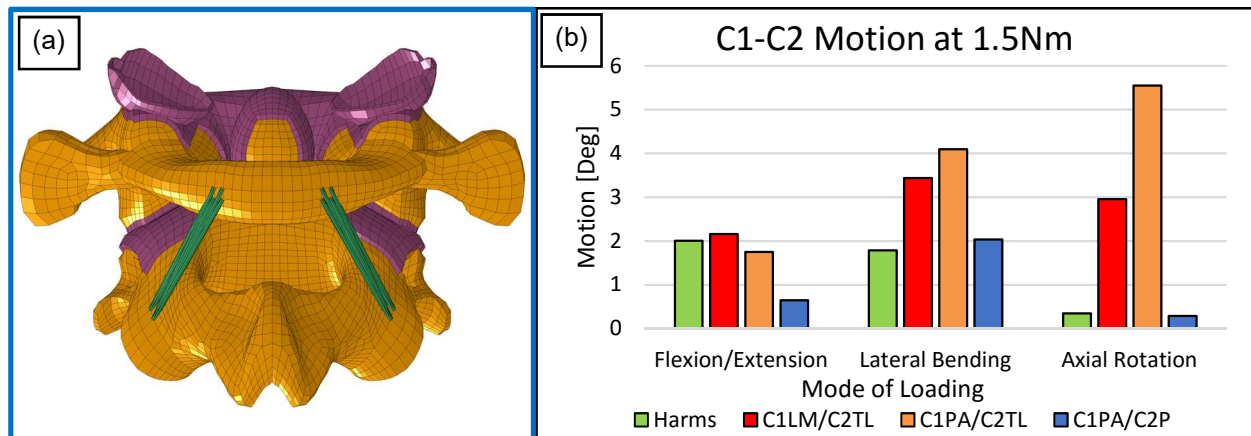
Figure 27: C1PA/C2P a) FE model and b) predicted construct stability

When the novel construct was revised to attach to the C2 pedicle rather than the C2 lamina, the stability was greatly improved in all types of motion. In fact, the FE model predicted

that this new construct configuration was more stable than the "gold standard" Harms procedure in flexion/extension. This was a logical finding since the C1PA/C2P construct has larger moment arms (than the Harms construct) to resist flexion/extension motion in the sagittal plane.

Despite stability concerns, the FE model with the C1PA/C2TL construct was the most clinically appealing for several reasons. The first reason was that the fixation locations were safer and out of the proximity of the C2 nerve root and the vertebral artery. The smaller lateral offset from the midline also allowed this hypothetical construct to have a smaller operating incision and thus be less invasive. A less invasive procedure was ideal because blood loss, operating time and recovery time would be reduced resulting in a larger patient population could be treated surgically. However, due to the narrower construct design, the FE model predicted that the C1PA/C2TL construct would be much less stable than the Harms construct under lateral bending and axial rotation loads. Although the C1PA/C2P construct would be more invasive than the C1PA/C2TL construct it would still be a much safer operating procedure because the C1 lateral mass is not used as a fixation location. Using the posterior arch of C1 as a fixation location instead of the C1 lateral mass eliminates both the need to sacrifice the C2 nerve root and the risk of injury the vertebral artery. Additionally, much less bleeding would be likely to occur when using the C1 posterior arch as a fixation point instead of the C1 lateral mass because the venous plexus around the vertebral artery would not be perturbed.

There were some limitations to the FE model due to the simplifications that were made when implementing the fusion constructs. Firstly, only the approximate fixation sites on the surface of the C1 and C2 vertebrae were connected using 2D beam elements. In reality, screws, clamps or plates would be used to secure the construct to the surface of the bone as well as the subsurface. Since the specific fixation components of the novel implants were not known at the time of modeling, implementing this level of fixation detail was not possible. As a result, the FE model could not be used to accurately predict the stresses that each construct would generate in the C1 and C2 vertebrae. This was not expected to be an issue because similar constructs with various fixation components had been used without traumatic failure of either the implant or bony anatomy. Also, since the fixation components of the constructs had not been modeled in detail, micro motion at the construct/bone interface could not be predicted. However, assuming no micro motion at the construct/bone interface has been common in FE modeling due to the complexity that would be required to implement and validate micro motion. Also, it was likely

that negligible amounts of micro motion would occur initially and perhaps this would remain the case until the fusion took hold. Thus, the FE model could be used as a design tool that provided a plausible prediction of the stability of each hypothetical construct relative to the Harms procedure.

3.2.1 Predicted Loading of Implant Constructs

As mentioned above, due to the simplifications that were used for construct modeling, predictions of the stresses in the bony anatomy could not yield realistic results. However, calculating loading of the beam elements yielded meaningful predictions about the loading that would be present in the rods of each hypothetical construct. These loads were helpful in the detailed design phase (presented subsequently in Chapter 4) to ensure that the implant design was strong enough to withstand the loads predicted by the FE model. The loads present in each hypothetical construct were calculated by first plotting the axial force in each lateral frame structure of 16 beam elements over the entire length of the simulation (Figure 28). It was found that each frame structure had beam elements that were under tension as well as elements that were under compression. This suggested that the 3.5 mm rods (that these beam element frame structures were intended to represent) would not only have to resist axial forces, but also bending moments.

To calculate the component forces in each lateral frame structure, the axial force in each beam element was summed at the time step when the boundary moment was equal to 1.5 Nm (shown by t^* on Figure 28).
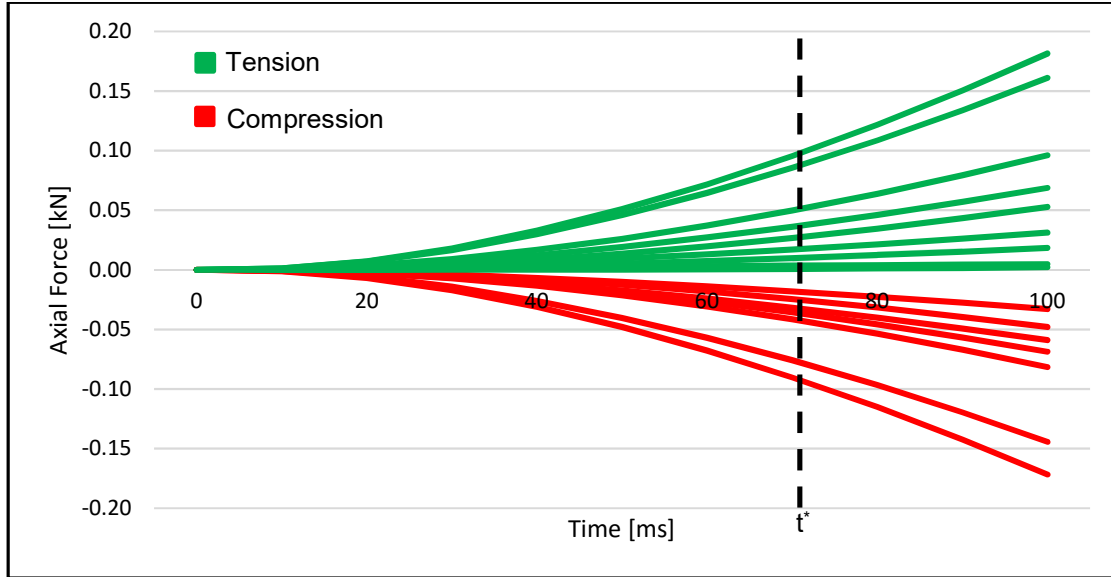
Figure 28: Axial forces predicted in C1PA/C2P construct frame by FE model in axial rotation at a applied load of 1.5 Nm (forces shown for the beam elements of one lateral rod only)

Calculating the component moments in each frame structure was not as trivial as calculating the forces and consisted of the following high level procedure (MATLAB code that showed a detailed example for right rod of Harms construct in axial rotation was described in Appendix A1). The calculation procedure was developed by the present author using vector mechanics and elementary statics. The first step was to select a point to calculate the moments about. This point was selected to be the centers of the shell elements (point O) that were used as the C2 fixation locations of each lateral frame member (Figure 29). The next step was to calculate the coordinates of O with respect to the coordinate system of the FE model. This was done by obtaining the coordinates of points n_{1-4} at time t^*, the nodal coordinates were then used to create diagonal vectors between n_1 and n_3 $(\overrightarrow{V_1})$ as well as n_2 and n_4 $(\overrightarrow{V_2})$. A series of cross product and dot product calculations were then performed to determine the coordinates of the point on $\overrightarrow{V_1}$ that had the shortest perpendicular distance to $\overrightarrow{V_2}$, these coordinates were used to define the point O.
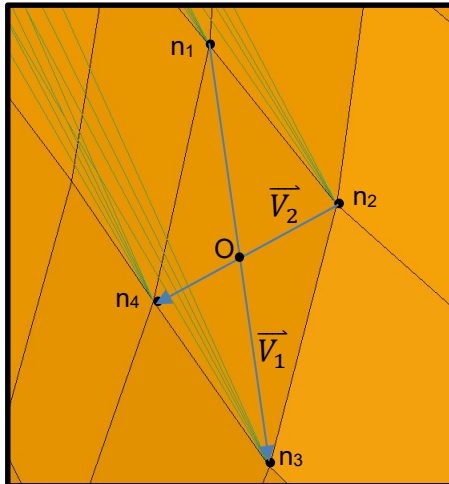
Figure 29: Center point O on shell element created from four nodes that represent the posterior-right C2 fixation location of the C1PA/C2P construct.

The next step was to calculate the magnitude and direction of the resultant force at each node at t* (each node had 4 forces corresponding to 4 beam elements). This was done by calculating the unit vector of each beam element and then multiplying the axial force in each beam element by this unit vector. The forces acting on each node were then summed resulting in four forces acting at each lateral C2 fixation location. After the magnitude and direction of these forces were known, the moments that these forces generated about point O were calculated using cross products. The moments were then summed about each axis and presented as M_x, M_y and M_z. These moments along with the component forces (F_x, F_y and F_z) under each mode of loading were used to predict the loads that were present in the left and right rod of each hypothetical construct (Figure 30 & Table 9).

43
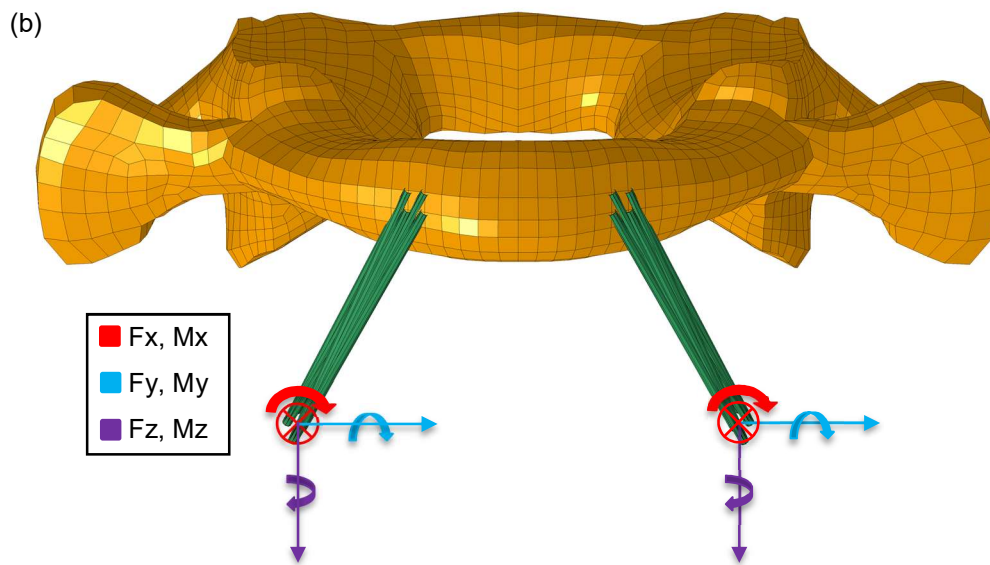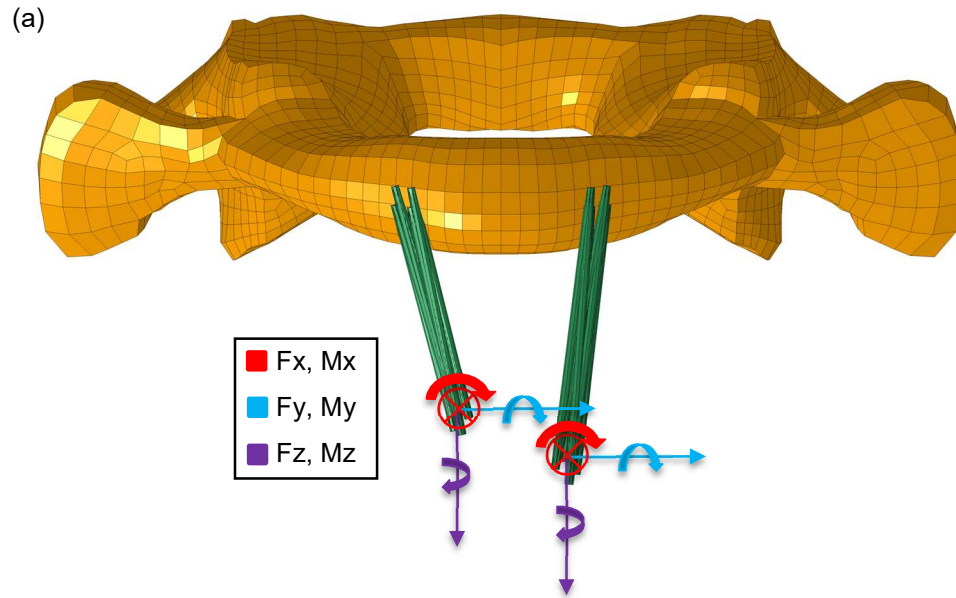
Figure 30: Illustration of component moments and forces for a) C1PA/C2TL construct and b) C1PA/C2P construct

Table 9: Summary of forces and moments predicted by FE model in all motion types for a) C1PA/C2TL construct and b) C1PA/C2P construct

(a) C1PA/C2TL	Extension		Flexion		Right Lateral Bending		Right Axial Rotation	
	Left rod	Right rod	Left rod	Right rod	Left rod	Right rod	Left rod	Right rod
F_x [N]	-15.0	1.3	4.6	-1.4	13.5	-6.0	10.0	15.1
F_y [N]	39.1	-7.0	11.4	-7.0	25.2	-2.0	35.7	16.2
F_z [N]	79.3	-87.0	35.0	19.0	118.1	-91.2	93.8	-33.8
M_x [Nm]	0.0	0.0	0.0	0.0	-0.2	-0.1	-0.2	0.0
M_y [Nm]	-0.3	-0.1	0.0	0.0	-0.1	0.1	-0.4	-0.2
M_z [Nm]	0.0	0.0	0.0	0.0	-0.1	0.1	-0.2	-0.2

(b) C1PA/C2P	Extension		Flexion		Right Lateral Bending		Right Axial Rotation	
	Left rod	Right rod	Left rod	Right rod	Left rod	Right rod	Left rod	Right rod
F_x [N]	11.7	12.9	9.6	9.6	27.0	26.9	-2.7	3.9
F_y [N]	-0.1	2.9	-4.0	4.6	-15.0	-21.5	3.2	3.6
F_z [N]	18.4	20.9	33.6	32.3	78.5	-55.8	0.6	-1.3
M_x [Nm]	-0.3	0.3	0.2	-0.2	-0.1	-0.1	0.0	0.0
M_y [Nm]	-0.4	-0.4	0.3	0.3	0.0	-0.1	0.0	0.0
M_z [Nm]	-0.1	0.1	0.0	0.0	-0.1	-0.1	0.0	0.0

The FE model predicted that the C1PA/C2TL construct would have to withstand higher loads than the C1PA/C2P construct. This was expected to be the case in lateral bending and axial rotation because the C1PA/C2TL construct was not as wide as the C1PA/C2P construct and therefore the forces in the frame structures had to be larger to resist the applied boundary moment. Additionally, loads in the C1PA/C2TL construct were also greater in extension. This was due to the non-symmetrical fixation on C2 that was intended to represent the insertion points of C2 translaminar screws. This non-symmetrical setup caused the right frame structure to be under compression and the left frame structure to be under tension. This uneven loading created torques that the construct had to resist in addition to that resulting from the applied boundary motion.

Overall, the forces and moments predicted by the FE model seemed very plausible. Using the FE model to approximate the loads in the rods of each hypothetical construct was very useful because it made strength analysis of critical construct components possible (presented subsequently in Chapter 4). Without these predictions, strength analysis would have been

difficult because the magnitude of the loads would have been unknown without performing tedious calculations for several input motion cases.

4.0   Design of a Fusion Device for the Posterior Arch of C1

In terms of construct stability, the FE model showed that using the C1 posterior arch as a fixation location was a feasible alternative to the C1 lateral mass. Two hypothetical constructs were proposed that utilized the C1 posterior arch. The C1PA/C2TL construct was intended to represent the case of a novel C1 implant and C2 translaminar screws connected by 3.5mm titanium rods. The C1PA/C2P construct was intended to represent the case of a novel C1 implant and C2 pedicle screws connected by 3.5mm titanium rods.

Both constructs greatly reduced motion compared to the UCS with a type II odontoid fracture. FE modeling predicted that the C1PA/C2P construct could achieve a level of stability that was equivalent to the Harms construct whereas the C1PA/C2TL, although less stable, might still be adequate for achieving fusion and was much less invasive. Thus, the next step was to design the C1 portion of the implant which could be used in conjunction with C2 translaminar screws or C2 pedicle screws.

4.1 Design Motivation

In addition to the encouraging results from the FE model, the decision to design an implant for the C1 posterior arch was made for several clinical reasons. Firstly, the C1 posterior arch presented a much safer alternative to the C1 lateral mass because there would be no risk of injuring the vertebral artery and no need to sacrifice the C2 nerve root in order to achieve optimal screw trajectory. The dissection required to expose the C1 posterior arch would also be less than the amount of dissection required to expose the C1 lateral mass. This would result in a less invasive procedure with a smaller incision, less blood loss and reduced operating time. Additionally, designing an implant for the C1 posterior arch that could be used with existing C2 instrumentation would give surgeons the flexibility to tailor the construct based on the needs of each individual patient. The C2PA/C2P construct could be used in cases where stability was considered to be the primary objective and the C2PA/C2TL construct could be used in cases where reducing the invasiveness of the surgery was considered to be the primary objective. Such judgements would be made by the surgeon and refined by their clinical experience with both

versions of the construct. Finally, utilizing the C1 posterior arch allows for the surgical technique to remain a posterior approach.

While a novel implant could perhaps have been designed for the anterior C1-C2 anatomy, it would have required designing novel instrumentation for C1 and C2. An anterior approach would also result in a much more invasive surgery with an increased chance of post-operative pneumonia, an unnecessary risk for the geriatric patient population.

As discussed in the literature review, C1-C2 fusion constructs that incorporate the C1 posterior arch already existed and pre-dated the use of C1 lateral mass screws. However, these existing constructs presented an additional risk to injuring the spinal cord because they required sublaminar passage either to place wires (Gallie technique[10]) or hooks (Halifax clamp[40]). Furthermore, these constructs promoted fusion by tying C1 and C2 together and did not achieve independent fixation on both C1 and C2. This resulted in poor construct stability and lower fusion rates[39,41]. For these reasons, the novel posterior arch implant presented in the present thesis was designed to achieve independent fixation on C1 and then achieved C1-C2 stability by the use of titanium rods connected to the fixation methods used in C2. Additionally, sublaminar passage was avoided which would reduce the risk of injury to the spinal cord.

4.2 Design Criteria and Design Constraints

To both guide and explain the design and development of alternative implant designs, sets of design constraints and design criteria had to be developed. In the context of the present thesis, design constraints were defined as bounds that all alternative designs must satisfy completely. In some cases, it was easy to demonstrate that a design constraint had been met completely but in other cases it depended on the judgement of the designer but this judgement could often be confirmed by prototype testing. The purpose of having constraints was to limit the design options by eliminating features that were likely to be counterproductive for an optimal final design and ensuring that only essential features remained. The selection of what would be counterproductive and what would be essential could be imposed by performance requirements of the final design and/or be imposed by the designer depending on their judgement.

Design criteria were defined as desirable design features that should be optimized by an alternative design. Design criteria provided a means to evaluate alternative designs which had to satisfy, or seem to satisfy, the design constraints to be considered. Design criteria allowed the selection of an optimal design from the feasible alternative designs for further design

47

development. However, compromises often had to be made between competing criteria to achieve the overall optimal design. The extent to which design criteria were satisfied depended initially on the judgement of the designer with perhaps a few supporting theoretical calculations. Eventually, more extensive theoretical calculations and prototype testing improved upon this judgement during the design development stage. Considerable designer judgement was also involved in deciding the relative importance of the various criteria in their contribution to the optimal design. In summary, design constraints defined the design space and design criteria were used to optimize the design within that space.

Additionally, the number of design criteria should be limited to the main ones because minor ones could often be addressed by iterative refinement in the design development stage. When too many design criteria were proposed, the designer tended to lose sight of the core design priorities and become bogged down with satisfying minute design features with the overall result of a suboptimal, non-innovative design.

Design was not considered to be an objective process, unless unlimited time and resources were available, and so design depended very much on subjective judgements of the designer.

4.2.1 Constraints

For the hypothetical C1 posterior arch implant the following design constraints were identified.

1. Material Selection
   - All materials used in alternative designs had to have a record of performance in spinal constructs that precluded any adverse tissue reaction to the bulk material
   - Essentially for screws, plates and rods this included implant grades of stainless steel, cobalt chromium alloy, pure titanium, titanium alloy and PEEK (polyether-etherkeytone)

2. Strength
   - Alternative designs could not fail under the physiological loads that were present in the upper cervical spine

- This essentially meant that rod diameters, screw sizes, screw attachments and plates would be of the size and general configuration that have been used in spinal constructs without overt early fracture

3. Fixation width

- Any portion of an alternative design that fixated to the superior side of C1 had to have a lateral profile of less than 10 mm from the midline in order to reduce the risk of injury to the vertebral artery

4. Transverse profile

- No portion of the implant profile (in the transverse plane) could protrude into the spinal canal in order to reduce the risk of spinal cord injury

5. Fixation location and integration

- Alternative designs only utilized the posterior portion of C1 as a fixation location so that the surgery remained to be a posterior approach and must integrate with existing C2 fixation options that include pedicle and translaminar screws

4.2.2 Criteria

For the hypothetical C1 posterior arch implant the design criteria listed below were identified. Each design criterion was given a score out of 10 that assessed how well it seemed to address the criterion. Also, each criterion was assigned a single weighting factor as a decimal fraction which represented its relative importance compared with the other criteria. The weighting factors of the criteria had to sum to the number one. The criterion scores were multiplied by their weighting factor and then all these values were summed to give an overall score (out of 10) for each alternative design. The highest overall score indicated the estimated optimal design. Furthermore, the overall scores were also used to assess (and explain the rationale for) different design revisions in the design development stage.

1. C1-C2 stability (Weight factor = 0.40)
    - Designs were intended to maximize construct strength and stability under physiological loads in order to minimize joint motion at C1-C2 and immediately stabilize the segment with the intent of achieving long term fusion
    - This criterion included minimizing micro motion at all locking mechanisms of the construct as well as well as minimizing micro motion at the implant/bone fixation interfaces (where micro motion could be caused by bone fracture due to high stresses)
    - Addressing this criterion was considered essential for the likelihood of successful C1-C2 fusion

2. Surgical Risk (Weight factor = 0.35)
    - Construct configurations should avoid areas where significant nerve or blood vessel damage was possible
    - Construct configurations should allow surgery to be as minimally invasive as possible (with as small a lateral dissection as possible) to reduce the time required for the surgery
    - Also, the implants involved should be simple and easy to install and adjust/tighten in situ to reduce the time required for the surgery

3. Spatial harmony (Weight factor = 0.20)
    - Adjustable to accommodate varying patient anatomy
    - Attach easily to the existing C2 fixation options
    - Minimal posterior length to avoid protruding bump at the skin surface
    - Design features in the construct to allow placement of bony fragments and/or bone matrix material to facilitate the fusion process

4. Manufacturing cost (Weight factor = 0.05)
    - Manufacturing process should be simple and inexpensive
    - Less important criterion because more complex and expensive manufacturing processes could be offset by the high profit margins

4.3 Alternative Designs

Two alternative designs were proposed for the treatment of AAI. The first alternative was an existing design that used C1 lateral mass screws, which was the C1 fixation used in the Harms procedure (Figure 31).
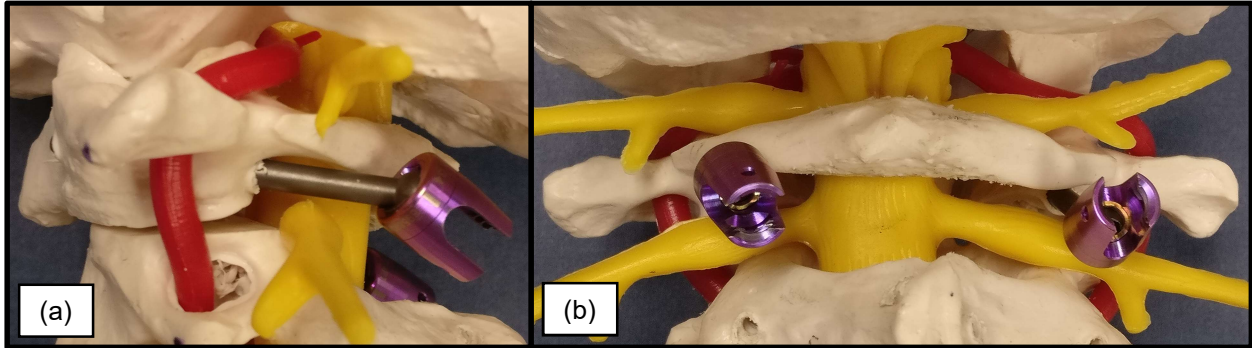
Figure 31: C1 lateral mass screws used in the Harms construct: a) lateral and b) posterior view

When C1 lateral mass screws were judged on the criteria developed for a C1 fixation device in the previous section, the screws achieved a score of 6.5 out of 10 (Table 10). The design scored high on the C1-C2 stability criterion because of the designs strong locking mechanisms, good stability and fixation, as well as the high probability of long term fusion. This high score was largely offset by low a score for the surgical risk criterion due to the large lateral construct width (which increased the invasiveness of the surgery) and poor safety consideration because of the location of the C1 lateral mass screws in relation to the vertebral artery and C2 nerve root. The spatial harmony criterion scored well because the posterior profile of C1 lateral mass screws did not largely extend beyond the posterior arch of C1 and polyaxial screws were highly adjustable, available in a variety of different sizes to address variations in anatomy and easily integrated with several C2 fixation options. Finally, the manufacturing score was good but slightly reduced due to the multiple moving components, exotic shapes and tight tolerances that must be achieved by the manufacturing process to ensure implant performance.

Table 10: C1 lateral mass screws scored against criteria

Design Criterion	Score /10	Weight Factor	Weighted Score
C1-C2 Stability	9.0	0.40	3.6
Surgical Risk	3.0	0.35	1.1
Spatial Harmony	7.5	0.20	1.5
Manufacturing	6.0	0.05	0.3
		Total	**6.5**

A clamp device for the posterior arch of C1 was envisioned as the second alternative design (Figure 32). It was decided to go with a clamping fixation mechanism over a screw/plate mechanism to avoid the technical demand required to safely place screws in the posterior arch of C1 and result in a good surgical risk score. Additionally, it was believed that the adjustability of a clamping device would better adapt to the varying size and shape of the posterior arch from patient to patient yielding a better spatial harmony score than a screw/plate mechanism. A stainless steel implant construction was envisioned for easier machining (compared with titanium alloy) of the complex geometry while still adhering to the material selection constraint.
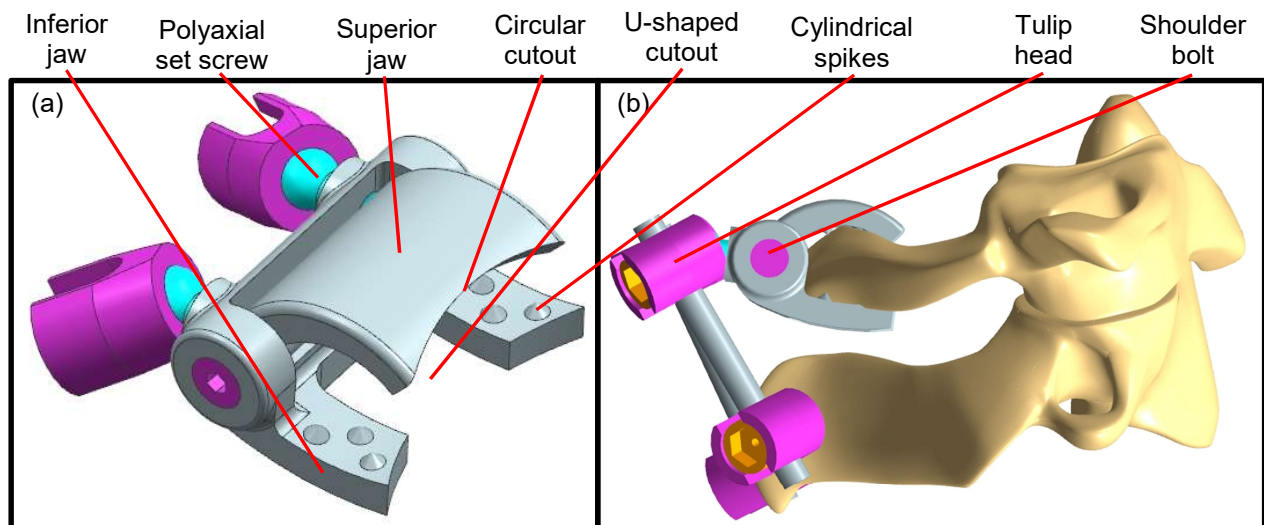
Figure 32: Alternative design showing the a) C1 posterior arch clamp and b) C1 posterior arch clamp used in conjunction with C2 translaminar screws to create a C1-C2 fusion construct

Key elements of the design included a superior and inferior jaw that were connected by two shoulder bolts that also acted as the clamp hinge. Cylindrical spikes were present on both the posterior jaw and superior jaw in order to improve fixation with the C1 posterior arch and

increase the C1-C2 stability score. A U-shaped cutout was present in the inferior jaw to allow a window for bone graft to be placed for the purpose of promoting long term fusion between the C1 posterior arch and the C2 lamina. Based on the recommendation from Stauffer et al[71], the lateral width of the superior jaw was specifically designed to be 20mm in order to prevent injury to the portion of the vertebral artery that sits atop the vertebral groove of C1. Since the vertebral artery does not contact the inferior portion of the posterior arch, the inferior jaw of the implant was designed to have a wider lateral width of 25mm to provide additional stability. The anterior profile of both the superior and inferior jaws were designed to have a circular cutout so that the jaws did not void the constraint of protruding past the posterior arch of C1 and into the spinal canal. The jaws were locked in place by polyaxial set screws which were threaded though the inferior jaw and tightened against the superior jaw. The polyaxial set screws were designed to have tulip heads so that the implant could easily integrate with existing spinal implants. More specifically, 3.5mm rods would be places into these tulip heads and the tulip heads of the screws used in C2, cap screws would then tighten the rods into place and lock the position of the construct.

The surgical procedure for implanting this construct was as follows:

1. Create a posterior midline incision and perform sufficient dissection to expose the posterior arch of C1 and fixation location of C2 (C2 lamina or C2 pedicle).
2. Place the C1 clamp on the posterior arch of C1 and obtain desired alignment.
3. Use pliers to apply pressure on the superior and inferior jaws in order to achieve the desired level of fixation strength between the clamp and the posterior arch.
4. While maintaining pressure with the pliers, thread the polyaxial set screws into the inferior jaw and tighten (at this point independent fixation between the clamp and posterior arch has been achieved).
5. Place two polyaxial screws into the desired anatomy of C2.
6. Place two 3.5mm rods in the tulips of the polyaxial set screws and the tulips of the C2 polyaxial screws.
7. Lock construct in place by tightening cap screws onto tulip heads.
8. Proceed with standard procedure to close up the surgical site and complete the operation.

When the first implant design was judged on the criteria, a total score of 6.6 out of 10 was achieved (Table 11).

Table 11: Alternative clamp design scored against criteria

Design Criterion	Score /10	Weight Factor	Weighted Score
C1-C2 Stability	6.5	0.40	2.6
Surgical Risk	7.5	0.35	2.6
Spatial Harmony	5.5	0.20	1.1
Manufacturing	5.0	0.05	0.3
		Total	**6.6**

When the scores of each alternative design were compared, it was found that the clamp implant scored slightly better than the C1 lateral mass screws. Specifically, the clamp implant scored much higher in the important criterion of surgical risk while still maintaining a good score for the C1-C2 stability criterion which were expected to be the best two criteria for predicting the implants ability to treat a larger patient population. It was also believed that the spatial design could be improved with further design revisions in the design development stage. For these reasons, it was decided that the clamp implant was a superior alternative design and it was the design that was selected for further development.

4.4 Design Development

After performing a critical review on the first generation design of the clamp implant, a major flaw was identified to be that profile of the construct extended too far posteriorly due to the placement of the polyaxial set screws. It was suggested by the team surgeon (co-supervisor Dr. Parham Rasoulinejad) that the posterior profile would probably cause interference issues with the base of C0 during extension so it was decided to orient the tulips laterally in the second generation of the design in order to improve the spatial harmony score (Figure 33).
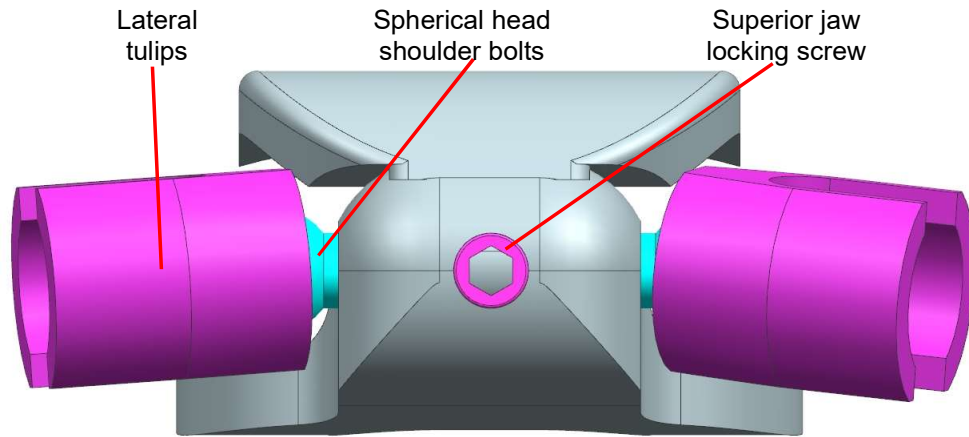
Figure 33: Posterior view of second generation clamp implant designed to have polyaxial tulip heads extend laterally

In order to achieve this design, the shoulder bolts from the first design had to be modified to have spherical heads so that the polyaxial tulips could attach to them. Additionally, to keep the lateral profile of the implant to a minimum, the width of the inferior jaw's rear body was reduced. As a consequence of this, only one set screw could be used to lock the jaws in place and maintain fixation with the C1 posterior arch which reduced the C1-C2 stability score. Also, this design became a compromise between reducing the length of the posterior profile and increasing the length of the lateral profile. Compared with the first design, the length by which the implant extended posteriorly beyond the C1 posterior arch was able to be reduced from 24 mm to 8 mm. However, as a tradeoff, the lateral profile of the implant was increased from 28 mm to 37 mm which increased the invasiveness of the surgical procedure required for this implant and therefore decreased the surgical risk score. Apart from these changes the implant remained the same as the first design and the high level surgical procedure remained unchanged.

This second generation construct was judged according to the criteria (Table 12) and achieved a scored a 6.7 out of 10 compared to the first design score of 6.6. While still an improvement, the benefit of improving the spatial harmony score was almost completely offset by the decrease in both the surgical risk and C1-C2 stability scores.

Table 12: Second generation implant scored against criteria

Design Criterion	Score /10	Weight Factor	Weighted Score
Surgical Risk	**6.0** *(↓0.5)*	0.35	**2.1**
C1-C2 Stability	**7.0** *(↓0.5)*	0.40	**2.8**
Spatial Harmony	**7.5** *(↑2.0)*	0.20	**1.5**
Manufacturing	5.0	0.05	0.3
		Total	**6.7**

4.4.1 Third Generation Design

When the second generation design was reviewed by a spinal orthopaedic surgeon (co-supervisor Dr. Rasoulinejad), a flaw was spotted with the placement of the polyaxial tulips. The issue was that lateral orientation of the tulips would make it very difficult to get tooling in place to tighten down the rod cap screws and lock the construct without making the surgery significantly more invasive than initially thought, thus reducing the surgical risk score. For this reason, the tulip head design was replaced with two lateral sockets integrated into the posterior body of the inferior jaw (Figure 34a) designed to each house a polyaxial rod (Figure 34b). The polyaxial rod consisted of a 3.5 mm shaft with an oversized spherical end designed to sit in a socket of the inferior jaw and allow ±30º of rotation in both the medial-lateral and anterior-posterior planes. The sockets were designed to have inferior openings to allow for easy posterior installation of the polyaxial rods. Unfortunately, this design change lowered the spatial harmony score by reducing the ability of the clamp implant to integrate with other surgical instrumentation because now custom polyaxial rods were required instead of conventional cervical rods. However, this was deemed to be acceptable since the new rods reduced the complexity of the implant design and the surgical procedure. Another major design change was also made to the locking mechanism of the jaws which consisted of changing the set screw to a cam and follower type mechanism (Figure 34c). The locking screw was moved above the center of rotation of the superior jaw and this allowed the screw to use the superior jaw surface as a cam. The tip of the screw was also rounded to allow for smoother motion as it was tightened against the superior jaw surface. This design change eliminated the need to use pliers to apply pressure and hold the clamp in place while locking the jaws into position, significantly simplifying the surgical procedure. The design now allowed the locking device to provide a progressive increase in

clamping force without the use of additional, cumbersome tooling. Slippage of the jaw locking mechanism has also been virtually eliminated due to the interference that was introduced with the cam/follower design. The cylindrical spikes used to improve fixation were also changed to square based pyramid spikes. This was done to reduce the manufacturing complexity and was not expected to have any adverse effects.

Once the clamp was securely in place on the C1 posterior arch, the rest of the construct could be installed (Figure 34d). This consisted of placing the desired C2 screws, placing the polyaxial rods in place and then locking the construct in place by tightening the rod cap screws. In the case of locking the spherical end of the polyaxial rod, an M8 cap screw was chosen to thread into the socket housing and tighten directly against the rod.
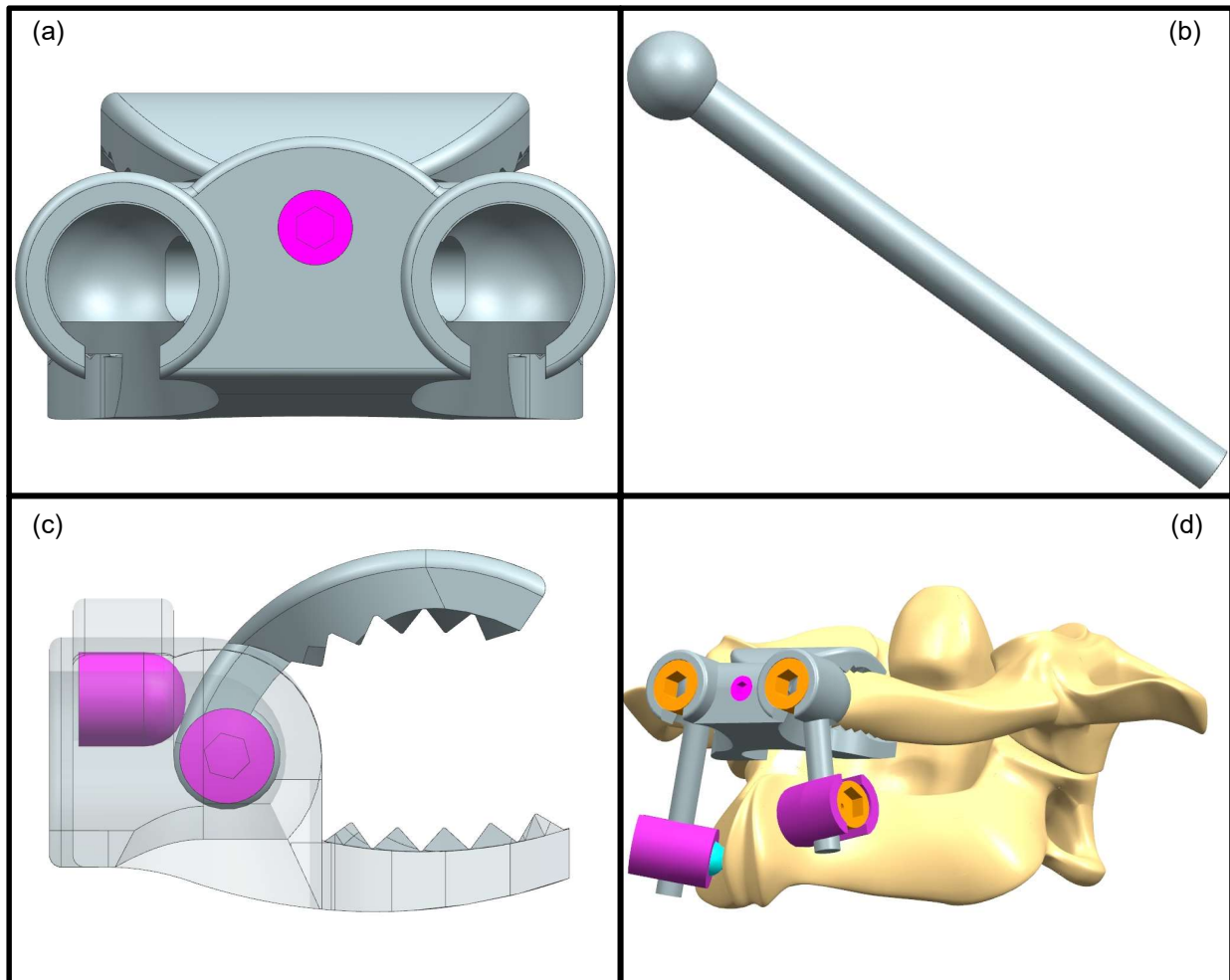
Figure 34: a) Posterior view of C1 clamp showing new socket design, b) 3.5mm polyaxial rod, c) detail to illustrate new cam locking mechanism and d) full construct utilizing C2 translaminar screws

57

At this point in the design development, it was decided to proceed with the first round of prototypes manufactured by 3D printing (selective laser melting) of stainless steel (Figure 35a). After the inferior and superior jaws were printed, three post processing steps were required. The first step was to tap an M2 thread all the way through the center of rotation of the superior jaw so that the shoulder bolts could be secured, in turn securing the superior jaw to the inferior jaw. The next step was to tap the M4 hole for the screw used to lock the superior jaw into place. Lastly, the M8 cap screws had to be threaded into the sockets for the polyaxial rods. However, while tapping the threads in the sockets, significant splaying of the sockets occurred due to the forces that were generated (Figure 35b). This caused the threading to be uneven and as a result the M8 cap screws could not be tightened with enough torque to lock the polyaxial rods before the threads stripped, thus voiding the strength constraint and requiring another round of design revisions.
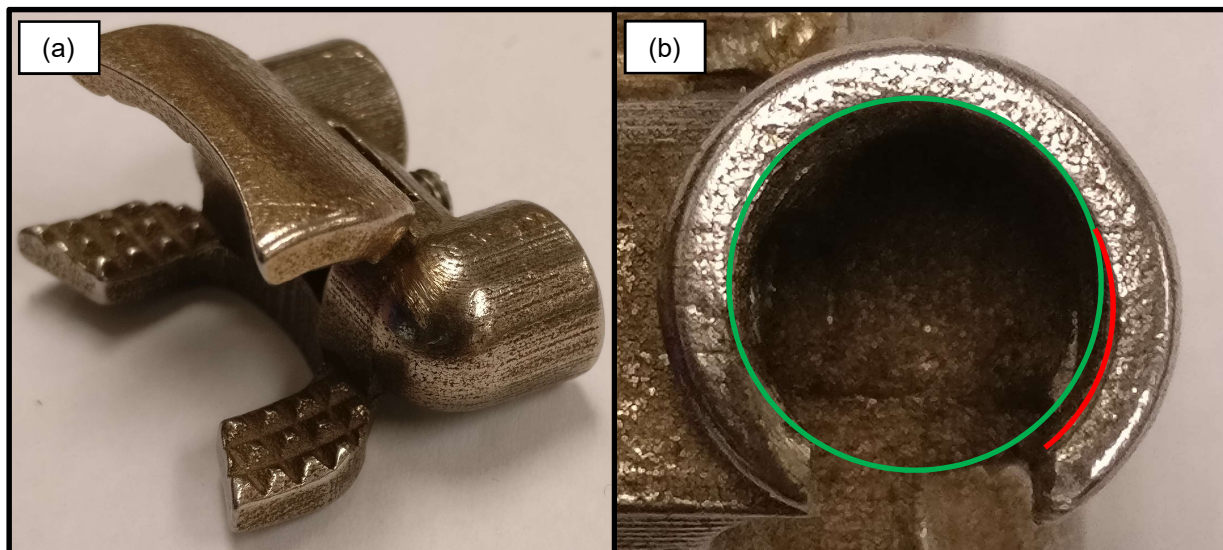
Figure 35: a) Stainless steel prototype manufactured by 3D printing and b) detail showing splaying that occurred during the thread tapping process

Anatomical models (Sawbones, Vashon Island, WA) of the upper cervical spine were also used to assess the form and function of the prototypes. During this assessment, it was noticed that the C1 posterior arch of the anatomical model was not symmetrical about the midline (Figure 36a). Specifically, from a posterior view, the height of the left side of the posterior arch (h_1) was smaller than the height of the right side of the posterior arch (h_2). After reviewing this finding with an orthopaedic surgeon (co-supervisor Dr. Rasoulinejad), it was

confirmed that this asymmetry was often observed in clinical practice and can vary significantly from patient to patient. Unfortunately, this asymmetry negatively affected the fit of the clamp implant and resulted in the superior jaw not achieving any fixation on the left side of the posterior arch (Figure 36b).
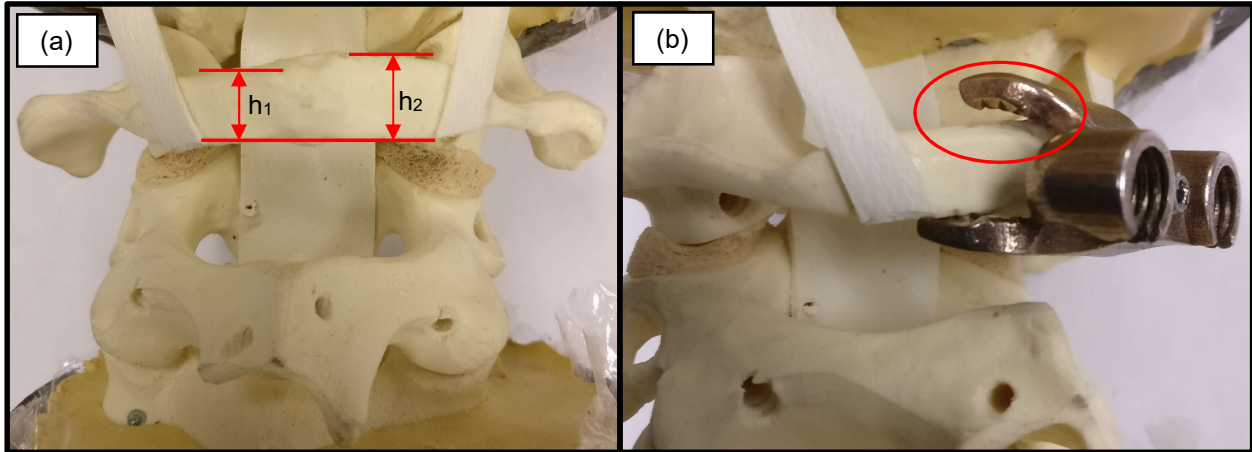
Figure 36: Anatomical model of upper cervical spine showing a) difference in posterior arch height and b) lack of fixation between clamp and posterior arch due to arch height asymmetry

This third generation implant was judged according to the criteria (Table 13) and achieved a score of 7.5 out of 10 compared to the second generation score of 6.7. The improved surgical risk score was a result of the increased simplicity and reduced invasiveness. The lower spatial harmony score was a result of the reduced integration with existing cervical rods and the increased manufacturing score was a result of improved machinability. However, it was the failure to meet the strength constraint that ultimately voided this design and required another round of revisions.

Table 13: Third generation implant scored against criteria

Design Criterion	Score /10	Weight Factor	Weighted Score
C1-C2 Stability	7.0	0.40	2.8
Surgical Risk	8.5 (↑2.0)	0.35	3.0
Spatial Harmony	7.0 (↓0.5)	0.20	1.4
Manufacturing	5.5 (↑0.5)	0.05	0.3
		Total	7.5

4.4.2 Fourth Generation Implant

After the first set of prototypes were produced, design concerns related to strength and fit were identified. To address the concern of clamp fit, the superior jaw was redesigned to have two separate jaws that articulate independently (Figure 37a). In order to accommodate these two jaws, the M2 shoulder bolts had to be replaced with a 2 mm diameter through axle to allow the jaws to articulate independently of each other. The mechanism to provide clamping pressure and lock the jaws in place remained the same as the previous iteration but now two M4 locking screws were required so that each jaw could be tightened and locked independently (Figure 37b). Additionally, the presence of two locking screws increased the overall strength of the clamp. Splaying of the M8 threads was addressed by removing the posterior slot for the 3.5mm polyaxial rods. This design changed the installation procedure for the polyaxial rods which now had to be inserted through the bottom of the inferior jaw (Figure 37c) and then slid forward into the socket when the M8 cap screw was tightened into place (Figure 37d).
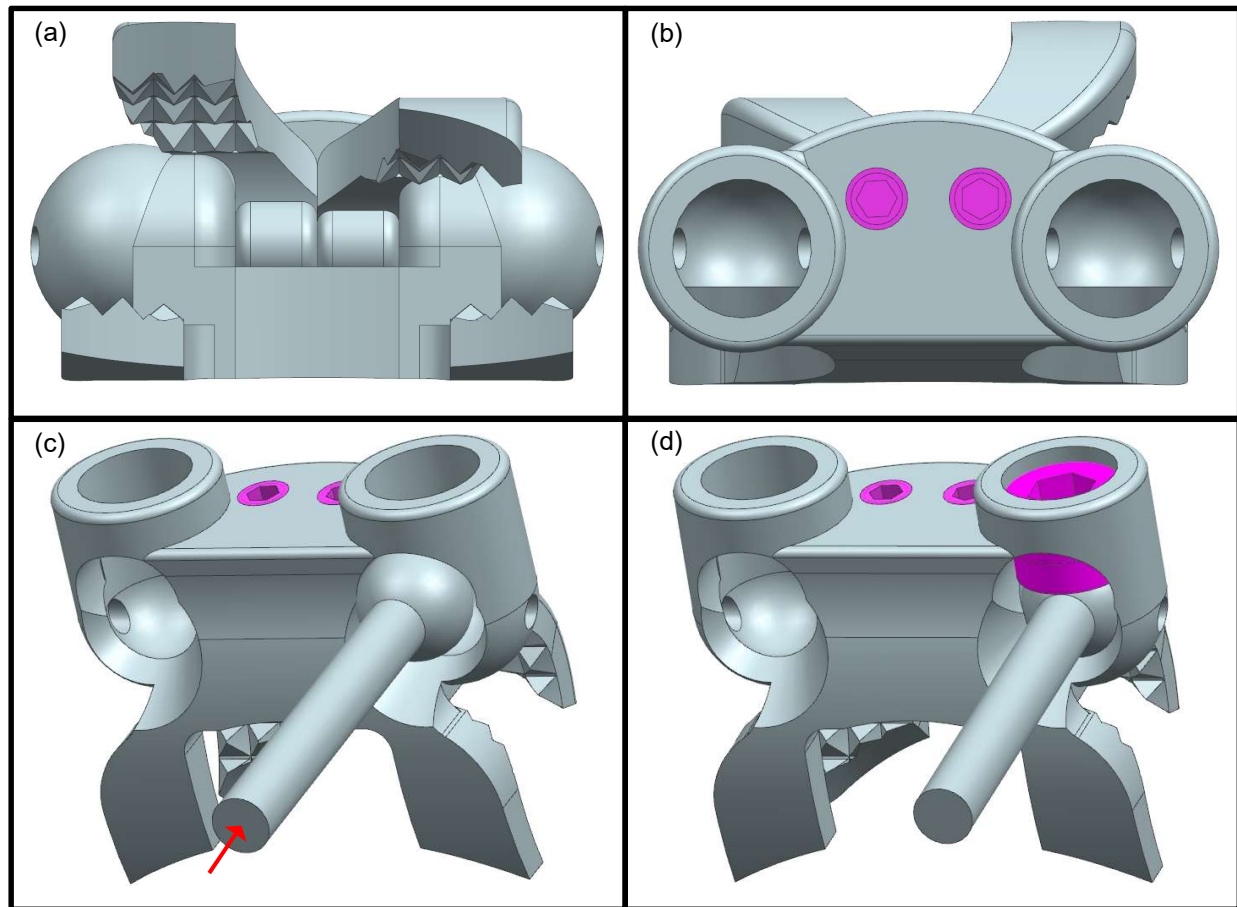
Figure 37: a) Front view of clamp implant showing independent superior jaws, b) rear view of clamp implant showing the addition of a second locking screw, c) bottom view showing insertion of polyaxial rod and d) bottom view showing final position of polyaxial rod locked in place by M8 cap screw

Once again, 3D printing was used to create prototypes. However, for this round of prototyping the material was changed from stainless steel to titanium alloy (Ti6Al4V) because this material was believed to be more osteoconductive (CES Edupack 2016, Granta Designs Limited, Cambridge, UK) and thus would hasten the fusion process. However, the during post processing, it was found that the titanium alloy was very brittle and two separate fractures occurred. The first fracture was formed during tapping because the 3D printed titanium alloy was not ductile enough to keep the cutting forces below the fracture limit of the material (Figure 38a). The second fracture occurred while testing the locking mechanism of the polyaxial rods (Figure 38b).
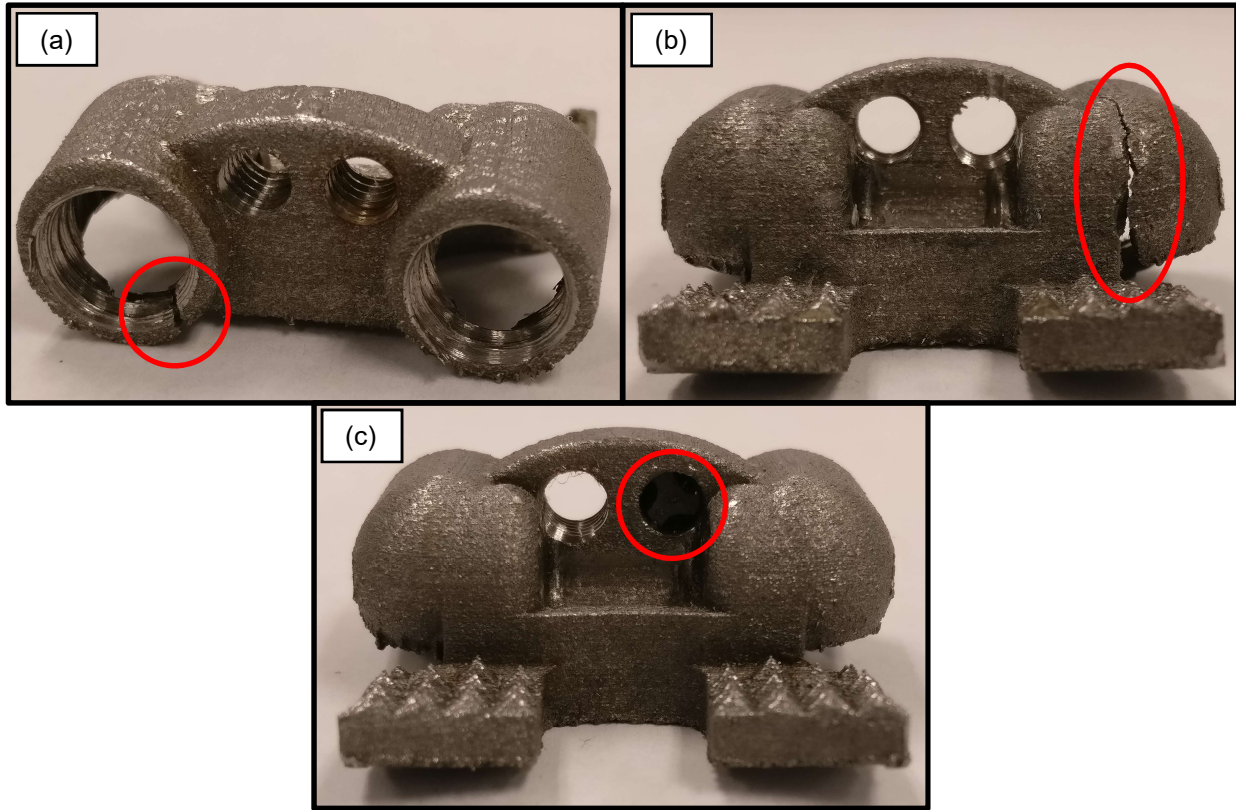
Figure 38: Examples of 3D printed titanium alloy prototypes that failed during post-processing: a) crack through wall during M8 thread tapping, b) crack in socket while locking polyaxial rod and c) M4 tap broken while tapping thread for jaw locking screw

After reviewing these failures with the manufacturer of the 3D printed parts (Renishaw Canada, Kitchener, ON), it was suggested that they occurred because the parts were not heat treated after the 3D printing process. The parts were created using a selective laser melting (SLM) 3D printer which rapidly melts and solidifies metal powder layer by layer until the desired 3D part was constructed by a series of thin slices. During the rapid cooling of the melt pool, a martensitic phase transformation occurred in the titanium alloy which introduced a complex grain structure with significantly altered mechanical properties compared with the medical grade of this titanium alloy[72]. This martensitic phase was responsible for making the parts very hard causing high cutting forces and very brittle thus encouraging fractures during the post-processing. These implant failures voided the strength constraint and another design iteration was necessary.

Aside from these implant failures, there was another design feature was identified for further optimization related to stresses generated on the C1 posterior arch as a result of the clamp

jaw configuration. When the jaws were being tightened into place on the posterior arch of a anatomical UCS model, it was found that the foam model material fractured on the inferior side of the posterior arch (Figure 39). This fracture was a consequence of the mismatch in width between the superior jaws and the inferior jaws (Δw). This difference in widths generated a large bending moment on the posterior arch of C1 and caused the inferior side of the arch to be under tension and the superior side of the arch to be under compression. Although these anatomical models were not designed to have the same mechanical properties as real bone, this stress concentration could still be identified as an issue that might cause problems with the implant in clinical practice if fracture occurred resulting in increased micro motion.
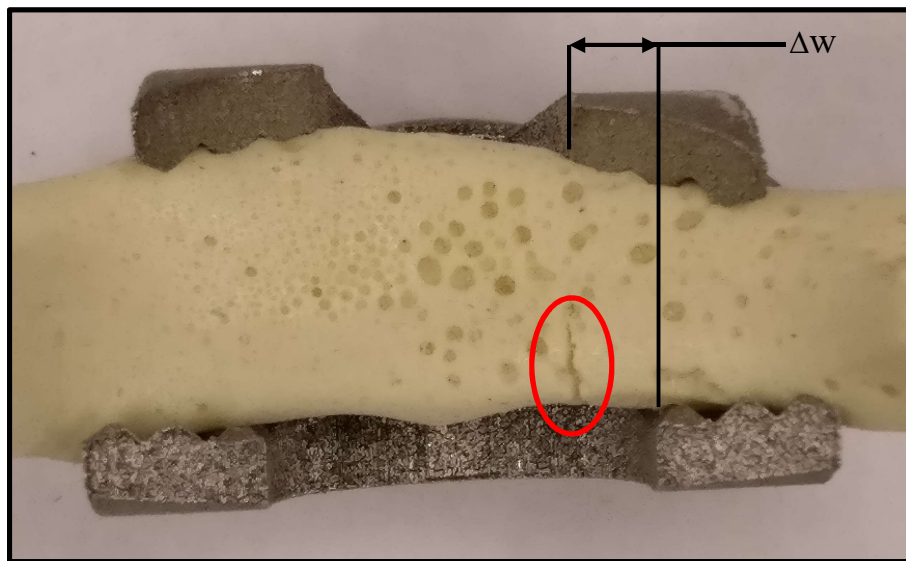
Figure 39: Model fracture on the inferior side of the C1 posterior arch due to bending moment caused by the clamp jaws

To better understand the loading that the clamp placed on the C1 posterior arch, shear and bending moment diagrams were developed by using beam analysis over the fixation area spanned by the clamp (Figure 40). It was assumed that each of the jaws applied an equal load, P, that was distributed along the width of each jaw (Figure 41). The clamp dimensions for the analysis were measured directly from the prototypes.
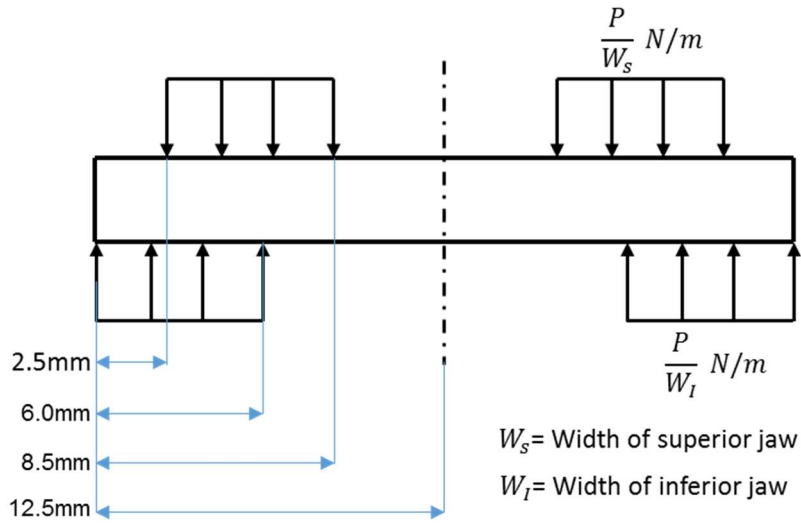
Figure 40: Simplified loading of C1 posterior arch (dimensions symmetric about center line)
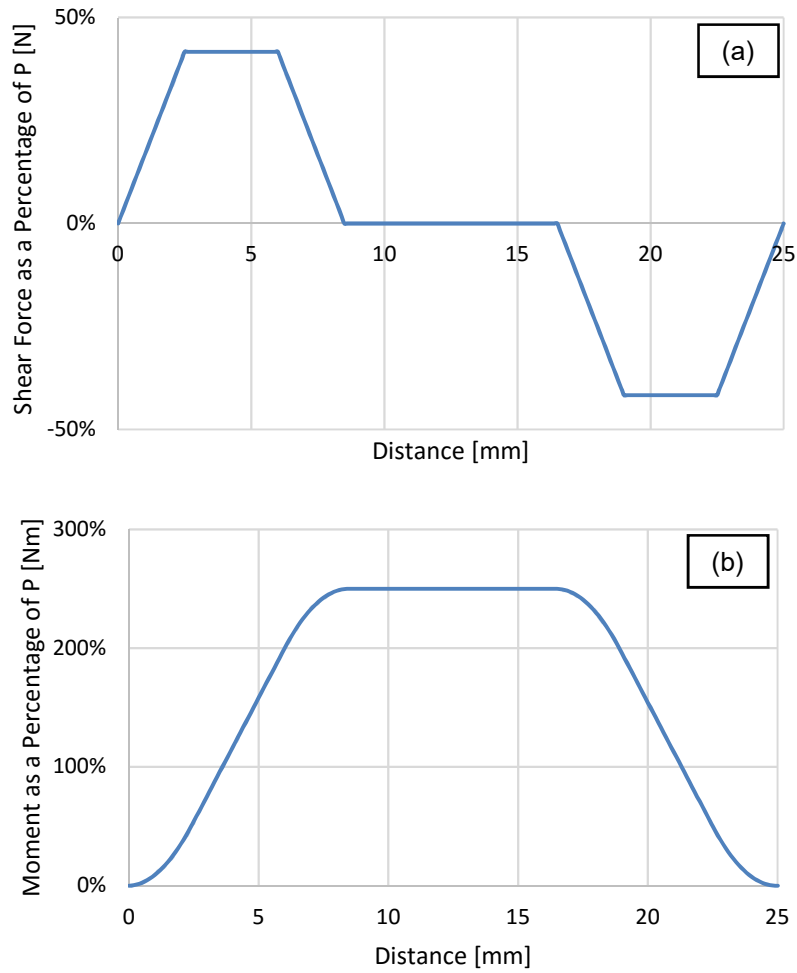
Figure 41: a) Shear diagram and b) bending moment diagram for clamp loading on C1 posterior arch

After reviewing the shear and bending moment diagrams, it was seen that the fracture in the anatomical models occurred at the location where the bending moment was at a maximum in the C1 posterior arch. Additionally, it was logical that the fracture occurred in line with the medial edge of the superior jaw due to the cross section of the C1 posterior arch decreasing in the lateral direction. This combination of maximum bending moment and reducing cross sectional area contributed to the anatomical model fracture because the bending stress was at a maximum at this point.

Finally, from a design functionality standpoint, it was found that the polyaxial rods had enough mobility to connect with the C2 screws in the C1PA/C2TL construct but more mobility was needed to connect to the C2 screws in the in the C1PA/C2P construct improve the integration of the clamp. For the C1PA/C2TL construct (Figure 42a) the angle of the left rod (θ) and the angle of the right rod (β) were both within the articulation allowed by the design of $\pm30^{\circ}$ with respect to the rod sockets. This ensured that the joint space at the C1-C2 capsules was maintained (Figure 42b). However, for the C1PA/C2P construct (Figure 42c), when the angles of the left rod (θ') and the right rod (β') were at the maximum allowable value there was still not enough mobility to reach the C2 pedicle screws. As a result, the joint space at the C1-C2 capsule (Figure 42d) would be distracted in order to make the construct fit. In reality, this distraction would not likely occur in a real patient due to resistance from ligaments around the C1-C2 joint capsule that are not present in the anatomical model shown. Rather, the additional height required to allow the rods to reach the C2 pedicle screws would put the C1-C2 segment in flexion and thus not allow the neck to be in its neutral state. Clinically, this was not considered to be ideal from a patient point of view because the natural curvature of the neck should be maintained during a fusion procedure to minimize the effect that the fusion has on day to day activities. Additionally, if the neck was fused in a non-neutral position other segment levels would be likely to overcompensate for the malposition which might cause an accelerated degeneration of the cervical spine requiring further surgical intervention.
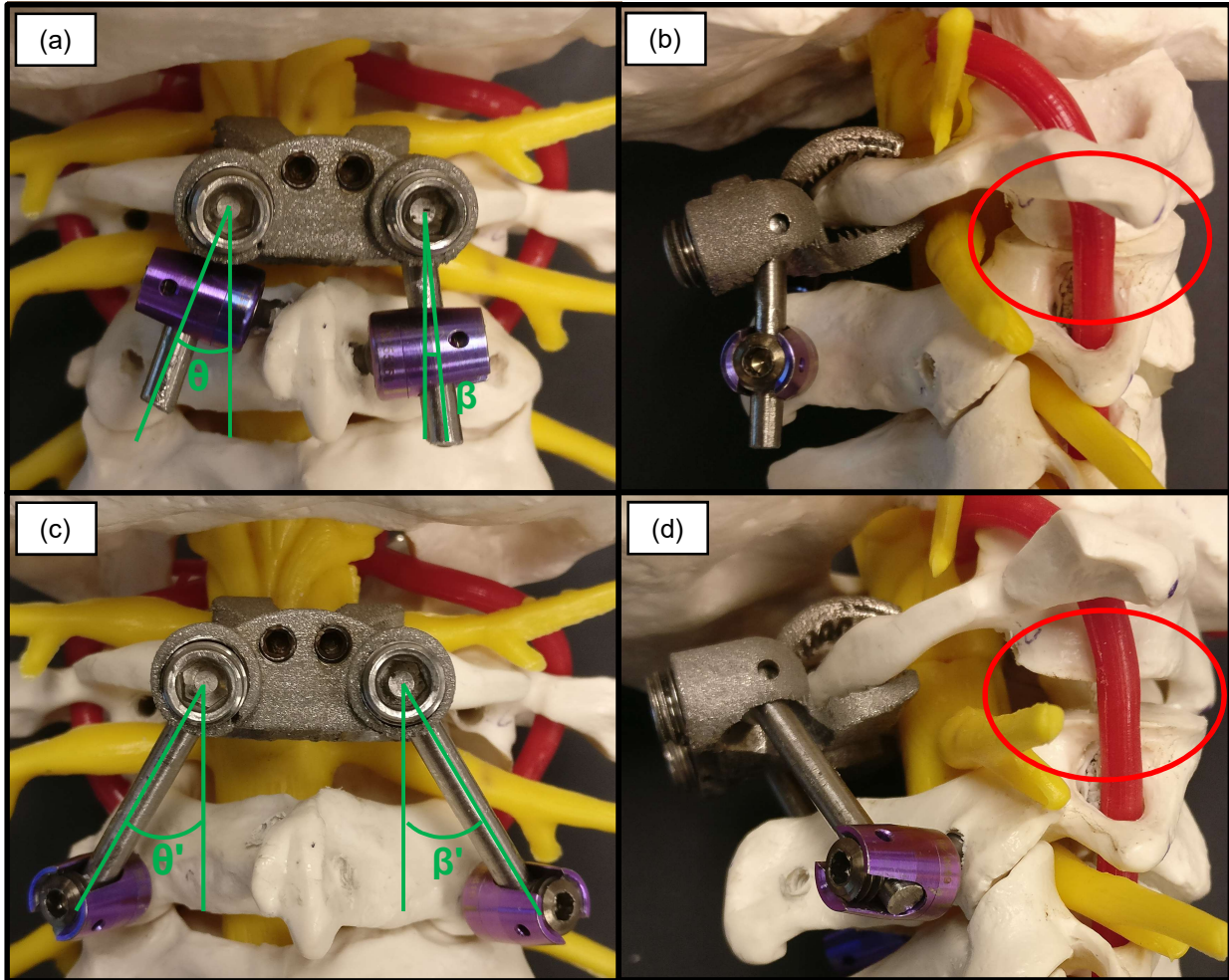
Figure 42: a) Rod positioning and b) C1-C2 joint spacing for C1PA/C2TL construct compared to c) rod positioning and d) C1-C2 joint spacing for C1PA/C2P construct

The fourth generation construct was judged according to the criteria (Table 14) and achieved a score of 7.9 out of 10 compared to the third generation score of 7.5. The spatial harmony score was improved due to the increased adjustability of the superior clamps and the C1-C2 stability score was improved by the more robust locking mechanisms. Changing the implant material to titanium alloy also helped improved the C1-C2 stability score but this was offset by lower manufacturing score. However, the brittle fractures of the titanium alloy once again voided the strength constraint and another round of design revisions was mandatory.

Table 14: Fourth generation implant scored against criteria

Design Criterion	Score /10	Weight Factor	Weighted Score
C1-C2 Stability	**7.5** *(↑0.5)*	0.40	**3.0**
Surgical Risk	8.5	0.35	3.0
Spatial Harmony	**8.0** *(↑1.0)*	0.20	**1.6**
Manufacturing	**5.0** *(↓0.5)*	0.05	**0.3**
		Total	**7.9**

4.4.3 Final Design

Several changes were made to the design of the C1 clamp implant to satisfy the strength constraint and further optimize the criteria score. Firstly, the wall thicknesses (t_w) of the sockets for the polyaxial rods were increased by 30% (Figure 43a) from 1.65 mm to 2.15 mm in order to prevent fracture of the socket during tapping and tightening of the M8 set screws. Additionally, to allow for the polyaxial rods to better reach C2 pedicle screws in the C1PA/C2P construct, the design of the socket was changed to allow 50º of lateral angulation and 10º of medial angulation (Figure 43b). Of course, this reduced the amount of rotation available in the medial direction from 30º to 10º but this was not seen as a concern since a large amount of medial rotation is not required to connect the polyaxial rods to the C2 translaminar screws in the C1PA/C2TL construct. Although the fixation was not flagged as a concern in earlier design revisions, it was decided to change the shape of the spikes on the jaws from square based pyramids to a saw tooth design (Figure 43c). The spikes were designed to help prevent the clamp from receding in the posterior direction. Movement of the clamp in the anterior direction was not expected to be a likely occurrence since the posterior arch of C1 buts up against the body of the inferior clamp and therefore the clamp cannot migrate further into the spinal canal after it has been locked in place. Finally, in order to reduce the bending stresses that were present in the posterior arch of C1 in that last design, the widths of the inferior jaws were increased medially so that the gaps between the superior jaws (L) and inferior jaws were equal (Figure 43d).
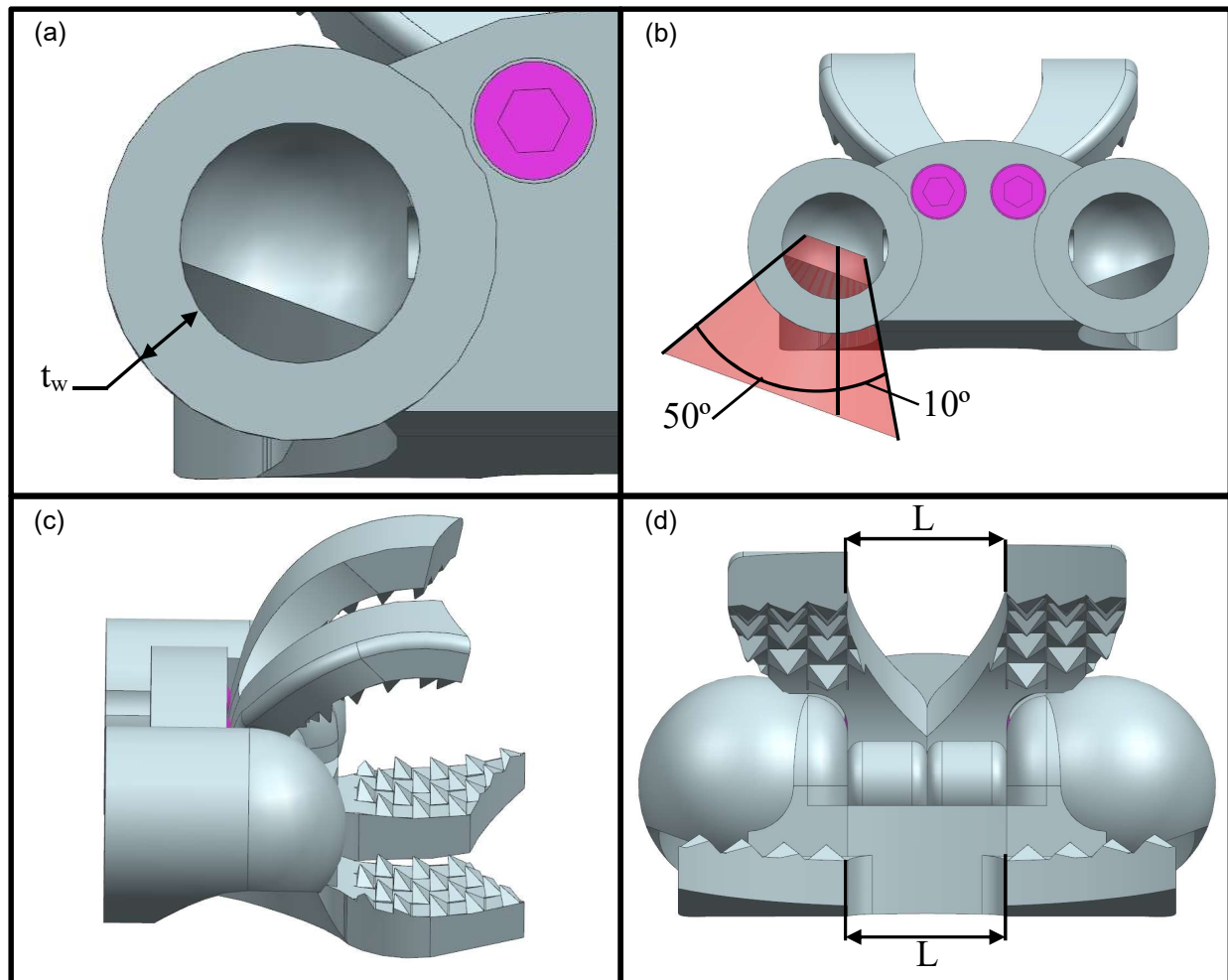
Figure 43: New design revision showing a) increased wall thickness of polyaxial socket, b) increased lateral rotation of polyaxial rods, c) new saw tooth design for improved fixation and c) increased medial width of inferior jaws to reduce bending stress

To compare the loading that the new clamp placed on the C1 posterior arch compared to the old design, shear and bending moment diagrams (Figure 45) were developed for the updated clamp geometry (Figure 44) using the same methodology presented earlier.
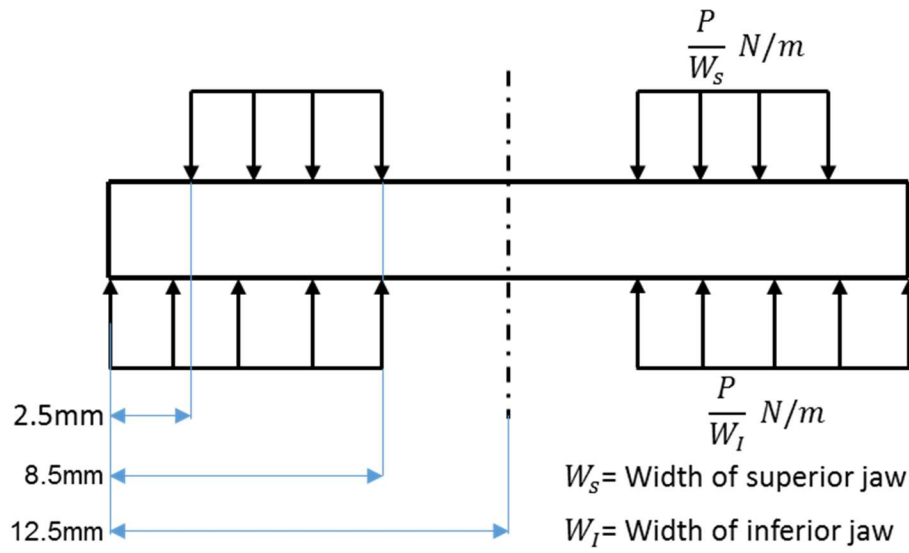
Figure 44: Simplified loading of C1 posterior arch for new clamp design (dimensions symmetric about center line)
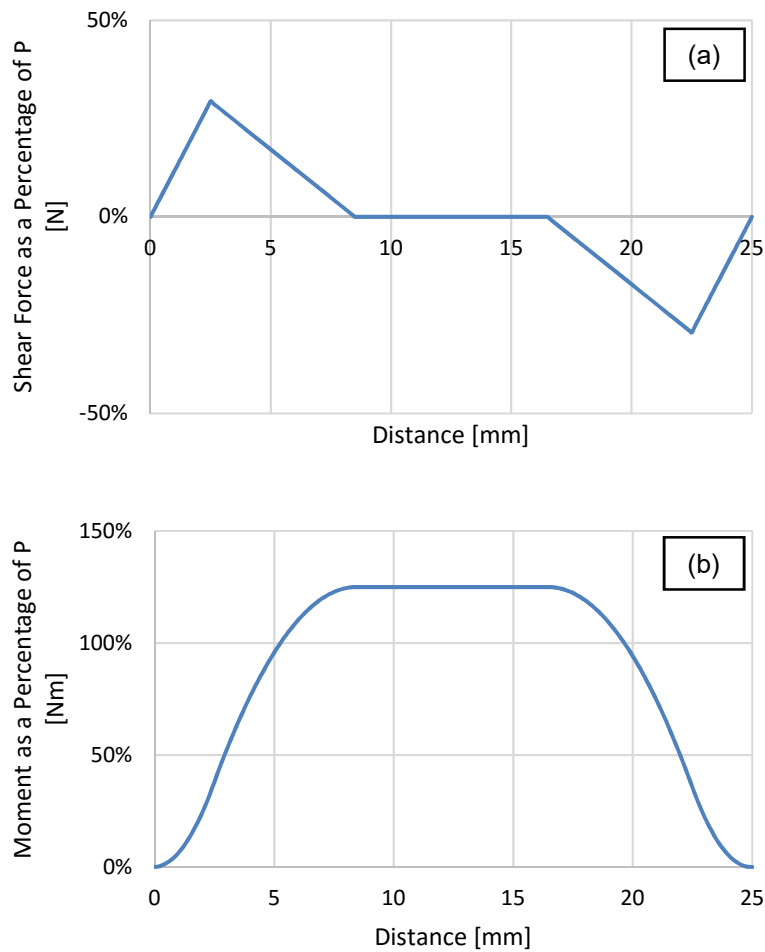
Figure 45: a) Shear diagram and b) bending moment diagram showing loading on C1 posterior arch for new clamp design

Increasing the width of the inferior jaws reduced the maximum bending moment in the C1 posterior arch by 50%. The downside of this design change was that it reduced the size of the window where bone graft could be packed posteriorly to promote fusion at C1-C2. However, to provide a relative comparison, the width of the bone graft window was only reduced by 38.5% to achieve a 50% drop in the bending moment. So, for that reason it was decided that the optimal design used this new inferior jaw configuration.

Once again, titanium alloy prototypes were manufactured using a SLM 3D printer. However, in order to satisfy the strength constraint, the parts were heat treated after printing to remove the martensitic phase. This was done using hot isostatic pressing at a pressure of 100Mpa and temperature of 1000ºC for 3 hours followed by a slow cooling to below 400ºC. This process significantly improved the ductility of the material and produced material properties that were equivalent to conventionally manufactured titanium parts[73]. As a result of heat treatment, there were no issues with post processing the parts. Both the M4 threads for the jaw locking screws and the M8 threads for the polyaxial rod cap screws were machined without any complications.

No further issues were identified when testing the functionality of both the C1PA/C2P and C1PA/C2TL constructs on anatomical UCS models (Figure 46). Increasing the lateral angulation of the polyaxial rods from 30º to 50º greatly improved the fit of the C1PA/C2P construct and eliminated the C1-C2 joint capsule distraction that was seen in the earlier prototype version. Conversely, reducing the medial rotation of the polyaxial rods from 30º to 10º did not negatively affect the fit of the C1PA/C2TL construct. Increasing the wall thicknesses of the polyaxial rod sockets had no effect on the form and function of the clamp implant and was not expected to cause any issues in practice. Finally, the new saw tooth spike design did not present any additional complexities during manufacturing and post processing.
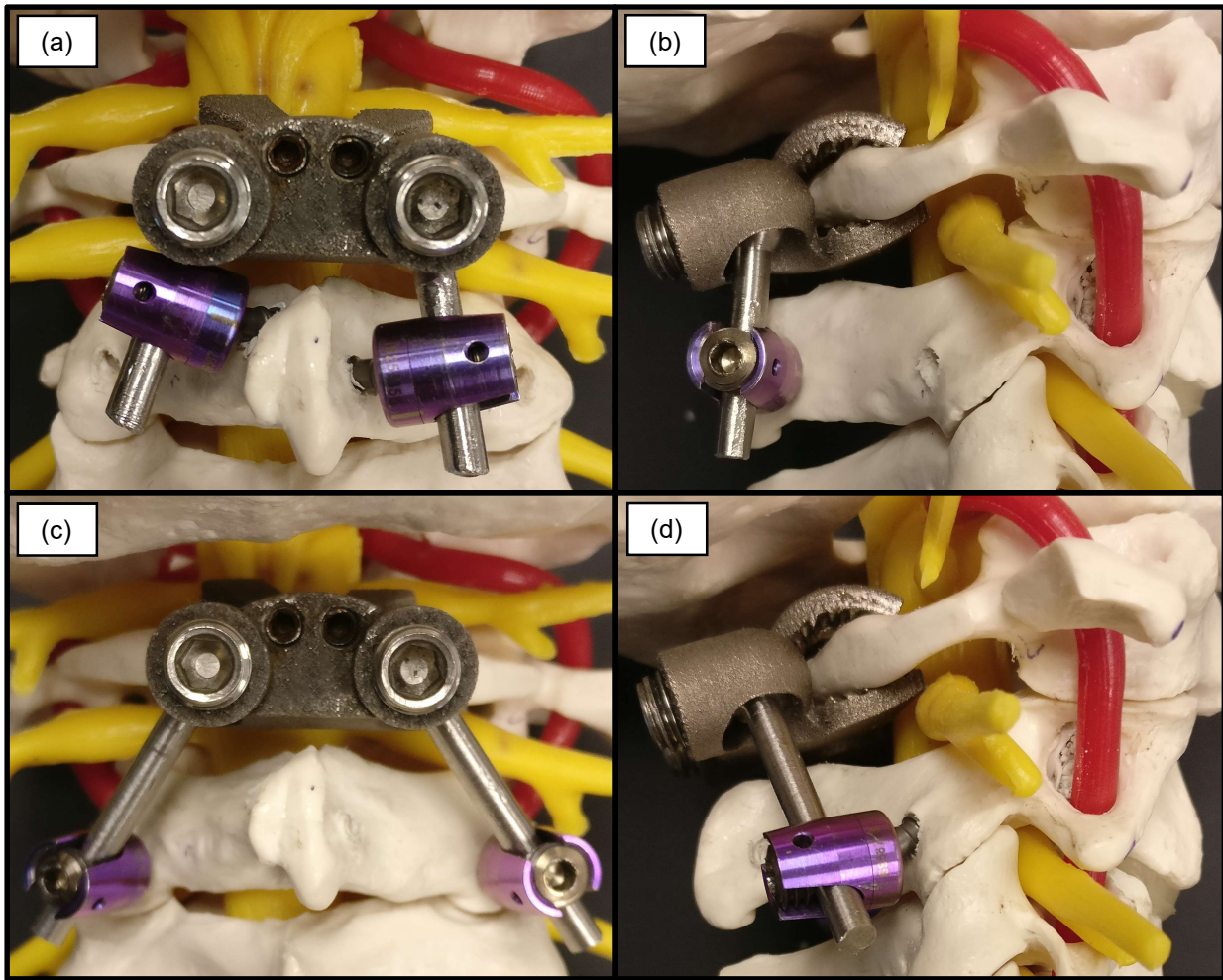
Figure 46: a) Posterior view of C1PA/C2TL construct, b) lateral view of C1PA/C2TL construct, c) posterior view of C1PA/C2P construct and d) lateral view of C1PA/C2P construct

The final implant design was judged according to the criteria (Table 15) and achieved a score of 8.2 out of 10 compared to the fourth generation score of 7.9. The C1-C2 stability score was improved with the saw tooth design as well as the reduced stress on the posterior arch. The spatial harmony score was improved by the increased lateral motion of the polyaxial rods but this was offset by a reduction in the size of the bone graft window. To further optimize the spatial harmony score, a second set of jaws were developed for larger posterior arch anatomy. The design of these jaws allowed an additional 3 mm of height in the C1 posterior arch (Figure 47). In practice, having two sets of jaw sizes (a small set and a large set) seemed reasonable since it is very common for implants to be offered in a variety of sizes to address the varying anatomy of

the entire patient population. Finally, the increased wall thickness and ductility of the implant eliminated fractures in the implant and satisfied the strength constraint.

Table 15: Final implant design scored against criteria and constraints

Design Criterion	Score /10	Weight Factor	Weighted Score
C1-C2 Stability	**8.0** *(↑0.5)*	0.40	**3.2**
Surgical Risk	8.5	0.35	3.0
Spatial Harmony	**8.5** *(↑0.5)*	0.20	**1.7**
Manufacturing	5.0	0.05	0.3
		Total	**8.2**
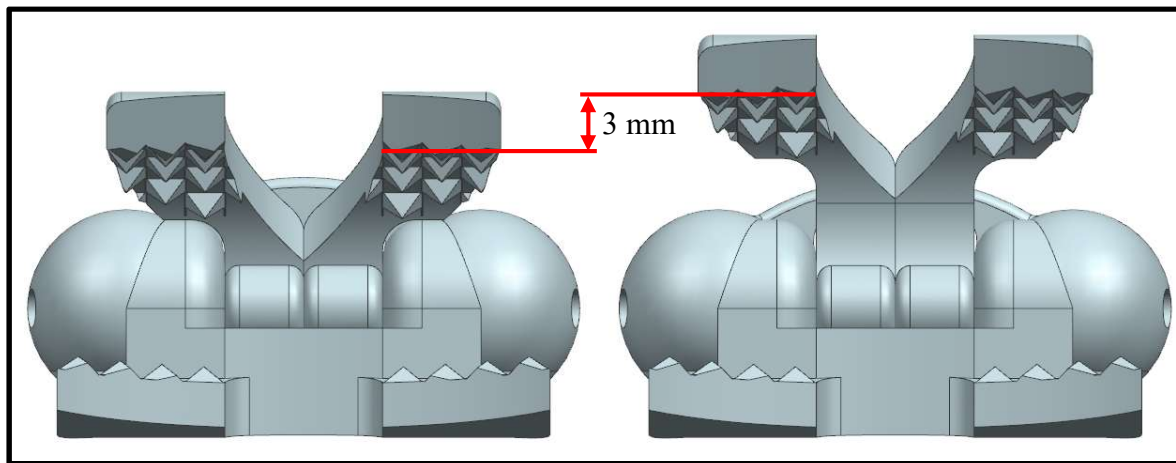
Figure 47: Size difference of small clamp implant (left) and large clamp implant (right)

4.5 C1 Posterior Arch Clamp for Multi-Level Fusion

Although the C1 clamp implant was primarily designed for C1-C2 fusion, the construct can be modified for a multi-level fusion that includes C0. For this case, the rod cap screws are replaced with cap screws that also have polyaxial heads (Figure 48). Standard cervical rods can then be attached to these polyaxial heads and connected to a C0 plate. Additionally, the construct can be extended below C2 by using longer polyaxial rods, these rods may be bent to allow better alignment with the rest of the cervical instrumentation.
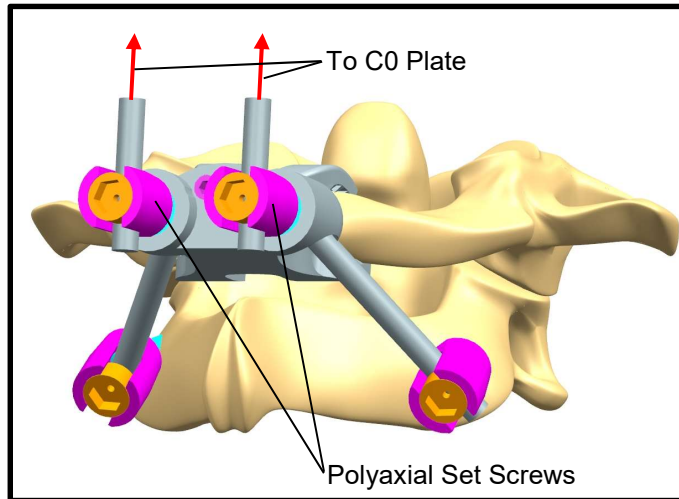
Figure 48: Modified C1PA/C2P construct to include C0 in a multi-level fusion

For the case of a multi-level fusion including C0, the posterior profile of the implant was not a large concern since the construct would prevent extension at C0/C1 and therefore eliminate interference concerns.

4.6 Predicted Loading

The final implant revision would probably have adequate strength during in-vivo loads because it has similar size and similar joints to existing UCS fusion constructs. However, this had to be verified. In order to do this, the predicted loads from the FE modeling phase (presented in section 3.2.1) were applied to each clamp construct for the case of flexion, extension, lateral bending and axial rotation. A high level description of the procedure used to verify the strength of the implants has been provided for the C1PA/C2P construct (detailed MATLAB code for the C1PA/C2P construct during axial rotation has been provided as an example in Appendix A2).

The first step was to link the approximate construct configuration used in the FE model to the final design of the construct as described in the CAD model. To do this, the projected angles of the frame structures in the FE model were measured and then the CAD model was reconfigured to match these angles (Figure 49). These three sets of angles were the angles that the lateral frame structures made with the XY plane (α), the angles that the lateral frame structures made with the XZ plane (β) and the angles that the lateral frame structures made with the YZ plane (θ) using the centers of the fixation points on the posterior arch of C1 as the

73

vertices for the measurement. When applying these angles to the CAD model, the centers of the spherical heads of the polyaxial screws were used as the vertices.

The second step was to find a place on the final construct design where the FE model would give forces that were likely to be about the same as would occur *if the actual construct with all its detail had been included in the FE model*. Thus, it was assumed that the forces and moments in the frame structures that were calculated in section 3.2.1 could be applied to the C2 ends of the polyaxial rods. This would then allow the forces and moments at certain points within the construct to be estimated using elementary statics.
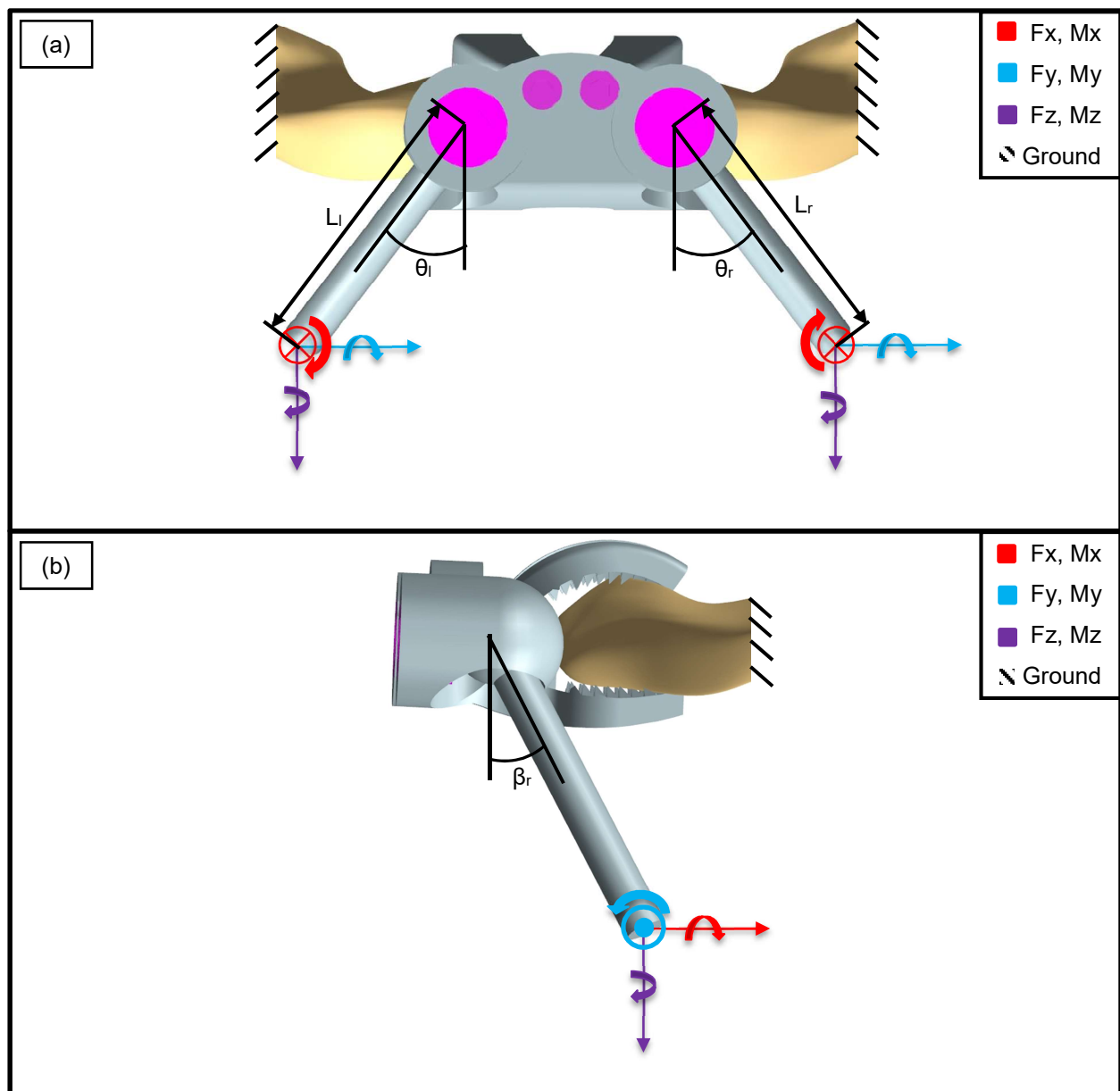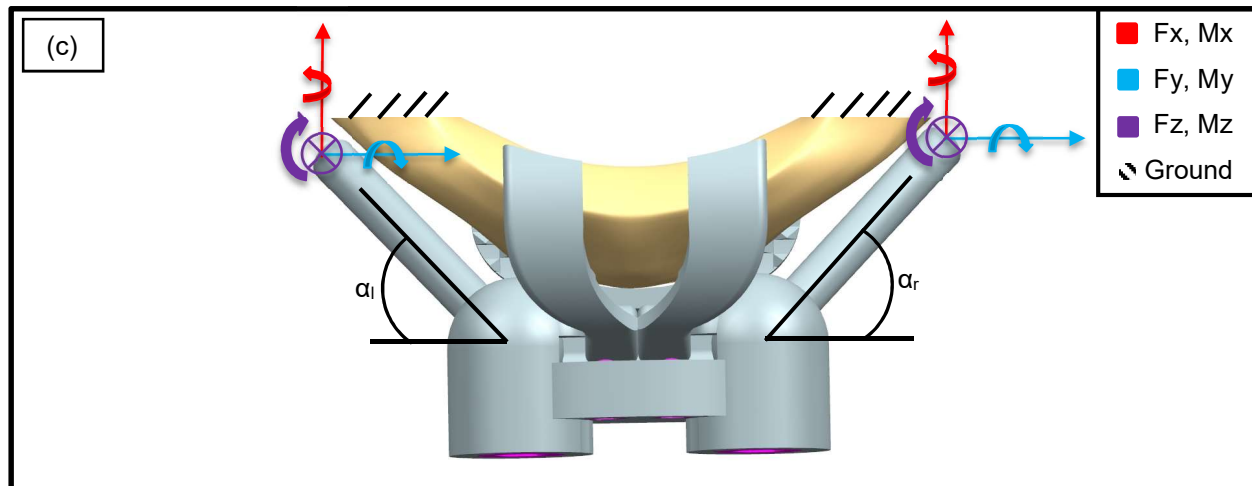
Figure 49: C1 Arch implant positioned to match the configuration of the FE model for the purpose of load analysis: a) coronal plane, b) sagittal plane and c) transverse plane.

So, the purpose of applying the forces and moments from the FE model (as calculated in section 3.2.1) to the detailed CAD model of the final design was to estimate the forces and moments that had to be resisted at the bone/clamp fixation interface and at the locking mechanism of the polyaxial rods to maintain static equilibrium. For example, a free body diagram (Figure 50) and elementary statics were used to generate the six equations of static equilibrium for the right polyaxial rod. Similar equations were generated for the left polyaxial rod and the reaction forces and moments at the spherical heads were calculated under motion conditions of extension, flexion, right lateral bending and right axial rotation for both the C1PA/C2TL and the C1PA/C2P constructs (Table 16). Left motions were the same as right motions due to the symmetry of the geometry.

Frx$_r$, Mrx$_r$

Fry$_r$, Mry$_r$

Frz$_r$,
Mrz$_r$

θ_r

L$_r$

Fx$_r$, Mx$_r$
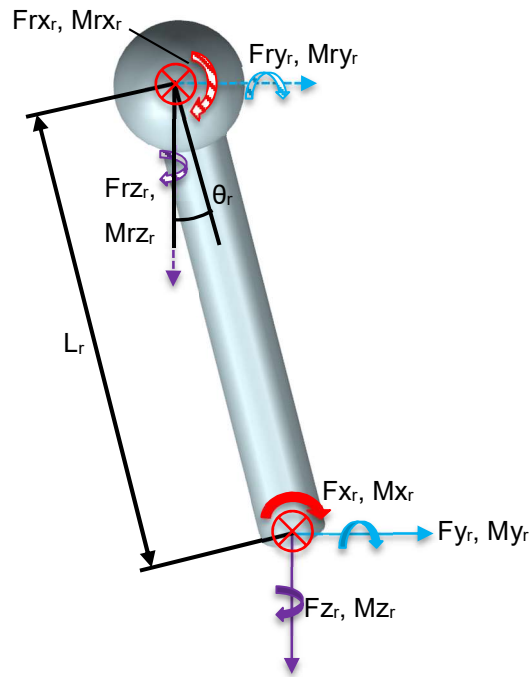
Fy$_r$, My$_r$

Fz$_r$, Mz$_r$

Figure 50: Free body diagram showing resultant forces and moments on right polyaxial rod in the coronal plane

$$Frx_r + Fx_r = 0 \tag{1}$$

$$Fry_r + Fy_r = 0 \tag{2}$$

$$Frz_r + Fz_r = 0 \tag{3}$$

$$Mrx_r + Mx_r - Fy_r \cdot \cos\theta_r \cdot L_r + Fz_r \cdot \sin\theta_r \cdot L_r = 0 \tag{4}$$

$$Mry_r + My_r + Fx_r \cdot \cos\beta_r \cdot L_r - Fz_r \cdot \sin\beta_r \cdot L_r = 0 \tag{5}$$

$$Mrz_r + Mz_r - Fx_r \cdot \cos\alpha_r \cdot L_r + Fy_r \cdot \sin\alpha_r \cdot L_r = 0 \tag{6}$$

Table 16: Reaction forces and moments at spherical heads of polyaxial rods for a) C1PA/C2TL construct and b) C1PA/C2P construct

(a) C1PA/C2TL	Extension		Flexion		Right Lateral Bending		Right Axial Rotation	
	Left rod	Right rod	Left rod	Right rod	Left rod	Right rod	Left rod	Right rod
Frx [N]	15.0	-1.3	-4.6	1.4	-13.5	6.0	-10.0	-15.1
Fry [N]	-39.1	7.0	-11.4	7.0	-25.2	2.0	-35.7	-16.2
Frz [N]	-79.3	87.0	-35.0	-19.0	-118.1	91.2	-93.8	33.8
Mxr [Nm]	-1.3	-2.2	-0.6	0.5	-2.1	-2.1	-1.5	-0.8
Myr [Nm]	0.7	0.3	-0.1	-0.1	0.0	0.3	0.3	-0.1
Mzr [Nm]	0.7	-0.2	0.3	-0.1	0.7	0.1	1.0	0.5

(b) C1PA/C2P	Extension		Flexion		Right Lateral Bending		Right Axial Rotation	
	Left rod	Right rod	Left rod	Right rod	Left rod	Right rod	Left rod	Right rod
Frx [N]	-11.7	-12.9	-9.6	-9.6	-27.0	26.9	2.7	-3.9
Fry [N]	0.1	-2.9	4.0	-4.6	15.0	21.5	-3.2	-3.6
Frz [N]	-18.4	-20.9	-33.6	-32.3	-78.6	55.8	-0.6	1.3
Mxr [Nm]	0.6	-0.6	0.3	-0.2	1.2	0.6	0.1	0.1
Myr [Nm]	0.4	0.4	0.0	0.0	0.6	-0.2	0.1	-0.1
Mzr [Nm]	-0.1	0.1	-0.4	0.2	-0.2	-0.1	0.1	0.0

The magnitudes of the forces at the spherical heads of the polyaxial screws were not expected to cause functionality issues with the implant. However, slippage of the locking mechanism due to the moments that must be resisted at the spherical heads was a concern. Rotations about the x-axis due to slippage were expected to be the most likely since the moments about the x-axis were the largest. More specifically, moments were the highest for the C1PA/C2TL construct in lateral bending and quite high for axial rotation, suggesting a higher risk of slip for this construct under these motions. Moments for flexion and extension were relatively low for the C1PA/C2TL construct and all moments for the C1PA/C2P construct were relatively low for all types of motion.

To determine the likelihood of slip at the bone/clamp interface, experiments were performed with a polymeric material to simulate the bone (presented later in Chapter 5). It was convenient in these experiments to use a test machine to apply a single force that acts through a moment arm to impose a force and a moment at the clamp/bone interface. However, before these experiments could be done, the forces and moments predicted above had to be applied at a single point so that they could be applied by a test machine. In order to simplify the loading, the forces

were transformed to act on a virtual point at the center of the jaws (Figure 51) rather than the ends of the polyaxial rods. These transformed forces and moments that acted at the virtual point were the same as reactions forces and moments that would hold the clamp and polyaxial rods in static equilibrium but opposite in direction. However, it was convenient in this section to think of them as transformed. This allowed for the forces and moments from the left and right rods to be combined so that the loading present in each type of motion could be represented by a set of three axial forces (F_{tx}, F_{ty}, F_{tz}) and three moments acting about these axes (M_{tx}, M_{ty}, M_{tz}). Mathematically, this was done by moving moments, forces, and moments generated by moving the forces to the virtual point (detailed equations available in Appendix A1). The combined forces and moments that act on the virtual point have been summarized for both constructs in flexion, extension, lateral bending and axial rotation (Table 17).
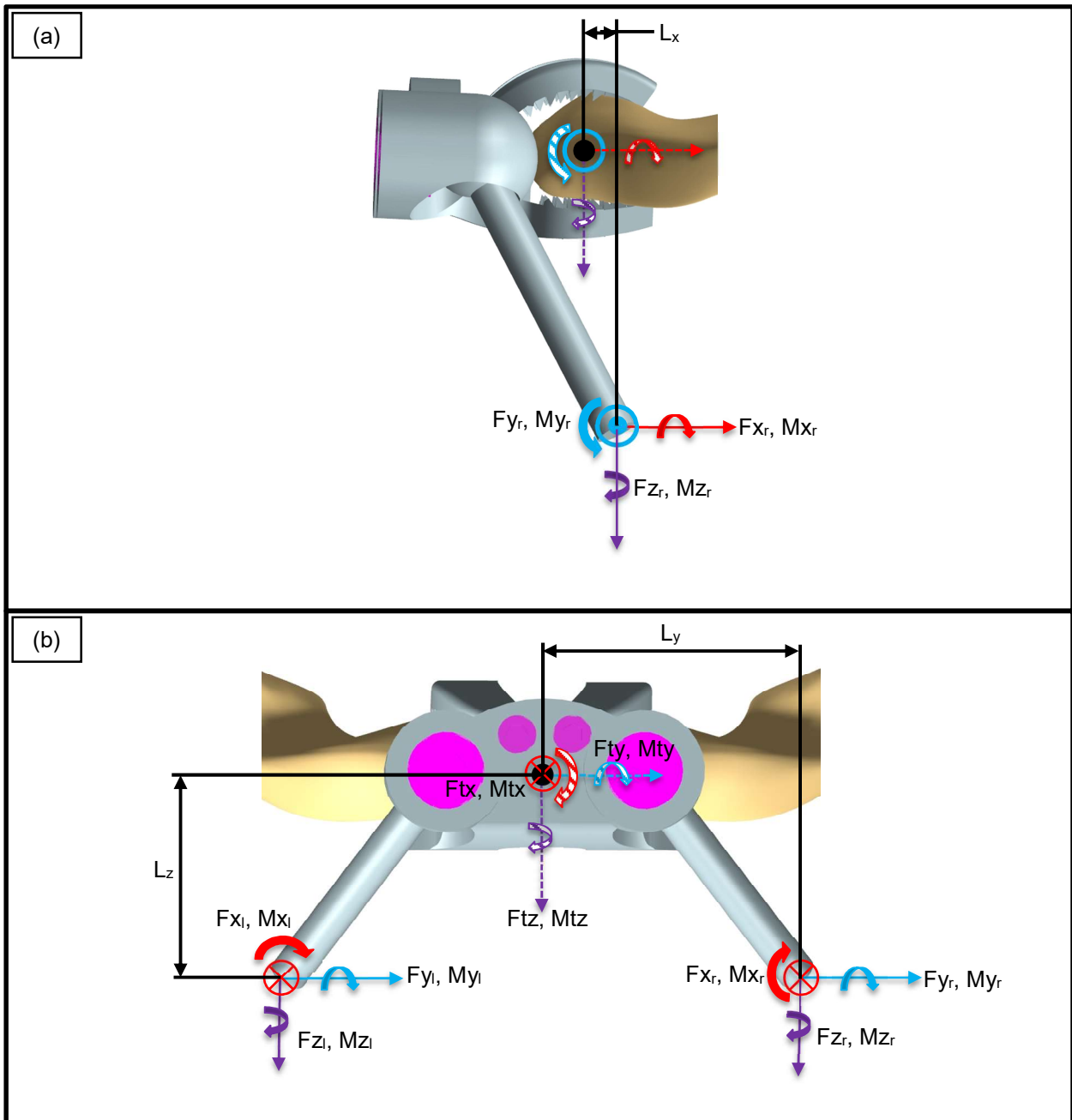
Figure 51: Loads from FE model transformed to act on a virtual point in the center of the jaws: a) sagittal plane and b) coronal plane

Table 17: Combined forces and moments to represent the loading at the virtual point of a) C1PA/C2TL construct and b) C1PA/C2P construct

(a) C1PA/C2TL	Extension	Flexion	Lateral Bending	Axial Rotation
Ftx [N]	-13.7	3.2	7.5	25.1
Fty [N]	32.1	4.4	23.3	51.9
Ftz [N]	-7.7	54	26.9	60.0
Mtx [Nm]	-0.1	0.0	-0.8	0.6
Mty [Nm]	-1.1	0.5	-0.2	0.2
Mtz [Nm]	-0.2	0.0	-0.2	-0.8

(b) C1PA/C2PA	Extension	Flexion	Lateral Bending	Axial Rotation
Ftx [N]	24.6	19.3	0.1	1.2
Fty [N]	2.8	0.6	-36.6	6.9
Ftz [N]	39.3	65.9	22.7	-0.7
Mtx [Nm]	0.1	0.1	-1.9	0.2
Mty [Nm]	0.1	1.5	-0.3	0.0
Mtz [Nm]	-0.0	0.2	0.4	-0.1

Reviewing the combined loads at the virtual point of each construct, it is seen that the loads vary significantly depending on the location of the screws in the C2 vertebrae. Not surprisingly, the combined forces in flexion and extension were higher in the C1PA/C2P construct than in the C1PA/C2TL construct because the configuration of the C1PA/C2TL construct can more effectively resist applied flexion/extension moments due to the rods of the construct creating larger moment arms. However, the wider lateral profile of the C1PA/C2P construct caused the combined forces in lateral bending and axial rotation to be lower than the forces present in the C1PA/C2TL construct for the same reason. Overall, moments and forces in either construct seemed feasible and it was decided to not alter the design further.

There were several limitations with this load prediction study. Firstly, the FE model used very simplified versions of each construct to predict the loading that would be present. More accurate load predictions could have been obtained if the construct was modeled in more detail in the FE model but this would have involved considerable effort and would have needed experimental validation to some extent. It was decided to just check the constructs experimentally. However, the estimates from the FE model were needed later in this thesis to establish torque specifications for the construct joints (polyaxial rod heads, clamp/bone interface) to function without slipping.

Another related limitation of the load prediction study was that specific geometries of the construct and bone interfaces (such as the bone/screw interface at C2 or the clamp surface interface with the posterior arch of C1) were not modeled in detail. This made accurately predicting local stresses in the bony anatomy due to the construct impossible because the stresses outputted by the FE model had artificially high values near the fixation points. Significantly more time would have been required to accurately model these interfaces since the protocol and methods for doing so have not yet been established in the literature. Furthermore, it was decided that this time investment was not merited since the constructs are intended for physiological loads and the stresses generated were expected to stay in the elastic zone of both the construct and the bony anatomy. Finally, in practice the location of both the clamp and C2 screws will vary slightly from patient to patient depending on each individual's anatomy. These variations were also expected to cause changes in the loading of the implant but the magnitude of these load changes were not expected to be large enough to detrimentally effect the performance of the construct. All of the above limitations have been addressed, to some extent by the cadaveric study of the stability of the final construct and various other constructs which is presented later in this thesis.

5.0 Methods for Experimental Testing of a Novel C1 Posterior Arch Clamp

After completing the detailed design phase in Chapter 4, the next step in the development process was to begin experimental testing of the C1PA/C2TL construct and C1PA/C2P construct. Experimental testing was broken down into two stages. The first stage was to test the C1 clamp implant under the expected loads that had been predicted by the FE model. The second stage was to test the stability of the full C1PA/C2TL and C1PA/C2P constructs in a cadaveric study.

5.1 C1 Clamp Strength Testing

Experimental strength testing was done on the clamp for two main reasons. The first reason was to estimate whether the polyaxial rod locking mechanism and the clamp/bone fixation interface could withstand the loads predicted in Section 4.7 without slippage occurring. The second reason was to ensure that mechanical failure of any of the components in the clamp did not occur under the predicted loading.

5.1.1 Polyaxial Rod Locking Mechanism

A separate fixture was created to test the strength of the polyaxial rod locking mechanism (Figure 52a) and determine a specification for the tightening torque on the polyaxial rod cap screws. The test fixture was designed to have the same internal dimensions as the sockets of the C1 clamp body but the external shape was made into a cube so that the jig could be easily held in the jaws of a tensile testing machine during testing. Another fixture (Figure 52b) was machined to allow for an eyebolt to be attached to the end of a polyaxial rod so that a cable could be tied to the eyebolt and connected to the other jaw of the tensile testing machine to apply moments to the polyaxial rod locking mechanism. In the full fixture assembly (Figure 52c), the polyaxial rod set screws were tightened. Three torque levels were initially tested as potential specifications: 4 Nm, 5 Nm and 6 Nm. The locked assembly was then placed into a tensile testing machine which applied tensile loading to the cable attached to the eyebolt. The tensile loads were applied in four directions (Figure 52d): north (N), east (E), south (S) and west (W). Tensile loads were increased until a load was reached at which slippage occurred at the locking mechanism. Three repeats were collected for each direction at each cap screw torque, this created a total of 36 data points.

The max tensile forces were then converted to moments by multiplying the force by the length of the fixture (43 mm). These moments represented the maximum moment that the locking mechanism could withstand without slippage in each direction (Figure 53). Later in this thesis, these moments were compared to the moments that the FE model predicted at the polyaxial rod heads (Table 16) in order to determine torque specification for the polyaxial rod set screws.
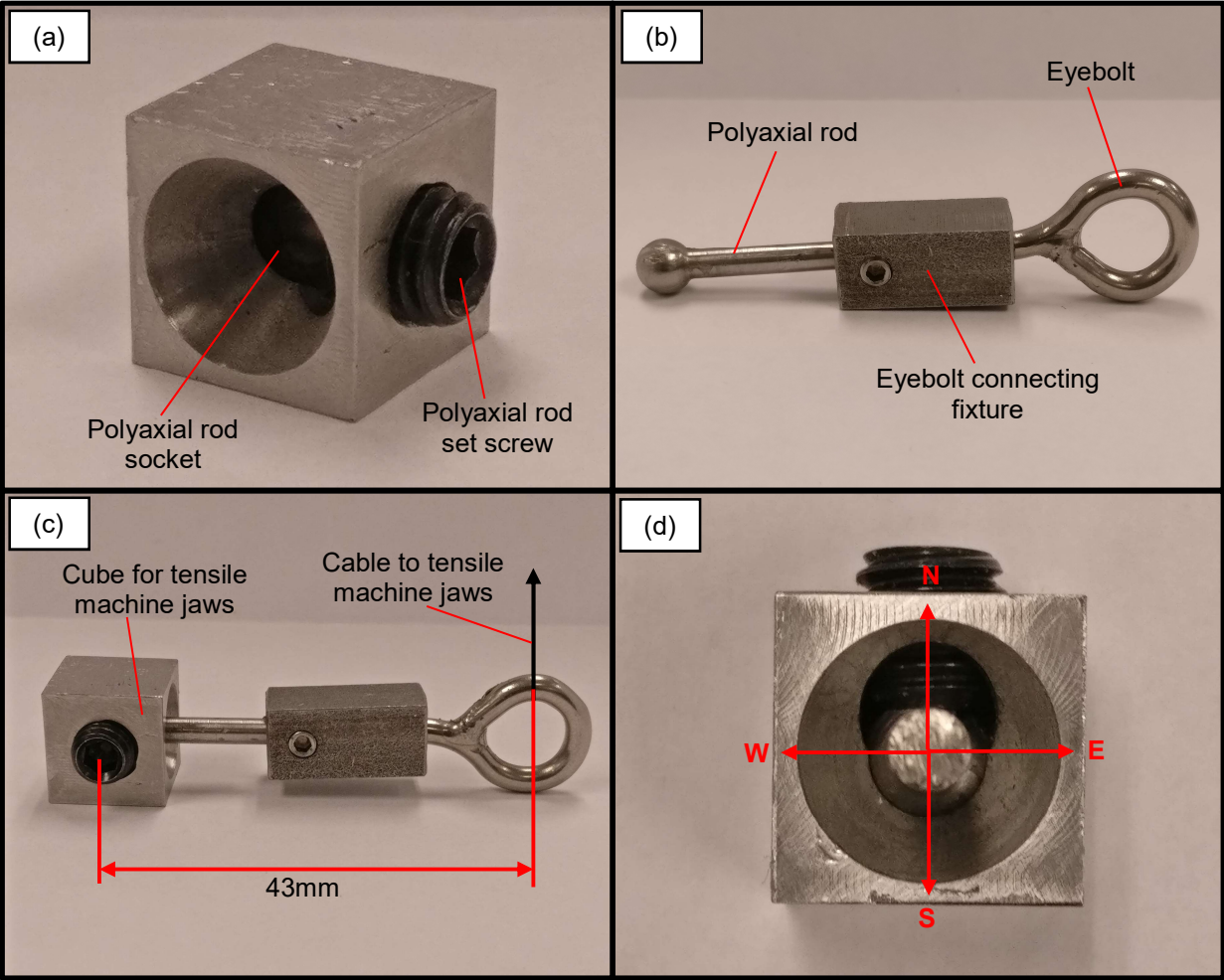
Figure 52: Testing apparatus for polyaxial locking screw mechanism: a) fixture to represent polyaxial rod locking mechanism, b) fixture for connecting eyebolt to polyaxial rod, c) fully assembled testing apparatus locked in place ready for tensile testing and d) directions of tensile loading
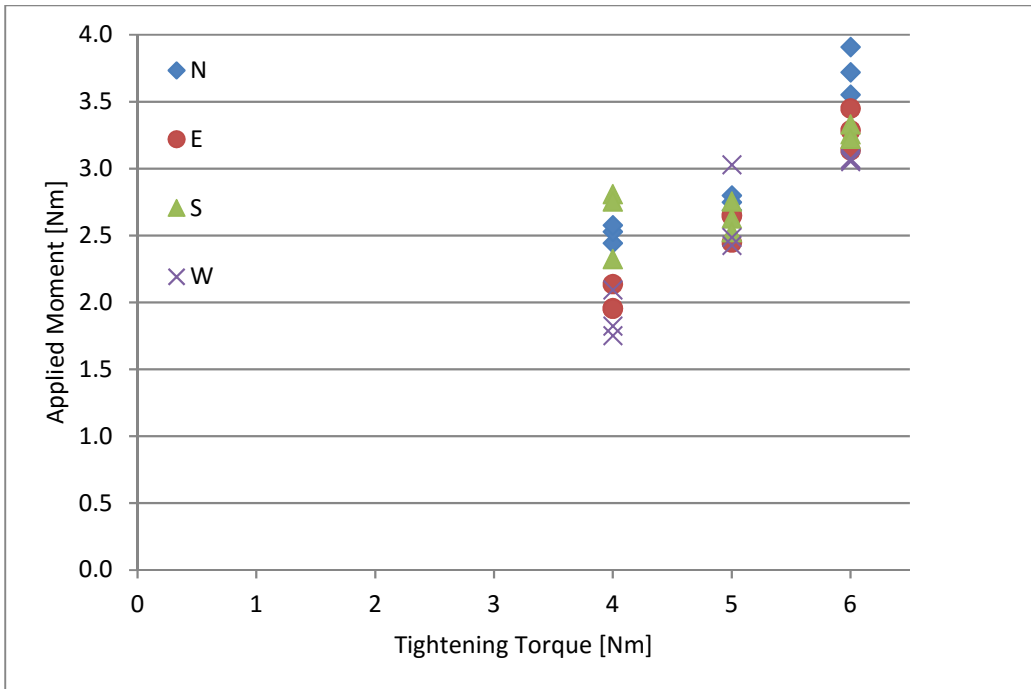
Figure 53: Results for strength testing of polyaxial rod locking mechanism

To better visualize the directional dependence of the strength of the locking mechanism, the deviation from the mean applied moment at each tightening torque was plotted against the load direction (Figure 54).
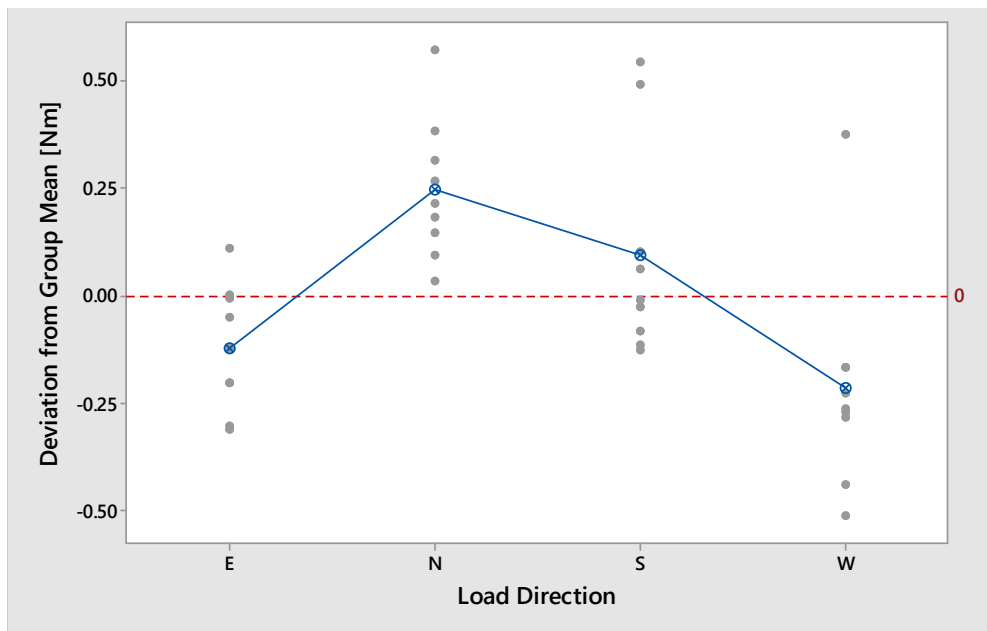
Figure 54: Directional dependence for the strength of the polyaxial rod locking mechanism

84

A balanced ANOVA was performed to test the effect that load direction and tightening torque had on the maximum applied moment (Table 18). After reviewing the ANOVA table, it was found that both the tightening torque and the load direction had a significant effect on the maximum moment that the locking mechanism could withstand without slippage occurring. More specifically, as the tightening torque increased, so did the maximum moment that the locking mechanism could withstand without slippage, an obvious finding. What was os some interest was the significant effect that the load direction had on the strength of the locking mechanism. It was found that the locking mechanism could withstand significantly higher loads in the N-S directions compared to the E-W directions. Although this result was not obvious, it did make sense based on the design of the locking mechanism. After the polyaxial rod set screw was torqued into place, the points on the spherical head with the highest contact forces were the contact areas between the head and the cap screw and the head and the anterior surface of the socket. The moment arms that these contact forces generated were larger in the sagittal plane than they were in the coronal plane and therefore it made sense that a larger moment could be applied in the N-S directions (corresponding to rotation about the y-axis in the FE model coordinate system) without slippage compared with the E-W directions (corresponding to rotation about the x-axis in the FE model coordinate system).

Table 18: Balanced ANOVA to determine the effect of tightening torque and load direction on maximum applied moment at the polyaxial rod locking mechanism

Source	DF	SS	MS	F-value	P-value
Tightening Torque	2	7.11	3.56	76.52	<0.01
Load Direction	3	1.18	0.39	8.44	<0.01
Error	30	1.39	0.05		
Total	35	9.68			

Testing the locking mechanism with the tensile testing machine was able to determine the maximum moments that the polyaxial rod locking mechanism could withstand without slipping about the anatomical x (E-W directions) and y (N-S directions) axes. However, another testing fixture was required to test the maximum moment that the locking mechanism could withstand when twisting about the anatomical z-axis (long axis of the rod) (Figure 55). This fixture allowed

for moments about the z-axis to be applied to a socket head cap screw attached to the end of the polyaxial rod. The polyaxial rod sets screws were tightened up to 4 Nm using a torque wrench, the jig was then placed in a benchtop vice and the same torque wrench was used to apply torques to the socket head cap screw. Torques up to 2.5 Nm were applied to the cap screw and slippage did not occur at the polyaxial rod locking mechanism. A maximum applied moment of 2.5 Nm without slippage occurring at the locking mechanism was deemed to be acceptable since it was higher than the predicted z-axis moments from the FE model (Table 16) and therefore higher tightening torques of 5 Nm and 6 Nm were not tested.
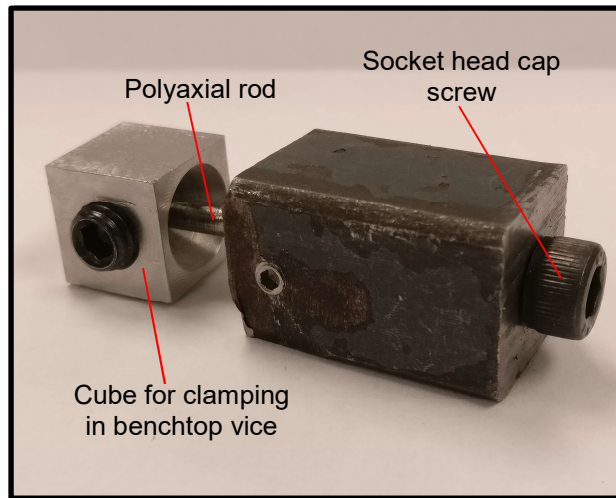
Figure 55: Fixture for testing strength of polyaxial rod locking mechanism against applied moments about the z-axis

When the maximum moments that the polyaxial rod mechanism could withstand without slipping were compared to the predicted moments about the x-axis and y-axis from the FE model (Table 16), it was found that the mechanisms ability to resist moments about the x-axis was the limiting factor. This was because the locking mechanism was the weakest at resisting moments about the x-axis and the FE model predicted that moments would be the highest about the x-axis. The largest predicted x-axis moment had a magnitude of 2.1 Nm and occurred in the C1PA/C2TL construct during lateral bending. In order for the polyaxial rod locking mechanism to resist this load without slipping, the experimental data suggested that the polyaxial rod set screws should be tightened to 5Nm. Additionally, no locking mechanism failures occurred at this tightening torque during testing. For these reasons, 5 Nm was adopted as the torque specification for the polyaxial rod set screws.

86

5.1.2 Fixation Strength

To experimentally test the fixation strength of the clamp jaws, a M4 hole was tapped into the body of the C1 clamp implant to allow for the placement of an eyebolt (Figure 56a). The clamp was then tightened onto a polyethylene rod by tightening the jaw locking screws. Three tightening torque values of 1.0 Nm, 1.25 Nm and 1.5 Nm were tested in the hopes of determining a specification for the jaw locking screws. These torques were lower than the torque range tested on the polyaxial rod M8 set screws because of the smaller M4 screws used in this mechanism and the reduced risk of the jaws slipping due to the cam design. Once the clamp was tightened onto the polyethylene rod, the assembly was placed in a tensile testing machine that applied tensile forces to test the fixation strength (Figure 56b). The tension forces were then multiplied by the moment arm created by the wire and the center of the jaws (Figure 56c). Tension forces were applied to the clamp in the ±z directions (representative of moments about the y-axis), -x direction (to test posterior pullout strength) and +y direction (representative of moments about the z-axis) (Figure 56d). The clamp was assumed to have equal strength in either lateral direction so only one direction was tested. Tests were done in each specified direction at each level of locking screw tightening torque and the full set of treatments was replicated once. The maximum tensile load was recorded for each test, this load was then multiplied by the moment arm to generate the maximum applied moment that the jaw could withstand in each direction (Figure 57). The maximum tensile load was defined as the load at which slippage began at the fixation interface or if a tensile load of 125 N (moment of 4.4 Nm) was hit without slippage occurring.
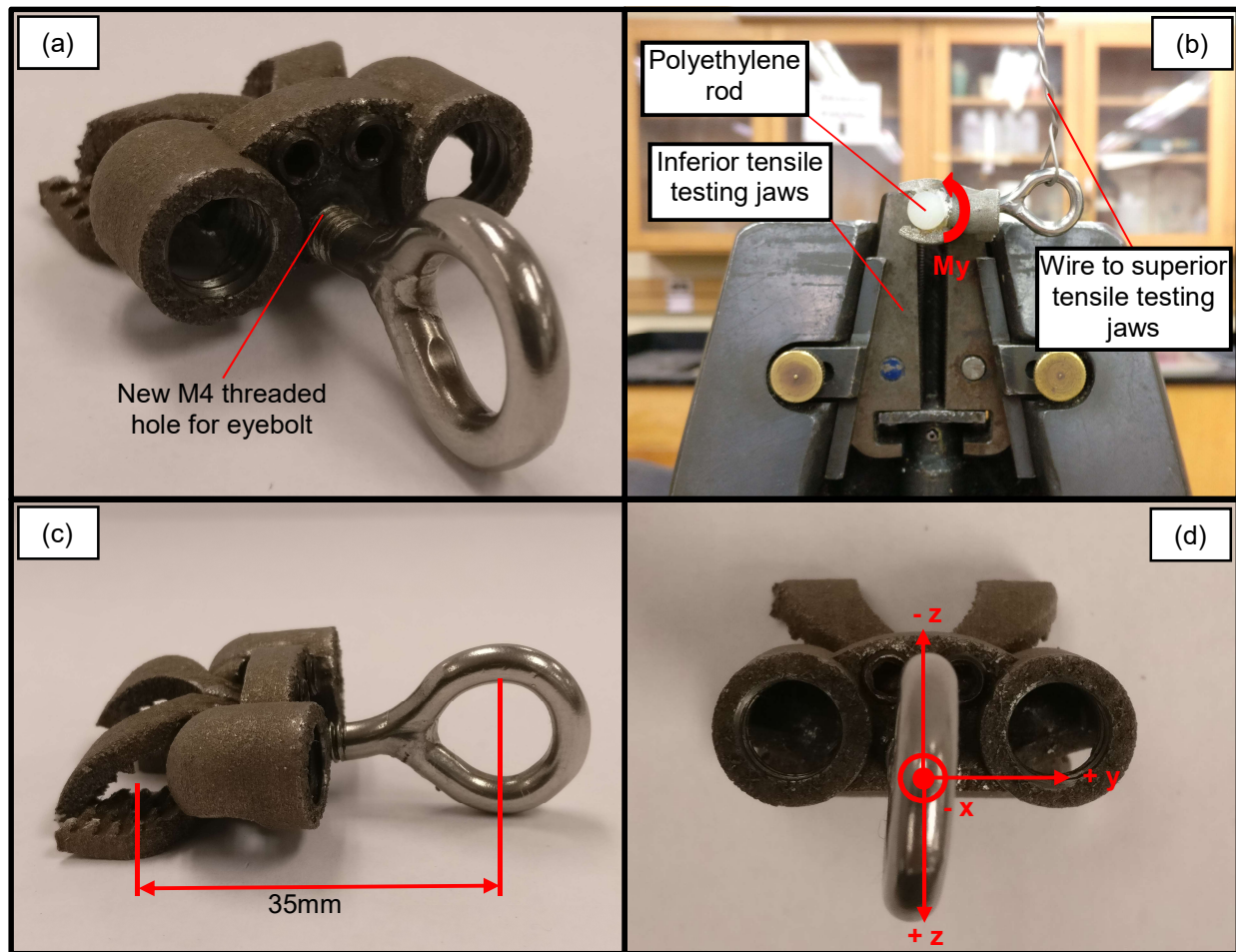
Figure 56: Modified C1 clamp to allow placement of an eyebolt in the implant body, b) example testing setup showing loading of the clamp in the inferior direction to generate a moment about the y-axis, c) side view of clamp showing moment arm length and d) load directions used for testing
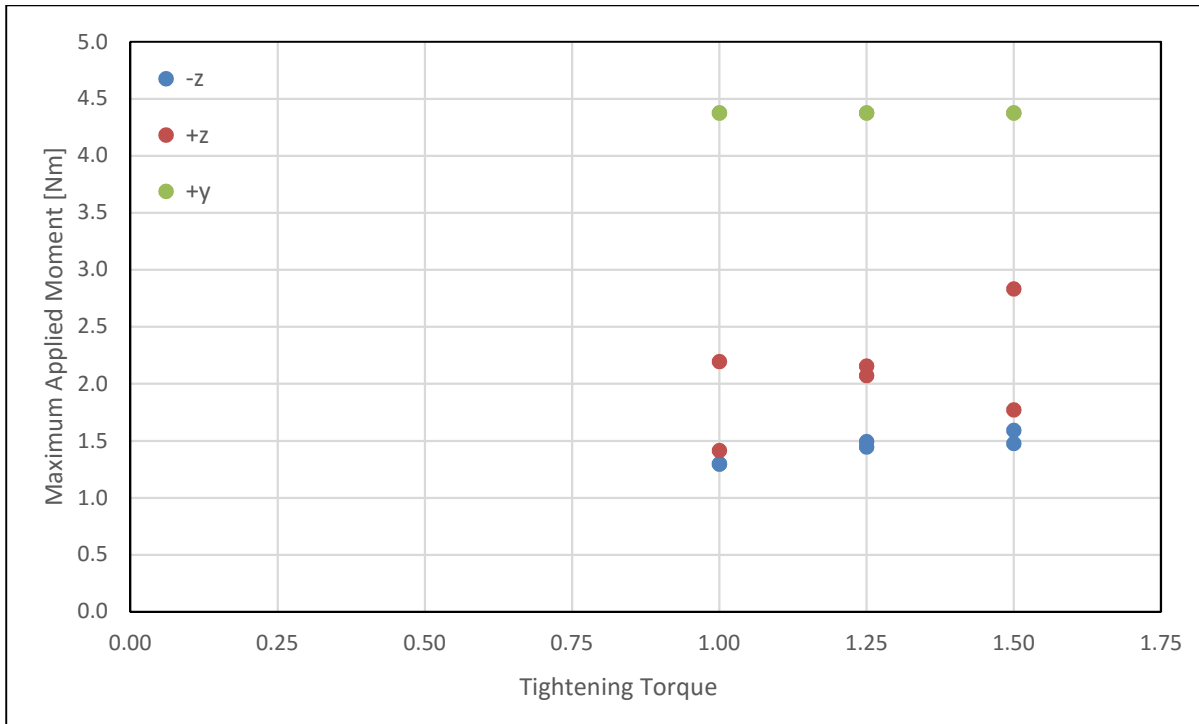
Figure 57: Applied moment that generated slippage at the fixation interface as a function of load direction and tightening torque

A balanced ANOVA was performed to test the effect that load direction and tightening torque had on the maximum applied moment that the fixation interface could withstand (Table 19). After reviewing the ANOVA table, it was found that load direction had a significant effect on the maximum moment that the fixation interface could withstand without slippage occurring but a significant effect was not detected for the tightening torque applied to the locking screws. When moments were applied about the z-axis, the maximum load limit was hit before slippage occurred at the fixation interface. Additionally, a post-hoc Bonferroni test showed the fixation strength differences between directions was significant with the +y direction resisting the highest applied moment without slipping, followed by the +z direction and -z direction. Although a significant effect for tightening torque was not detected, a positive trend was seen between tightening torque and fixation strength for all directions of loading. It is believed that with more replicates this trend would continue and become statistically significant. Tensile testing in the -x direction was omitted from the ANOVA since this force did not create a moment and was more representative of a pullout test. For all tests in the -x direction, the clamp was able to resist the

max load of 125 N without slippage occurring at the fixation interface regardless of the tightening torque applied to the jaw locking screws.

Table 19: Balanced ANOVA to determine the effect of tightening torque and load direction on maximum applied moment at the fixation interface

Source	DF	SS	MS	F-value	P-value
Load Direction	3	42.47	14.16	242.33	<0.01
Tightening Torque	2	0.14	0.07	1.19	0.33
Error	18	1.05	0.06		

Strength testing the fixation interface by using a tensile testing machine was able to determine the maximum moments that the interface could withstand without slipping about the y-axis and z-axis. However, another test was required to test the maximum moment that the fixation interface could withstand about the x-axis. For this test, the clamp jaws were tightened onto a wooden dowel and the polyaxial rod cap screws were threaded all the way into the sockets. The dowel was then clamped in a benchtop vice and a moment of 4.0 Nm was applied to the rod cap screws to simulate a moment about the x-axis. The jaw locking screws were torqued at different levels of 1.0 Nm, 1.25 Nm and 1.5 Nm, however the clamp did not slip under the applied load for all cases regardless of the tightening torque.

When the maximum moments that the clamp fixation interface could withstand without slipping were compared to the predicted moments about the virtual point from the FE model (Table 17), it was found that the strength of fixation interface in the ±z directions (rotations about the y-axis) was the limiting factor. This was because the fixation interface was the weakest at resisting moments about the y-axis and the FE model predicted that moments about the y-axis would be close to the magnitude needed to cause slip. However, in reality it was believed that the strength of the fixation interface to resist rotations about the y-axis would be adequate because the cross section of the C1 posterior arch (in the sagittal plane) is not circular. Rather, it is elliptical in shape and clamping to an elliptical cross section would provide better resistance to slip about the y-axis than a circular cross section. Additionally, no failure was noted in any of the components of the clamp implant under the loading conditions tested. For these reasons, it was decided to set the specification for the torque of the jaw locking screws to 1.5 Nm and proceed to testing the clamp in a cadaveric study.

5.2 Cadaveric Testing

No critical flaws were identified during benchtop testing of the C1 clamp implant and as a result, the next step was to experimentally test the full C1PA/C2TL and C1PA/C2P constructs in a cadaveric study. A detailed description of the testing protocol for the cadaveric study has been provided in this section and was based on the protocol proposed by Wilke et al[74]

The purpose of the cadaveric testing was to determine the stability of the novel C1PA/C2TL and C1PA/C2P constructs relative to commercially available constructs by measuring C1-C2 motions at specific boundary loads and specific motions. Additionally, a number of important things were observed during testing such as gross slippage of the constructs, failure of construct components and fractures in the bony anatomy as a result of stresses imposed by the constructs. Together, the stability of the novel constructs relative to the commercially available constructs and the qualitative observations presented above were the best predictor of clinical success in terms of long term C1-C2 fusion rates for the novel constructs.

5.2.1 Testing Apparatus and Materials

The spinal loading simulator used in the study was a modified Instron (Illinois Tool Works, Norwood MA) frame that was able to separately apply flexion/extension, axial rotation and lateral bending motions in a continuous fashion to cadaveric specimens held in the testing fixture (Figure 58). The fixture consisted of a superior cup attached to a frame that could apply flexion/extension and an inferior cup that sat on a ball bearing surface. A multi-linkage arm connected to a motor controlled the amount of flexion/extension motion applied to the superior cup. The same multi-linkage arm was used to apply lateral bending motion but to accomplish this, the testing fixture had to be rotated by 90º. Two hydraulic cylinders that actuated in opposite directions were used to apply axial rotation to the inferior cup of the fixture. A steel rod was used to connect the hydraulic cylinders to the inferior cup when performing axial rotation tests. The rod was removed when testing all other motion types to allow for the inferior cup to move freely on the ball bearing surface. An NDI (Northern Digital, Waterloo, ON) optical tracker was used to record the motions of the cadaveric specimens. This required the mounting of optical markers on the specimen as well as on the superior and inferior cups of the testing fixture.

Loading under each type of motion was recorded with a series of sensors. For flexion/extension, a torque sensor (not shown in Figure 58) was used to measure the applied moment during motion. Each hydraulic cylinder was equipped with a load cell to measure the

"axial rotation" force it applied in the horizontal direction that produced axial rotation of the inferior cup of the fixture. Also, the Instron frame was equipped with a load cell to measure compressive vertical forces.
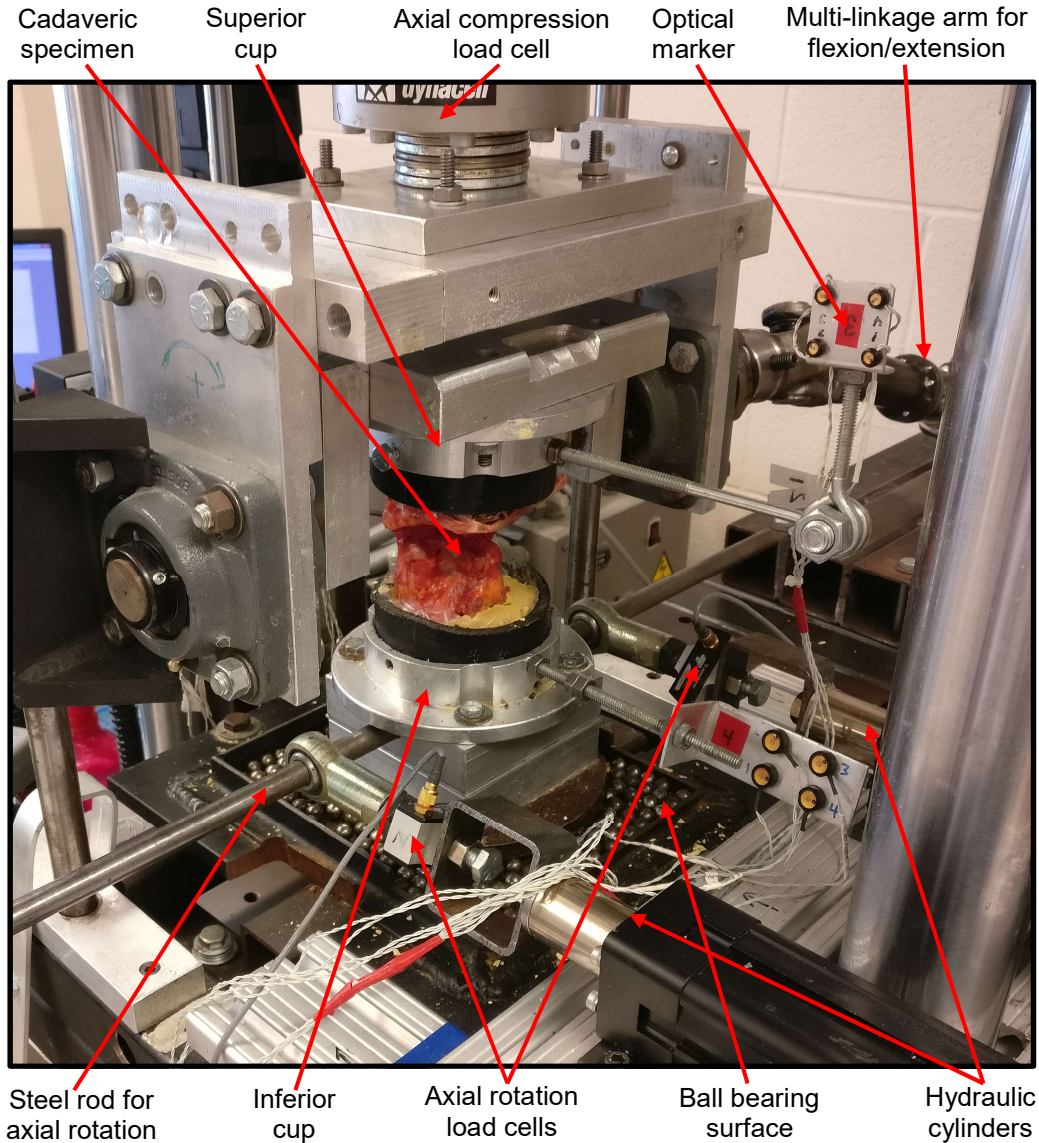
Figure 58: Spinal loading simulator used for the cadaveric study

For this study, 8 fresh frozen cadaveric specimens containing the C0-C3 vertebrae were used. The average age of the specimens was 76.5 yrs (range: 69 - 85 yrs) and there were 6 male specimens and 2 female specimens. These specimens were deemed to be an acceptable representation of the demographic that the clamp implant targeted. Before testing, the specimens were fully thawed and dissections were performed until only the bony anatomy and ligamentous

structures were intact. Dissections were performed under the supervision of an orthopaedic surgeon (thesis co-supervisor Dr. Parham Rasoulinejad), with some help from an orthopaedic resident (Dr. Supriya Singh) to ensure that the specimens were properly prepared without spurious damage to the ligaments or vertebral bodies. Additionally, the pilot holes required for the polyaxial screws were drilled by Dr. Rasoulinejad and Dr. Singh. Due to scheduling conflicts with the surgeons, all 8 specimens were dissected in one day and then refrozen until each specimen was required for testing. This was deemed to be acceptable due to a study by Tan et al[75] which reported that a significant change in NZ and ROM characteristics of cadaveric spines was not detected after 2 freeze thaw cycles.

The night before testing was scheduled to take place, a dissected cadaveric specimen was removed from the freezer to allow adequate time for thawing. The next morning, potting in the fixture cups was carried out as follows. The first step was to drills screws into C0 and C3 to increase the potting fixation strength (Figure 59a). Next, a 3.5 inch PVC tube was placed into the superior cup and lined with plastic wrap. Dental cement was then poured into the PVC tube and then the C0 end of the cadaveric specimen was placed in the cement until the cement had fully cured (Figure 59b). To ensure proper alignment, the superior cup (with the cadaveric specimen) was then attached to the Instron frame. The inferior cup was then aligned to the neutral position using the hydraulic cylinders and steel rod. Another section of PVC pipe was then placed into the inferior cup and lined with plastic wrap (Figure 59c). Using the Instron controls, the superior cup was then lowered until the screws placed in C3 were very slightly contacting the inferior cup (tests were run at 0N of axial compression). Modern Materials dental cement (Heraeus Kulzer, South Bend, IN) was then poured into the inferior cup and after curing the excess plastic wrap was trimmed off and optical markers were attached to the specimen (Figure 59d).

Figure 59: Potting procedure for cadaveric specimens: a) screws placed into C0 and C3 for additional potting strength, b) C0 potted first in dental cement, c) C3 potted second in Instron to ensure proper alignment and d) potted specimen with optical markers attached

Motion tracking of the cadaveric specimens was performed using a three camera optical tracker system with rigid body LED markers (Northern Digital, Waterloo ON). Four LED markers were used in the experimental setup: the first marker was attached to C2, the second marker was attached to C1, the third marker was attached to the superior cup of the testing jig and the fourth marker was attached to the inferior cup of the testing jig. A global coordinate system was established as follows: the superior direction was set to be the positive y-axis, the anterior direction was set to be the positive x-axis and the positive z-axis was in the lateral direction (based on the right hand rule). To establish a local coordinate system on each vertebra, anatomical reference points were digitized on each vertebra with respect to the LED marker on the same vertebra. Four anatomical reference points were used on each vertebra. For C2, the

right most (point 1) and left most (point 2) points on the transverse foramina as well as the inferior (point 3) and superior (point 4) points of the vertebral body were used. For C1, the right most (point 5) and left most (point 6) points of the transverse foramina as well at the inferior (point 7) and superior (point 8) points on the anterior arch were used as the anatomical reference points (Figure 60). Local axes were then set up on each vertebra by performing a series of cross product calculations. To use C2 as an example, vectors were created between point 1 and point 2, and point 3 and point 4. The vector created by points 1 and 2 was used as the local z-axis. The local x-axis was created by calculating the cross product of the local z-axis and the vector created by points 3 and 4. Finally, the local y-axis was created by calculating the cross-product between the local x-axis and the local z-axis. A similar procedure was used for C1 and the full MATLAB code is presented in Appendix A3.
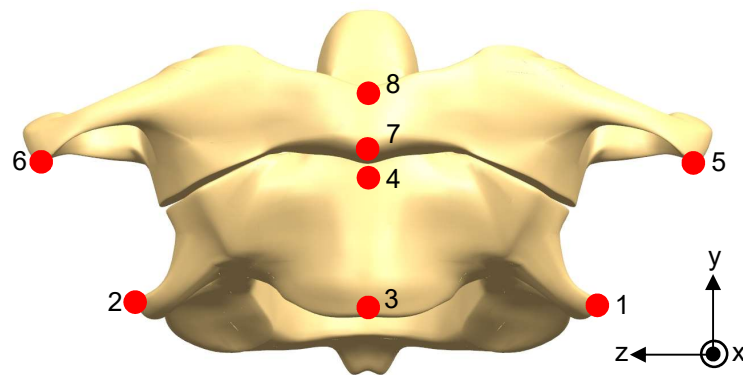
Figure 60: Anatomical reference points on C1 and C2 used in digitization process for optical tracking

The local coordinate systems established on C1 and C2 were used to calculate Euler angles which captured the rotation of C1 relative to C2. The order in which the Euler angles were calculated differed depending on the type of motion that the cadaveric specimen was being tested for. For flexion/extension, the Euler angles were first calculated about the z-axis (primary axis of motion) followed by the y and x axes of rotation (coupled axes of rotation). For axial rotation, the Euler angles were first calculated about the y-axis (primary axis of motion) followed by the z and x axes of rotation (coupled axes of rotation). For lateral bending, the Euler angles were first calculated about the x-axis (primary axis of motion) followed by the y and z axes of rotation (coupled axes of rotation). An existing MATLAB code was used for these Euler calculations and has been presented in Appendix A3.

To control the motion of this spinal loading simulator, a code was written (Appendix A4) using DMC smart terminal (Galil Motion Control, Rocklin CA). For all motion types, displacement controlled motion was applied at a rate of 2º/second until the specified load limit of 1.5 Nm was reached. For flexion/extension and lateral bending the torque sensor on the multi-linkage arm was able to directly measure the applied moment. For axial rotation however, the linear motion and axial loads of the hydraulic cylinders had to be converted to rotational motion and applied moments. This was done by passing a steel rod through the inferior portion of the testing jig and connecting it to the hydraulic cylinders through the use of ball joints. To apply axial rotation to the testing jig, the superior cup was held stationary while the hydraulic cylinders moved in opposite directions to rotate the inferior cup. The applied axial rotation moment (M_y) was calculated by multiplying the measured force applied by each load cell times the moment arm created between each hydraulic cylinder and the inferior cup (Figure 61).
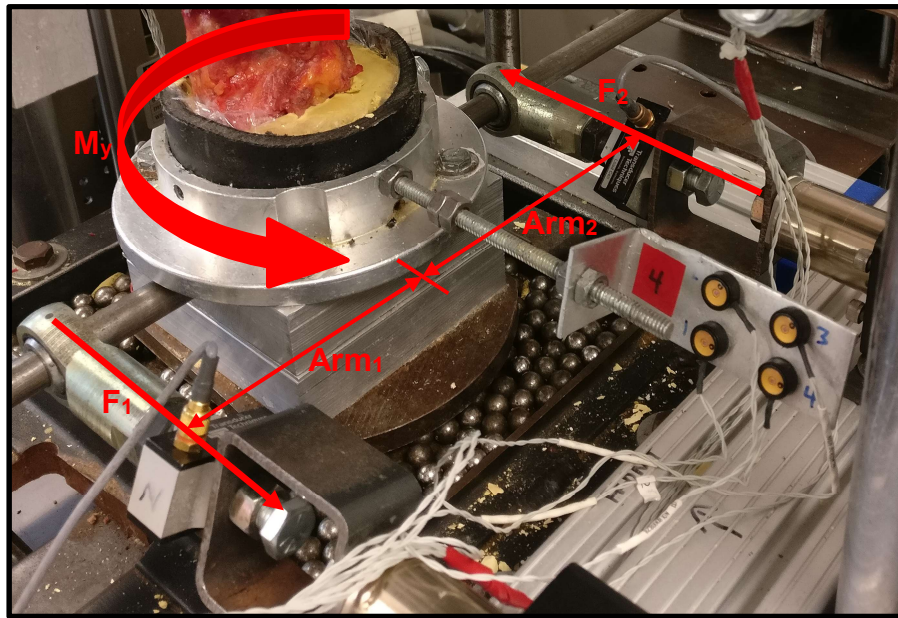
Figure 61: Axial loads and moment arms used to calculate the applied moment for axial rotation

Calibration procedures were used to maintain the accuracy of the load cells used in the spinal motion simulator. The load cells on the hydraulic cylinders were removed before testing each day and calibrated using a two-point linear fit. The first data point used for the linear fit was the measured voltage output from the load cell with no load applied. A hook was then attached to

the load cell and the voltage output when a 10 kg mass (applying a 98.1 N force) was hung from the load cell and this gave the second data point. Equations were then developed for the load control code so that voltage output (V) could be converted to the axial force (F) measured by the load cell in Newtons (Equation 7). Ideally, more than two points would have been used to calibrate the load cells used on the hydraulic cylinders to get an independent estimate of the error. However, the load cell response was known to be linear and accurate ($\pm\,0.02\%$) and so this two-point check performed daily was considered adequate.

$$F = \frac{(V_{10kg} - V_{no\ load})}{(F_{10kg} - 0)} \cdot (V - V_{no\ load}) \qquad (7)$$

$$\text{Where } F_{10kg} = 98.1N$$

To calibrate the torque sensor used to measure the moment applied to the multi-linkage arm for flexion/extension and lateral bending, a 6-point linear calibration, with 5 repeats at each point was used (Figure 62). A torque wrench was used to apply known torques to the multi-linkage arm and a zero load condition was also recorded. Regression analysis was performed using Minitab (Minitab Incorporated, State College, PA) to determine an equation for the output voltage (V) as a function of the applied moment (M) (Equation 8). The equation was then re-arranged to show applied moment as a function of output voltage in order to be used in the load control code (Equation 9). The torque sensor on the multi-linkage arm was not easily removable and as a result the calibration for this sensor was only done once. However, this calibration used multiple points and repeats and the regression was very strong ($R^2 = 99.83\%$).
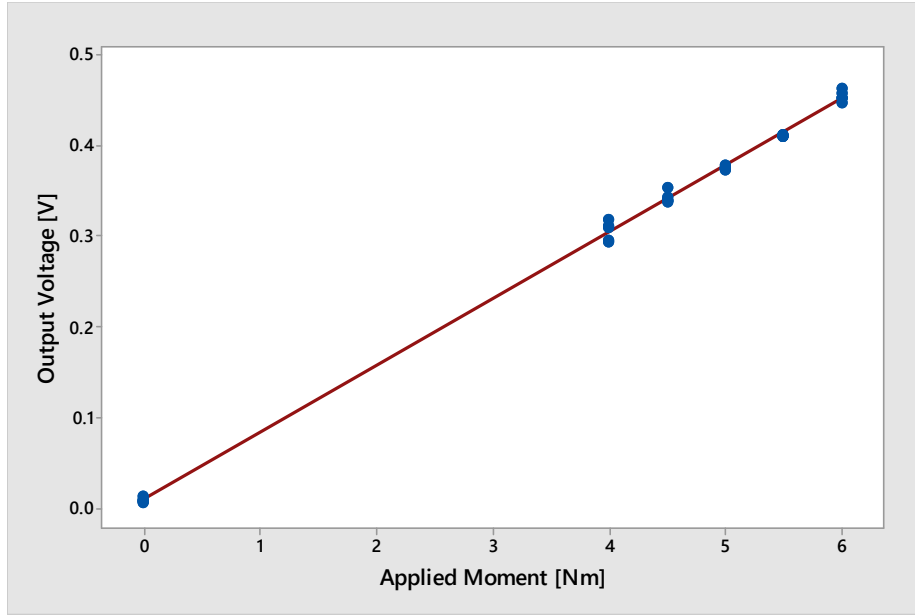
Figure 62: Calibration of torque sensor on multi-linkage arm

$$V = 0.074 \cdot M + 0.0089 \qquad (8)$$
$$M = 13.51 \cdot V - 0.12 \qquad (9)$$

When testing the control logic for the spinal loading simulator, it was found that there was considerable noise in the electrical signal coming from the load cells and the torque sensor. This caused the load limit of 1.5 Nm to be tripped early and resulted in inconsistent loading of the spine specimens due to the unpredictable nature of the signal noise. To fix this problem, a signal averaging technique which specified that the average of the last seven data points had to be greater than or equal to 1.5 Nm was implemented as the criteria for the load limit. Of course, signal averaging caused a slight lag in the control logic but this was not noticeable on a macro scale since the sample rate from the load cells and torque sensor was 1024Hz and motion was only applied at a rate of 2 °/s. Using signal averaging allowed the control logic to be very consistent and predictable, however the raw data that was recorded for analysis was still very noisy so for visualization purposes a Butterworth filter with a cutoff frequency of 2 Hz was used (Figure 63).
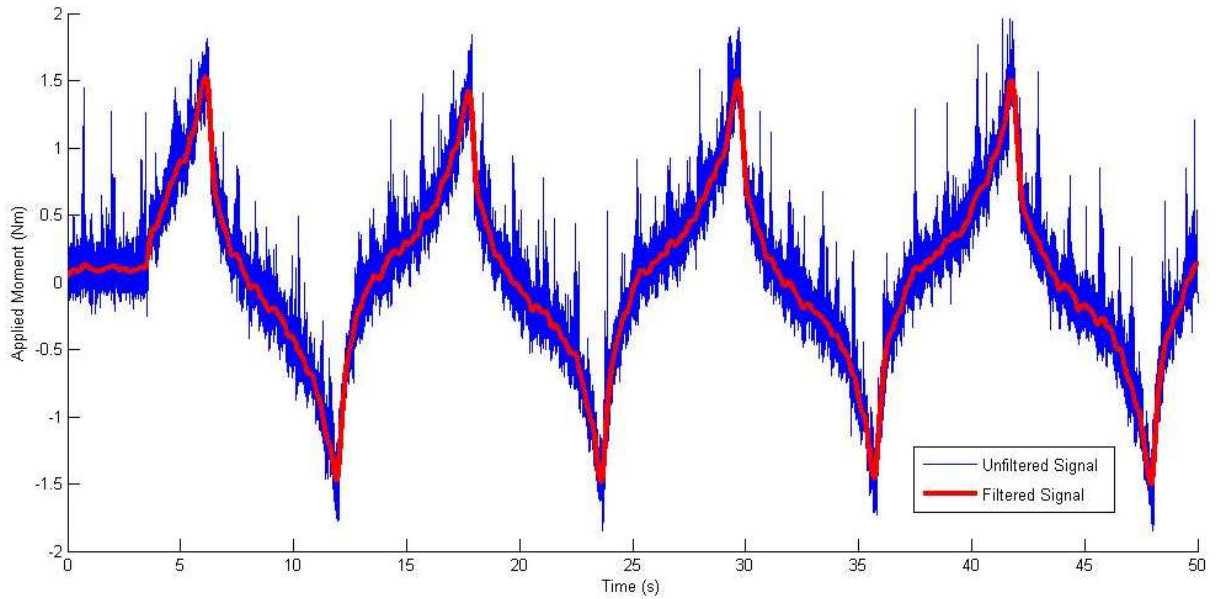
Figure 63: Example of filtered and unfiltered signal from torque sensor for the case of lateral bending

The amount of axial rotation that could be applied to the cadaveric specimens was limited to ±16.5º from the neutral position due to the stroke lengths of the hydraulic cylinders. This was deemed acceptable since all of the devices tested were fusion constructs designed to limit axial rotation to much less than 16.5º.

5.2.2 Testing Protocol

All of the cadaveric specimens were tested under flexion/extension, lateral bending and axial rotation for the following cases: intact specimen, destabilized specimen (simulated type II odontoid fracture), destabilized specimen with Harms construct, destabilized specimen with C1PA/C2TL construct and destabilized specimen with C1PA/C2P construct. The duration of testing for each specimen was less than 10 hours in all cases and was not expected to significantly affect the results of the study. After testing was completed on two specimens, it was decided to add an additional test case since the testing duration per specimen was fairly short. The case that was added was a C1LM/C2TL construct. For all specimens, the intact case was always tested first, followed by the destabilized case and then each construct. The order in which the constructs were tested was randomized and the testing order of the motion types was also randomized within each construct case. The destabilization (simulated odontoid fracture) was created from the anterior side of the C2 vertebra using a high speed burr (Figure 64). Specimens

were kept moist throughout the entire duration of testing by spraying them with a 0.9% NaCl saline solution periodically. The average temperature of the testing laboratory was 20.9°C (range 20.0 °C to 23.5 °C) and the average humidity of the testing laboratory was 22.1%RH (15.0%RH to 26.0%RH). For each motion type, a total of four cycles were run with a single cycle consisting of motion in the positive and negative directions until the load limit of 1.5 Nm was reached. The first three cycles were used to precondition the specimen and minimize the viscoelastic effect of the specimens. ROM (average absolute values of C1-C2 motion at a load of ±1.5 Nm) data was collected from the fourth cycle and used for analysis.
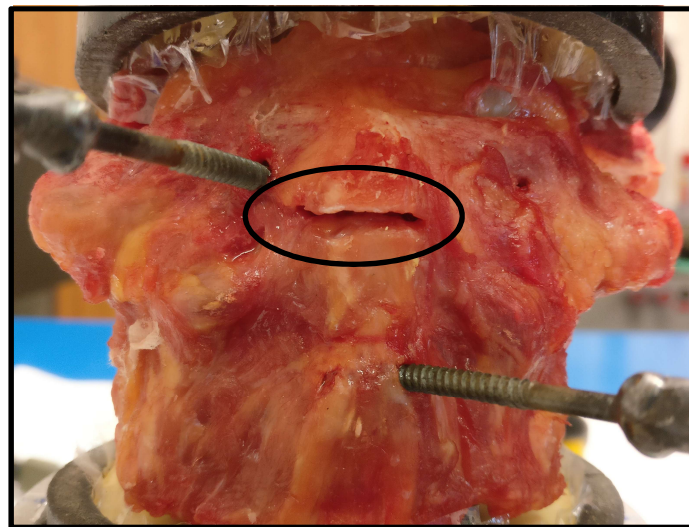
Figure 64: Type II odontoid fracture created from the anterior side of the C2 vertebra using a high speed burr

As mentioned previously, the pilot holes necessary for each construct were placed by an orthopaedic surgeon (Dr. Rasoulinejad) or an orthopaedic resident (Dr. Singh). Fit of the C1 clamp on the posterior arch was then assessed and a decision to use either the small clamp of the large clamp was made for each specimen. Specimens were removed from the spinal load simulator every time a construct change was made (Figures 65 & 66). Before testing, a torque wrench was used to tighten each construct to the torque specification. For constructs requiring a C1 clamp, the jaw locking screws were torqued to 1.5 Nm and the polyaxial rod cap screws were torqued to 5.0 Nm (based on the specifications determined from benchtop testing). Additionally, commercially available polyaxial screws were used and the cap screws for these screws were

tightened to 1.5 Nm as specified by the manufacturer (Medtronic Sofamor Danek, Memphis, TN).
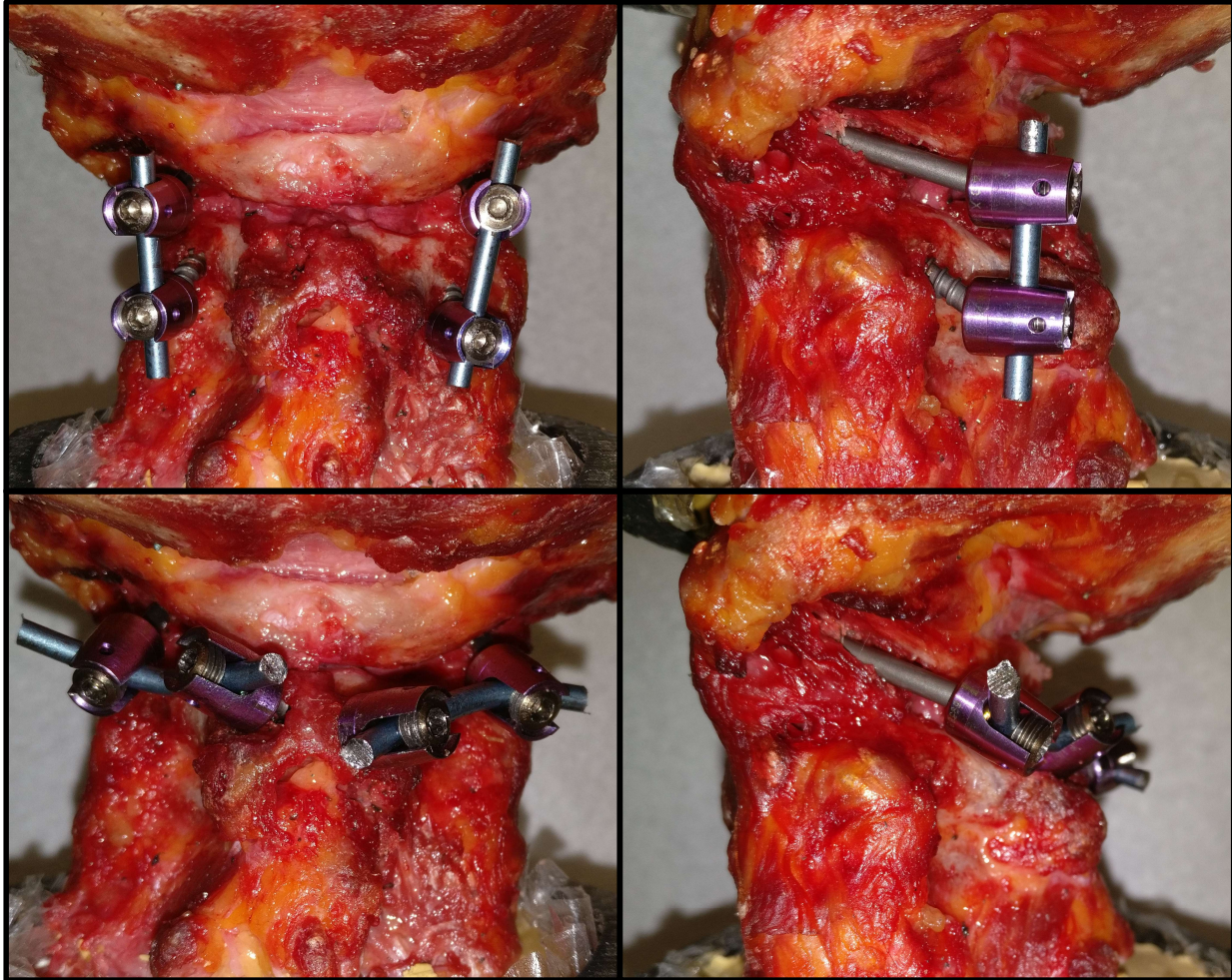
Figure 65: Clinically available constructs that were tested: Harms construct shown in a) posterior view and b) lateral view and C1LM/C2TL construct shown in c) posterior view and d) lateral view
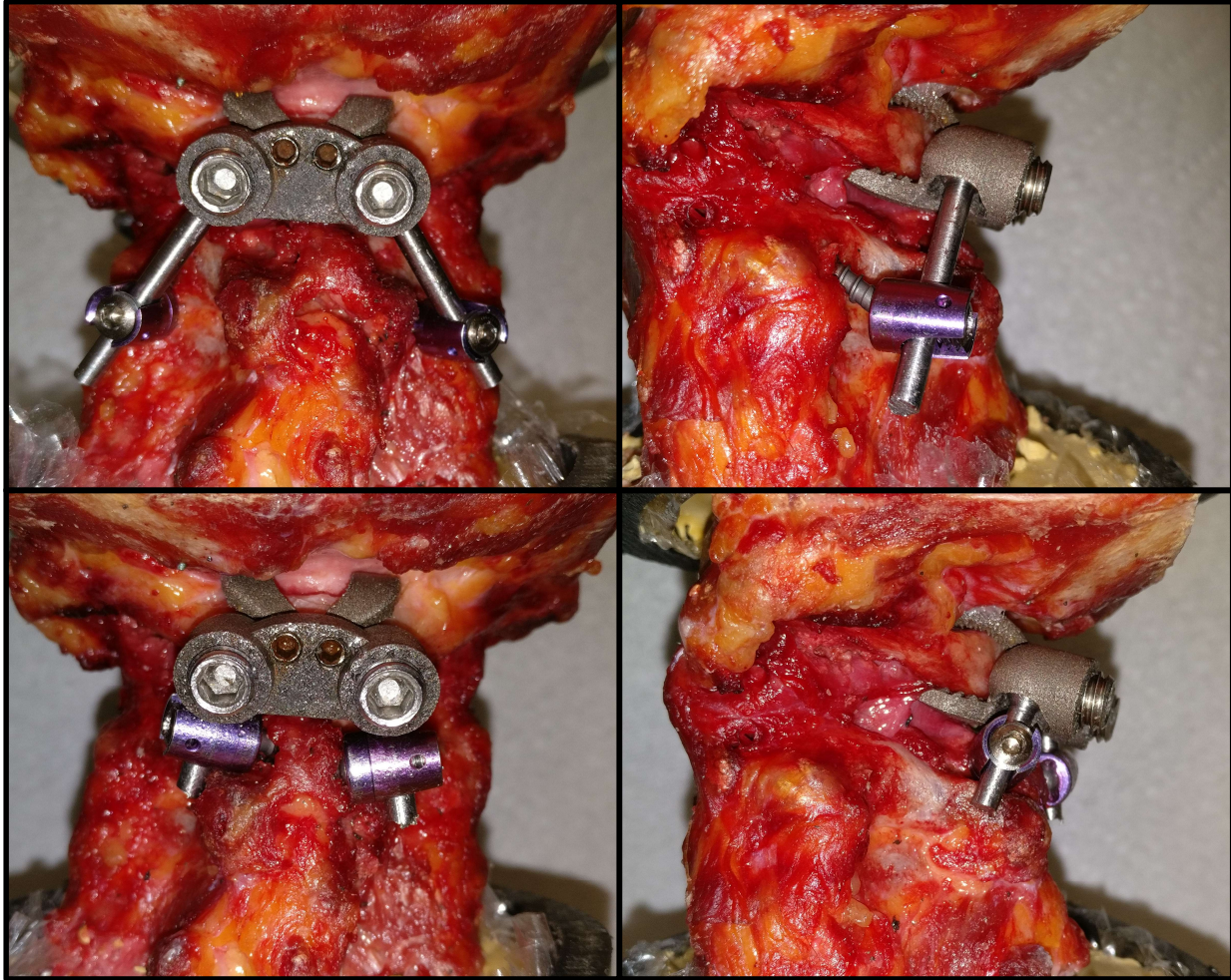
Figure 66: Novel constructs with C1 clamp that were tested: C1PA/C2P construct shown in a) posterior view and b) lateral view and C1PA/C2TL construct shown in c) posterior view and d) lateral view

5.2.3 Statistical Analysis

Statistical analysis was performed using Minitab (Minitab Incorporated, State College PA). Statistical analysis was independently performed for each motion type (flexion/extension, lateral bending and axial rotation) and the experimental data for each motion type was broken down into two sets. The first dataset included the ROM data for the intact and destabilized states and was used to determine if there was a significant difference in ROM between states by performing a repeated measures ANOVA. A repeated measures ANOVA accounts for the fact that multiple states were tested on each cadaveric specimen and therefore is able to isolate the specimen to specimen variability from the construct to construct variability[76]. The second dataset

included the ROM data for each construct state (Harms, C1LM/C2TL, C1PA/C2P, C1PA/C2TL) and was used to determine if there was a significant difference in ROM between states by once again performing a repeated measures ANOVA. Multiple comparisons were then made post hoc using the Bonferroni method to determine which pairs of constructs showed a significant difference in ROM[77]. In all cases, a confidence interval of 95% was used to determine significance.

For the statistical methods used, it was assumed the ROM data for each testing case followed a normal distribution and that the variances of all cases tested were equal. Since the sample size was relatively small (maximum of 8 ROM values per testing case) normality could not be confirmed or denied. Small sample size is an inherent limitation of cadaver studies due to time and cost constraints, the effects of this limitation are further detailed in the proceeding discussion section. To test the equal variance assumption, a Barlett's test was performed for each dataset within each motion type.

6.0 Results for Cadaveric Testing of Fusion Constructs for the C1-C2 Vertebrae

All 8 cadaveric specimens were tested following the protocol described in the previous section. Important information related to each specimen has been provided in Table 20.

Table 20: Summary of specific data related to the testing of each cadaveric specimen

Specimen ID	Age	Sex	Clamp Size	Temperature	Duration	Notes
1611025	69	M	Large	23.5ºC	9.5 hrs	Loosening in C2TL screws
1611001	82	M	Large	20.0ºC	7.5 hrs	Loosening in C2TL screws
1611032	82	M	Small	20.0ºC	6.5 hrs	Strong fixation in C2TL screws
1610057	68	M	Small	20.0ºC	6.5 hrs	Strong fixation in C2TL screws
1611037	69	F	Large	21.5ºC	6.5 hrs	Strong fixation in C2TL screws
1601038	79	M	Small	21.0ºC	7.0 hrs	Strong fixation in C2TL screws
1612052	78	F	Small	20.5ºC	6.0 hrs	Loosening in C2TL screws
1612055	85	M	Small	21.0ºC	7.0 hrs	Loosening in C2TL screws

6.1 Load-Displacement Plots

Two time dependent plots for each testing case were obtained during experimental data collection: the applied moment plot (Figure 67) and the C1-C2 primary rotation plot (Figure 68). The first three cycles of each plot represented the preconditioning region and the fourth cycle was the analysis cycle used to generate load-displacement plots (Figure 69). Analyzing how the shapes of these plots changed from test case to test case was not considered important for analyzing the performance of each construct. However, it is important to understand how the ROM value for each test case was calculated so plots have been provided for intact test case in lateral bending for specimen 1611001 for illustration. The full raw data for each test case would be available upon written request to the present author.
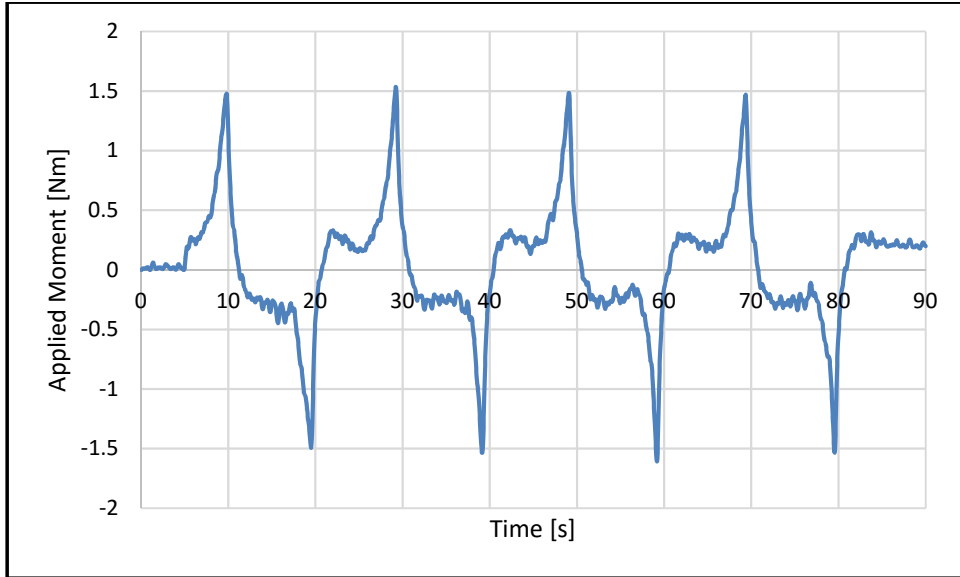
Figure 67: Example applied moment plot for the intact case in lateral bending
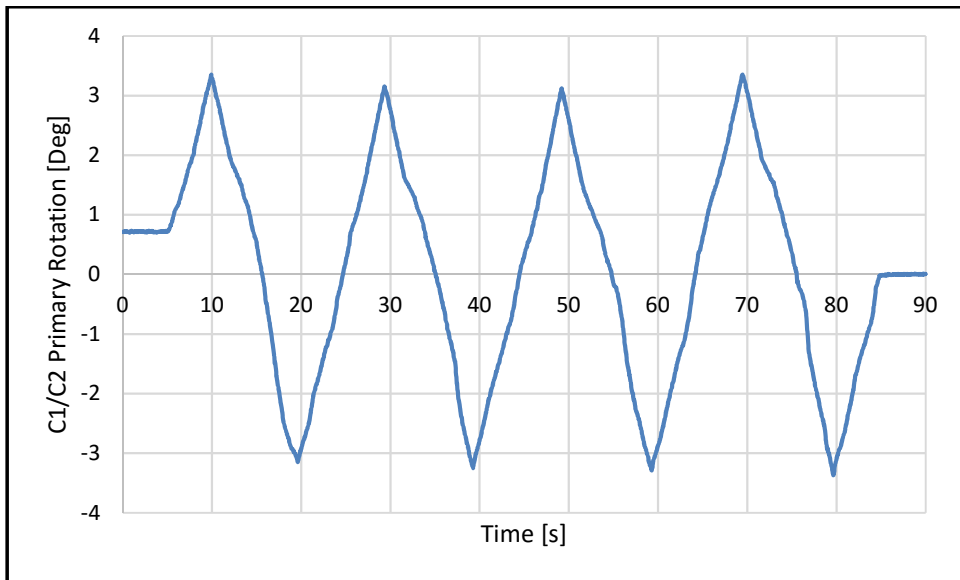
Figure 68: Example of C1-C2 primary rotation plot for the intact case in lateral bending
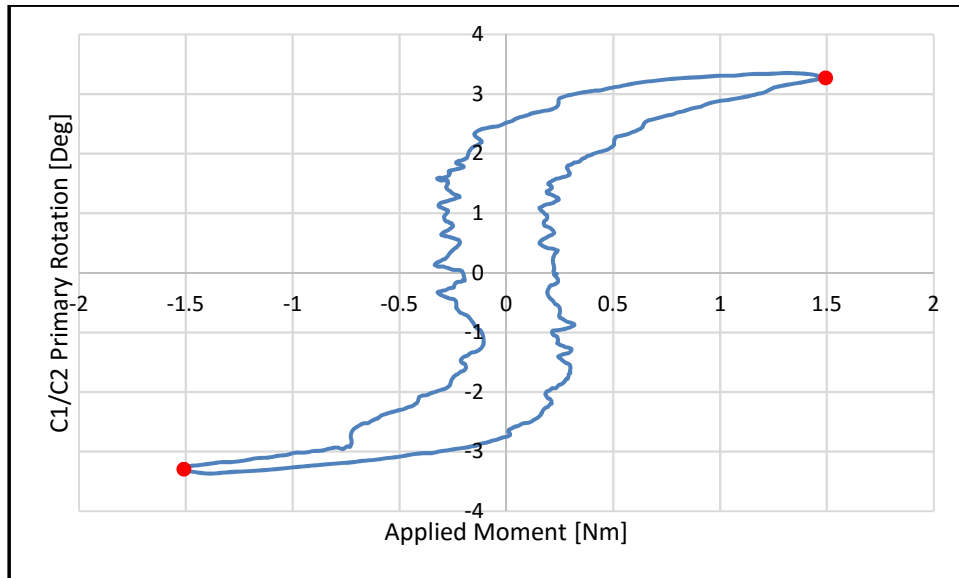
Figure 69: Example of load-rotation curve for the intact case in lateral bending (absolute values of red points averaged to calculate ROM)

6.2 ROM of Intact Case and Destabilized Case

In general, the ROM significantly increased for all cases ($p<0.05$) when a type II odontoid facture was created for the destabilized case (Figure 70). The only exception to this was for axial rotation where the ROM of the destabilized case was equal to the ROM of the intact case due to the physical limitation of the spinal loading simulator. For flexion/extension the significant increase was reflected in a p-value of 0.02 and for lateral bending the significant increase was reflected in a p-score of 0.01. Barlett's analysis suggested that the equal variance assumption held true for both flexion/extension ($p = 0.24$) and lateral bending ($p = 0.81$).
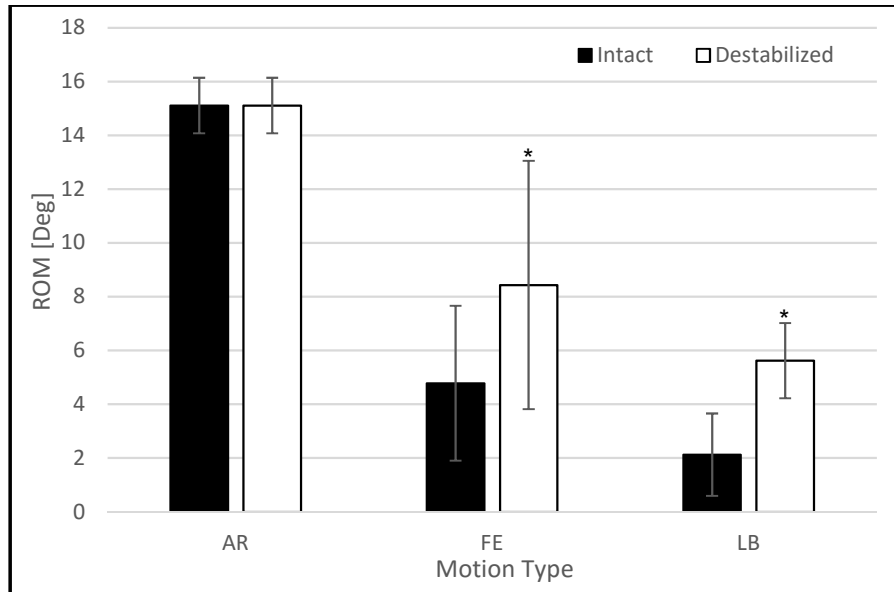
Figure 70: Comparison of intact case to destabilized case for all motion types (* indicates a significant difference compared to the intact state)

6.3 ROM of Construct Cases

In flexion/extension (Figure 71), it was found that the type of construct had a significant effect on the ROM response (p = 0.001). Performing Bonferroni multiple comparisons showed that constructs incorporating the C1 posterior arch clamp had significantly less ROM than constructs that did not incorporate the C1 posterior arch clamp. Additionally, no significant difference was detected between the ROM of the C1PA/C2P and C1PA/C2TL constructs and no significant difference was detected between the ROM of the C1LM/C2TL and Harms constructs (Figure 72). Barlett's analysis showed that the equal variance assumption did not hold true (p = 0.01).
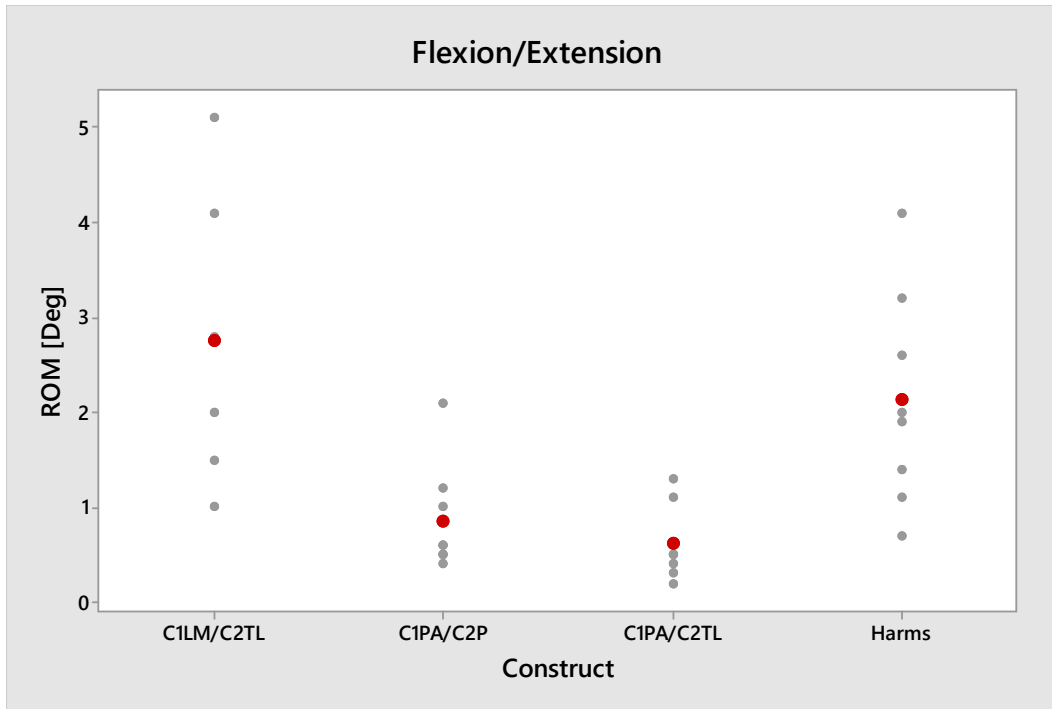
Figure 71: Individual values plot for construct ROM's in flexion/extension (group average shown in red)
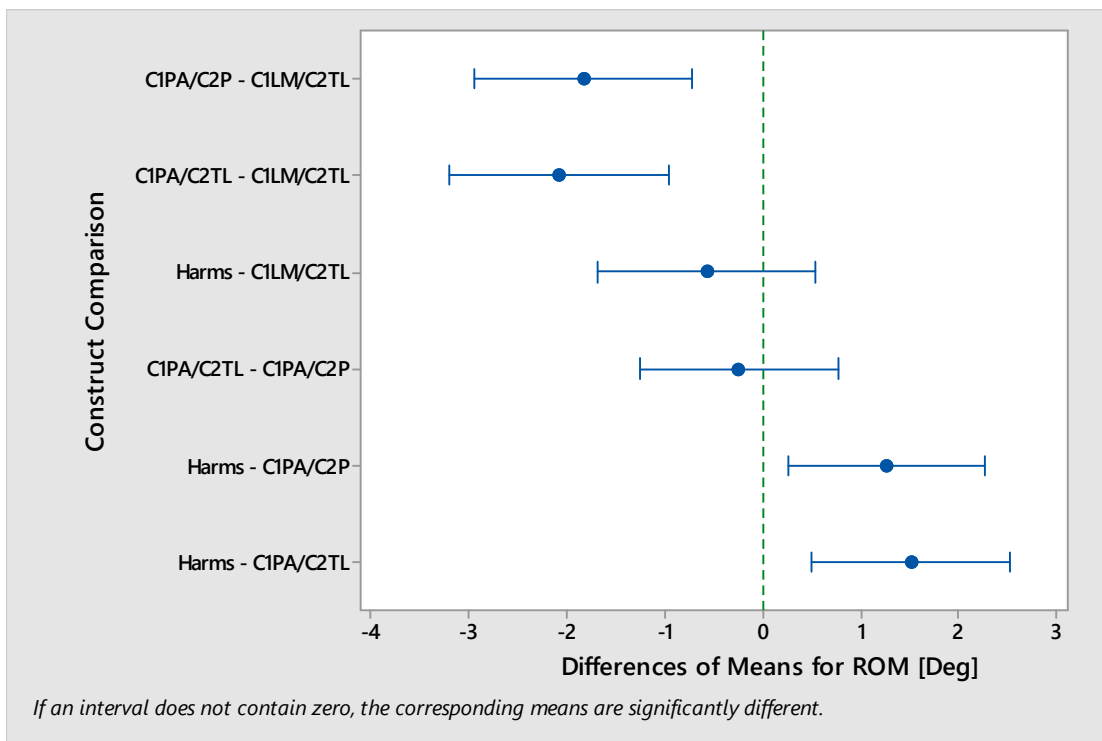
Figure 72: Multiple comparisons of construct ROM differences using Bonferroni method for flexion/extension

In axial rotation (Figure 73), it was found that the type of construct had a significant effect on the ROM response (p = 0.001). Performing Bonferroni multiple comparisons showed that the Harms construct and constructs incorporating the C1 posterior arch clamp had significantly less ROM than the C1LM/C2TL construct. Additionally, no significant differences were detected for all other construct comparisons (Figure 74). Barlett's analysis showed that the equal variance assumption did not hold true (p = 0.04).
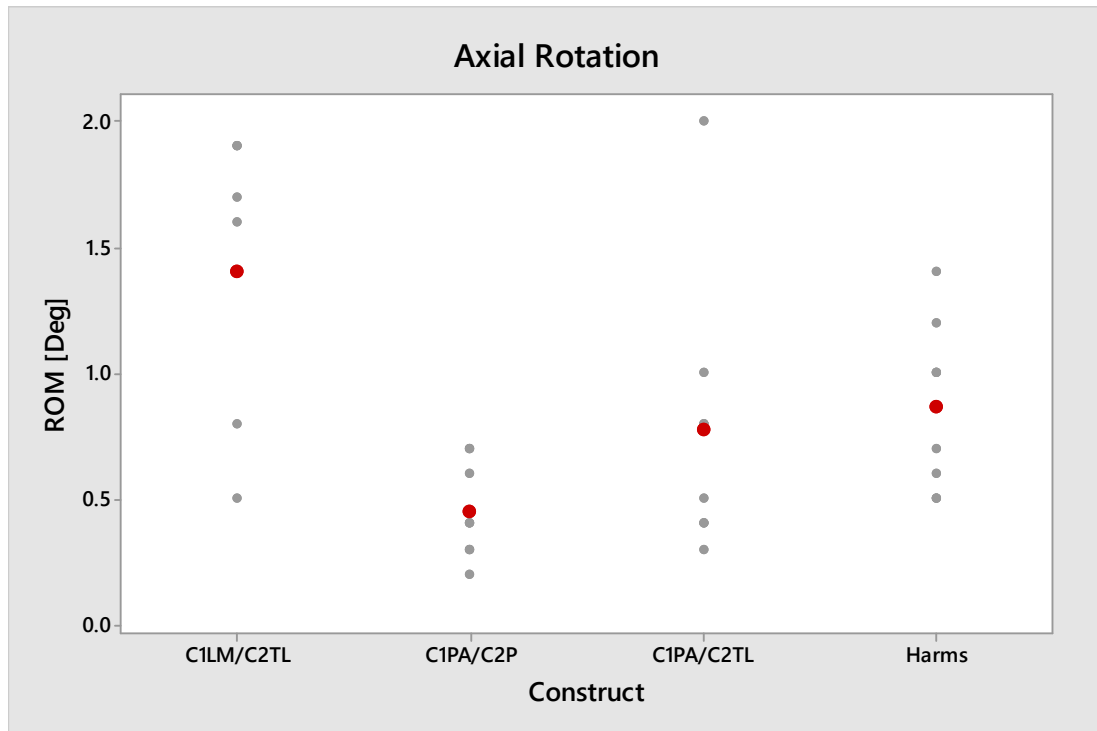
Figure 73: Individual values plot for construct ROM's in axial rotation (group average shown in red)
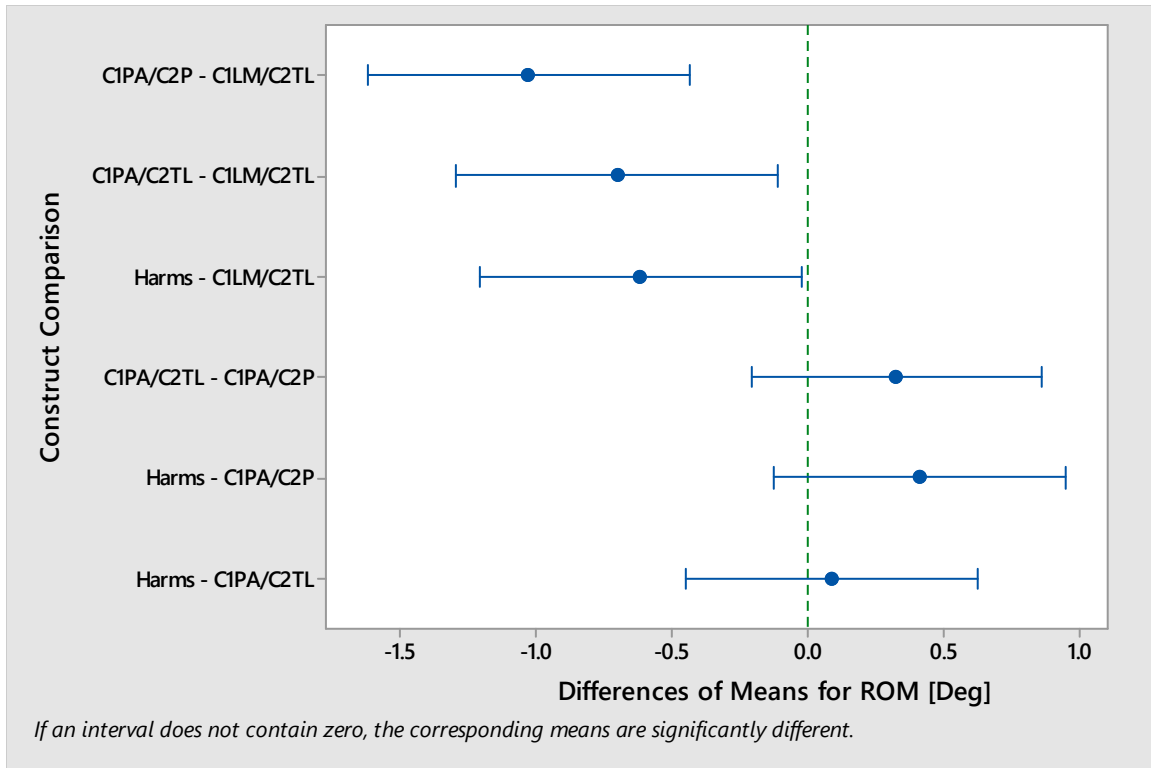
Figure 74: Multiple comparisons of construct ROM differences using Bonferroni method for axial rotation

In lateral bending (Figure 75), it was found that the type of construct had a significant effect on the ROM response (p < 0.001). Performing Bonferroni multiple comparisons showed that constructs incorporating the C2 translaminar screws had significantly more ROM than constructs that incorporated C2 pedicle screws. Additionally, no significant difference was detected between the ROM of the C1PA/C2TL and C1LM/C2TL constructs and no significant difference was detected between the ROM of the C1PA/C2P and Harms constructs (Figure 76). Barlett's analysis showed that the equal variance assumption did not hold true (p = <0.001).
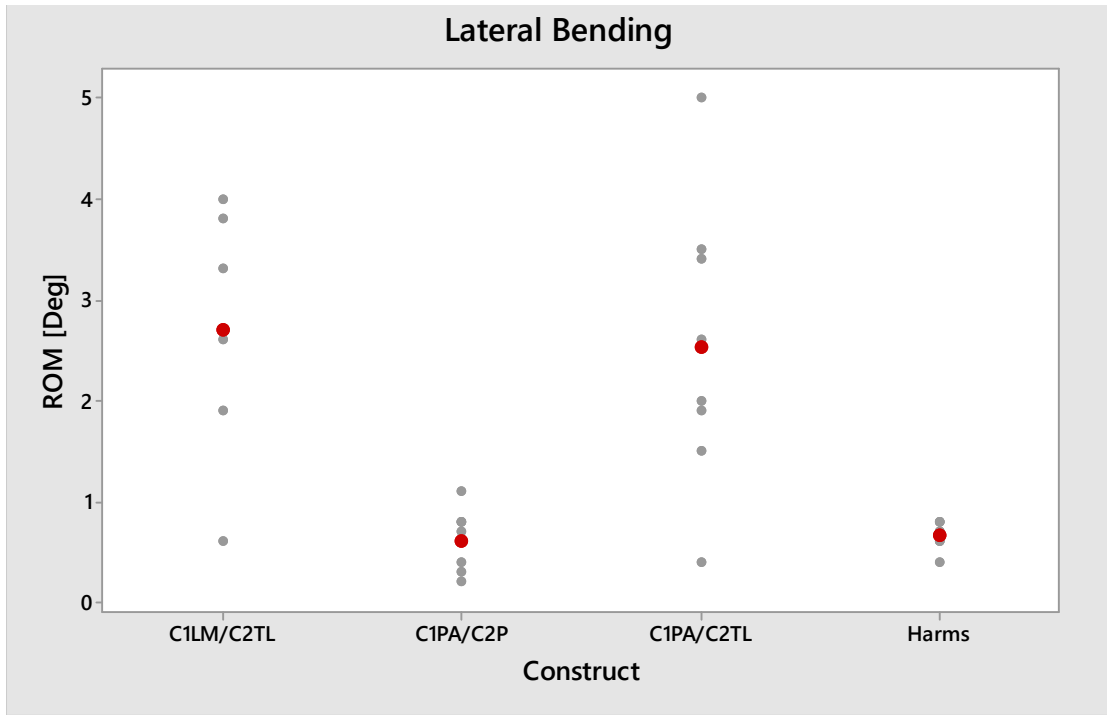
Figure 75: Individual values plot for construct ROM's in lateral bending (group average shown in red)

If an interval does not contain zero, the corresponding means are significantly different.
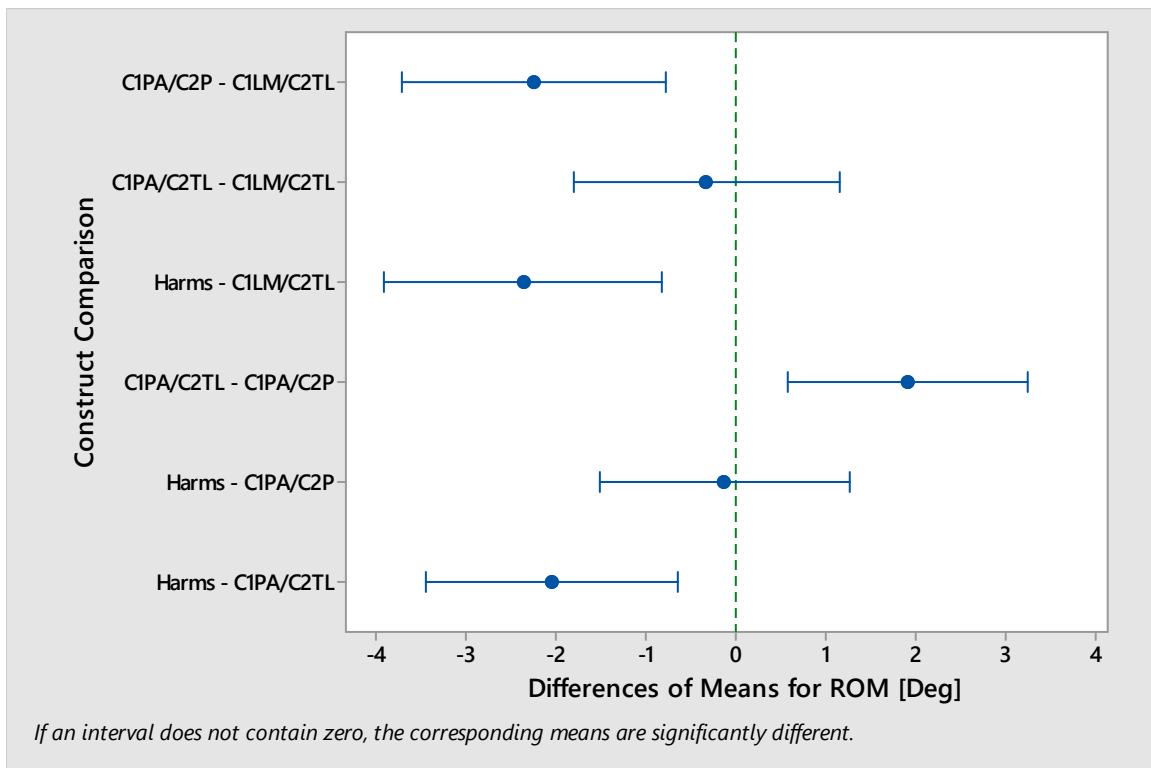
Figure 76: Multiple comparisons of construct ROM differences using Bonferroni method for lateral bending

111

To provide a comparison of each construct to the Harms procedure, the ROM results from all motion types have been summarized (Table 21).

Table 21: Comparison of ROM for each construct to the Harms

Construct	Flexion/Extension	Axial Rotation	Lateral Bending
C1LM/C2TL	Failed to detect significant difference to Harms	Significantly more ROM than Harms	Significantly more ROM than Harms
C1PA/C2TL	Significantly less ROM than Harms	Failed to detect significant difference to Harms	Significantly more ROM than Harms
C1PA/C2P	Significantly less ROM than Harms	Failed to detect significant difference to Harms	Failed to detect significant difference to Harms

7.0   Discussion and Conclusions

The approach to design that was presented in this thesis proved to be very efficient for developing a new implant for the posterior arch of C1. Starting with the FE modeling phase, a set of optimized ligament laxities were determined to achieve the best agreement between the model and experimental ROM data under physiological loads. The methodology used in the ligament laxity optimization allows for the laxity values presented in this thesis to be implemented in other FE models as a lateral shift in the force displacement curves for each ligament. This is beneficial because it allows future researchers to incorporate ligament laxity into their models to generate realistic ROM values without having to perform another optimization study.

Ensuring that the FE models with an intact odontoid and a fractured odontoid generated realistic ROM values were the best indicators that the predicted ROM values in the FE models with simplified fusion constructs would also be accurate. Modeling simplified fusion constructs was very useful in the design process for two reasons. Firstly, the simplified fusion constructs were able to assess the feasibility of using the C1 posterior arch as a fixation location by predicting the stability of novel constructs that utilized the C1 posterior arch as a fixation site to the predicted stability of clinically available constructs that utilized the C1 lateral mass as a fixation site. A direct result of these comparisons was the introduction of the C1PA/C2P construct after the FE model predicted that the C1PA/C2TL construct would not be as stable as the Harms construct in lateral bending and axial rotation. The second benefit of modeling simplified fusion constructs was that construct loads were also predicted. These loads were used during benchtop testing of the posterior arch clamp to determine the tightening specifications necessary for the clamp locking mechanisms to avoid slippage under physiological loads.

Benchtop testing of the clamp was able to assess the strength of the locking mechanisms and clamp fixation without additional FE modeling. While FE modeling could also have been used for this strength assessment, the complexity and further validation that would have been required for the model was deemed to be too time consuming and likely would not have yielded results that were any better than those obtained through benchtop testing.

In cadaveric testing, all constructs effectively reduced ROM at C1-C2 compared to the destabilized state. Statistical analysis between the destabilized and stabilized states (by means of construct implantation) was omitted because the reduction in ROM caused by construct implantation was obvious and substantial. What was more important, and not as obvious, was the

comparisons of construct ROM and more specifically how the constructs incorporating a C1 posterior clamp compared to the Harms construct. Based on the biomechanical results of the cadaveric testing, both the C1PA/C2TL and C1PA/C2P constructs have proven to be feasible alternatives to the Harms procedure in terms of stabilizing the C1-C2 joint and reducing ROM. In fact, statistical analysis of the experimental data showed that the C1PA/C2P and the C1PA/C2TL constructs were superior to the Harms procedure at reducing ROM in flexion/extension. This result was logical and expected because the constructs that incorporated the C1 posterior arch clamp created larger moment arms to resist against motion in the flexion/extension plane. For most other types of motion, statistical analysis failed to detect a significant difference in the ROM of the Harms construct and the ROM of both the C1PA/C2P and the C1PA/C2TL constructs. The only exception to this was the C1PA/C2TL construct, which showed significantly more ROM that the Harms procedure in lateral bending. This result was also logical due to the C1PA/C2TL construct having smaller moment arms to resist against motion in the lateral bending plane compared to the other constructs. However, a significant difference was not detected between the ROM of the C1PA/C2TL construct and the C1LM/C2TL construct in lateral bending. This suggests that the C1PA/C2TL construct is still clinically feasible since the C1LM /C2TL construct has been used clinically with great success in terms of high C1-C2 fusion rates. Additionally, the C1PA/C2TL construct is much safer than the C1LM/C2TL construct because there is no disturbance to the vertebral artery or C1 nerve root, further improving the clinical feasibility. In practice, the decision to use C2 translaminar screws instead of C2 pedicle screws should be made by the surgeon based on the size and integrity of the C2 lamina. The C2 lamina of the cadavers in the present study were not screened prior to testing and as a result some of the specimens were not ideal for C2 translaminar screws leading to larger ROM values during testing. It is believed that with better assessment of the C2 lamina prior to surgery, the values and variability of the ROM for the C1PA/C2TL construct would be equivalent to the C1PA/C2P construct. Further studies are needed to confirm this suggestion but if it were found to be true then it is reasonable to propose that the C1PA/C2TL construct and the C1PA/C2P construct would have the same clinical performance in terms of C1-C2 fusion rates. The only difference between these two constructs would be that the C1PA/C2TL construct would serve a slightly smaller patient population due to some patients having a small C2 lamina causing them to be poor candidates for C2 translaminar screws. To summarize, the C1PA/C2P

construct was the best at reducing ROM out of all the constructs tested and is biomechanically superior to the Harms construct. Additionally, the C1PA/C2TL construct was biomechanically superior to the C1LM/C2TL construct and should therefore still exhibit high C1-C2 fusion rates while also presenting a much safer surgical procedure when used clinically.

When performing the statistical analysis, the equal variance assumption did not hold true for all motion types when comparing the ROM of different constructs. While this reduces the strength of the conclusions that can be drawn from the statistical analysis, the increased variability of the ROM data for the C1PA/C2TL and C1LM/C2TL constructs does not have to be accepted as random error because it was believed to be a result of the C2 translaminar screws. More specifically, the anatomy of the C2 lamina of the cadaveric specimens that were tested varied largely resulting in compromised fixation strength and screw loosening for some of the C2 translaminar screws (Table 20). In future studies, the ROM variance of constructs incorporating C2 translaminar screws could be reduced by ensuring that all cadaveric specimens had adequately sized C2 lamina.

When comparing the predictions of the FE model to the experimental data, it was seen that the FE model did a fantastic job of predicting the stability of both the C1PA/C2TL and C1PA/C2P constructs. Without the use of FE modeling early in the design process, the idea to design the C1 clamp for use with either C2 translaminar screws or C2 pedicle screws would not have surfaced and as a result the clinical feasibility of the C1 posterior arch clamp would not have been as strong. Additionally, it is important to note that the constructs in the FE model were very simplified and still accurately represented the ROM performance seen in the experimental data. This builds a compelling case for the use of FE modeling early in the design iteration process because it allowed for only one round of experimental testing to act as the implant validation case (in terms of biomechanical stability).

No C1 posterior arch clamps failed during testing and gross slippage was not observed for any of the locking mechanisms, suggesting that the clamp design and benchtop testing phase adequately met the strength demands for the implant under physiological loading. Furthermore, the torque specifications for both the polyaxial rod cap screws and the jaw locking screws were validated from the experimental data because the rigidity of both clamp constructs led to ROM values that were within the range of the clinically available (Harms and C1LM/C2TL)

constructs. Additionally, there was no observable difference between the performance of the small and large C1 clamp and both have been deemed feasible C1 fixation options.

The major limitation of the present study was that it assumed that the biomechanical stability (assessed by ROM) of the novel constructs was directly correlated to the clinical feasibility, and ultimately the clinical success of each construct. In reality, the clinical success of a C1-C2 fusion construct depends primarily on maximizing the C1-C2 fusion rate and minimizing the mortality rate of type II odontoid fractures, neither of which can be tested directly in a cadaveric study. As a result, the clinical success of the novel clamp constructs had to be predicted based on how closely they could match the biomechanical stability of the Harms construct. Additionally, patients are externally immobilized after surgery with a hard collar which further reduces motion at C1-C2 but is not measureable in a cadaveric study. While biomechanical stability is a good predictor of C1-C2 fusion rates, predicting how a novel construct will effect mortality rates is difficult. However, there are no reasons to believe that the novel constructs proposed in the present study will negatively affect patient mortality rates. If anything, mortality rates associated with the novel clamp constructs will be improved, especially for the C1PA/C2TL construct, due to the less invasive procedure, shorter operating time and no disturbance to the C2 nerve root or vertebral artery.

Based on the work presented in this thesis, the following conclusions have been made:

1) The ligament laxity optimization process greatly improved the response of the FE model for physiological ROM and the optimized laxity values presented in this thesis are available for use in future FE models.

2) The hybridized approach of using simplified construct FE modeling and benchtop testing to determine tightening specifications for the locking mechanisms of the C1 posterior arch clamp proved to be very efficient was expected to be more effective than just developing FE models with more detailed clamp constructs.

3) Based on the results of cadaveric testing, both the C1PA/C2P and the C1PA/C2TL constructs are expected to be feasible alternatives to the Harms construct for C1-C2 fusion procedures.

4) The C1PA/C2P construct has shown to more effective at reducing ROM than the Harms construct in flexion/extension and equally effective in axial rotation and lateral bending.

116

5) Although not as stable as the Harms construct in lateral bending, the C1PA/C2TL construct is hypothesized to be the most clinically appealing due to a safer, faster and less invasive procedure. The decision to use this construct should be based upon whether the anatomy of the C2 lamina is a good candidate for C2 translaminar screws.

8.0 References

1. Shih Y-T, Kao T-H, Pan H-C, Chen H-T, Tsou H-K. The surgical treatment principles of atlantoaxial instability focusing on rheumatoid arthritis. *Biomed Res Int*. 2015:1-8.

2. Crockard HA, Heilman AE, Stevens JM. Progressive myelopathy secondary to odontoid fractures: clinical, radiological, and surgical features. *J Neurosurg*. 1993;78(4):579-586.

3. Ochoa G. Surgical management of odontoid fractures. *Injury*. 2005;36(2):54-64.

4. Anderson LD, D'Alonzo RT. Fractures of the odontoid process of the axis. *J bone Jt surgery Am*. 1974;56(8):1663-1674.

5. Southwick WO. Management of fractures of the dens (odontoid process). *J bone Jt surgery Am*. 1980;62(3):482-486.

6. Jaiswal AK, Sharma MS, Behari S, Lyngdoh BT, Jain S, Jain VK. Current management of odontoid fractures. *Indian J Neurotrauma*. 2005;2(1):3-6.

7. Smith HE, Kerr SM, Fehlings MG, et al. Trends in epidemiology and management of type II odontoid fractures: 20-year experience at a model system spine injury tertiary referral center. *J Spinal Disord Tech*. 2010;23(8):501-505.

8. Chapman J, Smith JS, Kopjar B, et al. The AOSpine North America geriatric odontoid fracture study. *Spine (Phila Pa 1976)*. 2013;38(13):1098-1104.

9. Magerl F, Seemann PS. *Stable Posterior Fusion of the Atlas and Axis by Transarticular Screw Fixation*.; 1987.

10. Gallie W. Fractures and dislocations of the cervical spine. *Am J Surg*. 1939;46:495-499.

11. Mummaneni P V, Haid RW. Atlantoaxial fixation: overview of all techniques. *Neurol India*. 2005;53(4):408-415.

12. Harms J, Melcher RP. Posterior C1-C2 fusion with polyaxial screw and rod fixation. *Spine (Phila Pa 1976)*. 2001;26(22):2467-2471.

13. Huang D-G, Hao D-J, He B-R, et al. Posterior atlantoaxial fixation: a review of all techniques. *Spine J*. 2015;15(10):2271-2281.

14. Squires J, Molinari RW. C1 lateral mass screw placement with intentional sacrifice of the C2 ganglion: Functional outcomes and morbidity in elderly patients. *Eur Spine J*. 2010;19(8):1318-1324.

15. Wright NM. *Posterior C2 Fixation Using Bilateral, Crossing C2 Laminar Screws: Case Series and Technical Note*. Journal of spinal disorders & techniques 17, 158-162 (2004).

16. Meyer D, Meyer F, Kretschmer T, Börm W. Translaminar screws of the axis-an alternative technique for rigid screw fixation in upper cervical spine instability. *Neurosurg Rev*. 2012;35(2):255-261.

17. Gray H. *Anatomy of the Human Body*. 20th ed. Philadelphia: Lea & Febiger; 1918. www.bartleby.com/107/.

18. Bogduk N, Mercer S. Biomechanics of the cervical spine. I: Normal kinematics. *Clin Biomech*. 2000;15(9):633-648.

19. Sorrentino S. Arcuate Foramen. Radiopaedia. Published 2017.

20. Sabuncuoglu H, Ozdogan S, Karadag D, Kaynak ET. Congenital hypoplasia of the posterior arch of the atlas: case report and extensive review of the literature. *Turk Neurosurg*. 2011;21(1):97-103.

21. Werne S. Studies in spontaneous atlas dislocation. In: *Acta Orthop Scand Suppl*. 23rd ed. ; 1957:1-150.

22. Goel VK, Clark CM, Gallaes K, Liu YK. Moment-rotation relationships of the ligamentous occipito-atlanto-axial complex. *J Biomech*. 1988;21(8):673-680.

23. Panjabi M, Dvorak J, Duranceau J, Yamamoto I. Three dimensional movements of the upper cervical spine. *SPIE*. 1988;1030:370-377.

24. Panjabi M, Dvorak J, Crisco III J, Oda T, Hilibrand A, Grob D. Flexion, extension, and lateral bending of the upper cervical spine in Response to alar ligament transections. *J Spinal Disord*. 1991;4(2):157-167.

25. Panjabi MM, Dvorak J, Crisco JJ, Oda T, Wang P, Grob D. Effects of alar ligament transection on upper cervical spine rotation. *J Orthop Res*. 1991;9(4):584-593.

26. Panjabi MM, Crisco J, Vasavada A, et al. Mechanical properties of the human cervical spine as shown by three-dimensional load-displacement curves. *Spine (Phila Pa 1976)*. 2001;26(24):2692-2700.

27. Goel VK, Winterbottom JM, Schulte KR, Chang H, Gilbertson LG. Ligamentous laxity across C0-C1-C2 complex. *Spine (Phila Pa 1976)*. 1990;15(10):990-996.

28. Dailey AT, Hart D, Finn MA, Schmidt MH, Apfelbaum RI. Anterior fixation of odontoid fractures in an elderly population. *J Neurosurg Spine*. 2010;12(1):1-8.

29. Joaquim AF, Patel A a. Surgical treatment of Type II odontoid fractures: anterior odontoid screw fixation or posterior cervical instrumented fusion? *Neurosurg Focus*. 2015;38(4):1-

6.

30.   Löhrer L, Raschke MJ, Thiesen D, et al. Current concepts in the treatment of Anderson
       Type II odontoid fractures in the elderly in Germany, Austria and Switzerland. *Injury*.
       2012;43(4):462-469.

31.   Scheyerer MJ, Zimmermann SM, Simmen H-P, Wanner G a, Werner CM. Treatment
       modality in type II odontoid fractures defines the outcome in elderly patients. *BMC Surg*.
       2013;13:54.
       http://www.pubmedcentral.nih.gov/articlerender.fcgi?artid=3833842&tool=pmcentrez&re
       ndertype=abstract.

32.   Harrop JS, Hart R, Anderson P a. Optimal treatment for odontoid fractures in the elderly.
       Spine (Phila Pa 1976). 2010;35(21 Suppl):S219-S227.

33.   Böhler J. Anterior stabilization for acute fractures and non-unions of the dens. *J Bone
       Joint Surg Am*. 1982;64(1):18-27.

34.   Babak Kalantar S. Fractures of the C1 and C2 Vertebrae. *Semin Spine Surg*.
       2013;25(1):23-35.

35.   Reindl R, Sen M, Aebi M. *Anterior Instrumentation for Traumatic C1-C2 Instability.*
       Spine 28, E329-E333 (2003).

36.   Graffeo CS, Perry A, Puffer RC, et al. Deadly falls: operative versus nonoperative
       management of Type II odontoid process fracture in octogenarians. *J Neurosurg Spine*.
       2016;26(January):1-6.

37.   Vasudevan K, Grossberg JA, Spader HS, Torabi R, Oyelese AA. Age increases the risk of
       immediate postoperative dysphagia and pneumonia after odontoid screw fixation. *Clin
       Neurol Neurosurg*. 2014;126:185-189.

38.   Brooks AL, Jenkins EB. Atlanto-axial arthrodesis by the wedge compression method. *J
       Bone Joint Surg Am*. 1978;60(3):279-284.

39.   Richter M, Schmidt R, Claes L, Puhl W, Wilke H-J, Richter Marcus; Schmidt RCLPW&
       WH-J. Posterior atlantoaxial fixation: biomechanical in vitro comparison of six different
       techniques. *Spine (Phila Pa 1976)*. 2002;27(16):1724-1732.

40.   Holness RO, Huestis WS, Howes WJ, Langille RA. Posterior stabilization with an
       interlaminar clamp in cervical injuries: Technical note and review of the long term
       experience with the method. *Neurosurgery*. 1984;14(3):318-322.

41. Rihn JA, Winegar CD, Donaldson WF 3rd, Lee JY, Kang JD. Recurrent atlantoaxial instability due to fracture of the posterior C1 ring: a late finding following posterior C1-C2 fusion using the Halifax clamp. *J Surg Orthop Adv*. 2009;18(1):45-50.

42. Jeanneret B, Magerl F. Primary Posterior Fusions C1-2 in Odontoid Fractures: Indications, Technique, and Results of Transarticular Screw Fixation. *J Spinal Disord*. 1992;5:464-475.

43. Guo X, Ni B, Wang M, Wang J, Li S, Zhou F. Bilateral atlas laminar hook combined with transarticular screw fixation for an unstable bursting atlantal fracture. *Arch Orthop Trauma Surg*. 2009;129(9):1203-1209.

44. Haid RW. C1-C2 transarticular screw fixation: Technical aspects. *Neurosurgery*. 2001;49(1):71-74.

45. Madawi AA, Solanki G, Casey ATH, Crockard HA. Variation of the Groove in the Axis Vertebra for the Vertebral Artery. *J Bone Jt Surg*. 1997;79(5):820-823.

46. Terterov S, Taghva A, Khalessi A a, Hsieh PC. Symptomatic vertebral artery compression by the rod of a C1-C2 posterior fusion construct: case report and review of the literature. *Spine (Phila Pa 1976)*. 2011;36(10):E678-E681.

47. Dmitriev AE, Lehman RA, Helgeson MD, Sasso RC, Kuhns C, Riew DK. Acute and long-term stability of atlantoaxial fixation methods: a biomechanical comparison of pars, pedicle, and intralaminar fixation in an intact and odontoid fracture model. *Spine (Phila Pa 1976)*. 2009;34(4):365-370.

48. Parker SL, McGirt MJ, Garcés-Ambrossi GL, et al. Translaminar versus pedicle screw fixation of C2: Comparison of surgical morbidity and accuracy of 313 consecutive screws. *Neurosurgery*. 2009;64(SUPPL. 5):343-349.

49. Gorek J, Acaroglu E, Berven S, Yousef A, Puttlitz CM. Constructs incorporating intralaminar C2 screws provide rigid stability for atlantoaxial fixation. *Spine (Phila Pa 1976)*. 2005;30(13):1513-1518.

50. Taghva A, Attenello FJ, Zada G, Khalessi AA, Hsieh PC. Minimally invasive posterior atlantoaxial fusion: A cadaveric and clinical feasibility study. *World Neurosurg*. 2013;80(3):414-421.

51. Kantelhardt SR, Keric N, Conrad J, Archavlis E, Giese A. Minimally invasive instrumentation of uncomplicated cervical fractures. *Eur Spine J*. 2015.

52. Kelly BP, Glaser JA, DiAngelo DJ. Biomechanical comparison of a novel C1 posterior locking plate with the harms technique in a C1-C2 fixation model. *Spine (Phila Pa 1976)*. 2008;33(24):920-925.

53. DiAngelo DJ, Foley KT. An improved biomechanical testing protocol for evaluating spinal arthroplasty and motion preservation devices in a multilevel human cadaveric cervical model. *Neurosurg Focus*. 2004;17(3):E4.

54. Robertson PA, Tsitsopoulos PP, Voronov LI, Havey RM, Patwardhan AG. Biomechanical investigation of a novel integrated device for intra-articular stabilization of the C1-C2 (atlantoaxial) joint. *Spine J*. 2012;12(2):136-142.

55. Xu T, Guo Q, Liu Q, et al. Biomechanical Evaluation of a Novel Integrated C1 Laminar Hook Combined with C1-C2 Transarticular Screws for Atlantoaxial Fusion: An in Vitro Human Cadaveric Study. *World Neurosurg*. 2016;92:133-139.

56. Puttlitz CM, Goel VK, Traynelis VC, Clark CR. A finite element investigation of upper cervical instrumentation. *Spine (Phila Pa 1976)*. 2001;26(22):2449-2455.

57. Cai X-H, Liu Z-C, Yu Y, Zhang M-C, Huang W-B. Evaluation of biomechanical properties of anterior atlantoaxial transarticular locking plate system using three-dimensional finite element analysis. *Eur Spine J*. 2013;22:2686-2694.

58. Cai X, Yu Y, Liu Z, Zhang M, Huang W. Three-dimensional finite element analysis of occipitocervical fixation using an anterior occiput-to-axis locking plate system: A pilot study. *Spine J*. 2014;14(8):1399-1409. http://dx.doi.org/10.1016/j.spinee.2013.08.025.

59. Zhang B-C, Liu H, Cai X-H, et al. Biomechanical comparison of a novel transoral atlantoaxial anchored cage with established fixation technique - a finite element analysis. *BMC Musculoskelet Disord*. 2015;16:261-272.

60. Brolin K, Halldin P. Development of a finite element model of the upper cervical spine and a parameter study of ligament characteristics. *Spine (Phila Pa 1976)*. 2004;29(4):376-385.

61. Zhang H, Bai J. Development and validation of a finite element model of the occipito-atlantoaxial complex under physiologic loads. *Spine (Phila Pa 1976)*. 2007;32(9):968-974.

62. Schwartz D, Guleyupoglu B, Koya B, Stitzel JD, Gayzik FS. Development of a Computationally Efficient Full Human Body Finite Element Model. *Traffic Inj Prev*.

2015;16(sup1):S49-S56.

63. Shateri H, Cronin DS. Out-of-position rear impact tissue-level investigation using detailed finite element neck model. *Traffic Inj Prev*. 2015;16(7):698-708.

64. Panzer MB, Cronin DS. C4-C5 segment finite element model development, validation, and load-sharing investigation. *J Biomech*. 2009;42:480-490.

65. DeWit JA, Cronin DS. Cervical spine segment finite element model for traumatic injury prediction. *J Mech Behav Biomed Mater*. 2012;10:138-150.

66. Mattucci SFE, Moulton JA, Chandrashekar N, Cronin DS. Strain rate dependent properties of human craniovertebral ligaments. *J Mech Behav Biomed Mater*. 2013;23:71-79.

67. Nightingale RW, Winkelstein BA, Knaub KE, Richardson WJ, Luck JF, Myers BS. Comparative strengths and structural properties of the upper and lower cervical spine in flexion and extension. *J Biomech*. 2002;35(6):725-732.

68. Lasswell TL, Cronin DS, Medley JB, Rasoulinejad P. Incorporating ligament laxity in a finite element model for the upper cervical spine. *Spine J*. 2017:1-10.

69. Ma X-Y, Yin Q-S, Wu Z-H, et al. C1 pedicle screws versus C1 lateral mass screws: comparisons of pullout strengths and biomechanical stabilities. *Spine (Phila Pa 1976)*. 2009;34(4):371-377.

70. Lehman RA, Dmitriev AE, Wilson KW. Biomechanical analysis of the C2 intralaminar fixation technique using a cross-link and offset connector for an unstable atlantoaxial joint. *Spine J*. 2012;12(2):151-156.

71. Stauffer SE. Posterior atlanto-axial arthrodesis: the Gallie and Brooks techniques and their modifications. *Tech Orthop*. 1994;9(1):43-48.

72. Reclaru L, Susz C, Ardelean L. Laser Beam Welding. 2010;60(1):86-89.

73. Dutta B, (Sam) Froes FH. *The Additive Manufacturing (AM) of Titanium Alloys*. Elsevier Inc.; 2015.

74. Wilke HJ, Wenger K, Claes L. Testing criteria for spinal implants: Recommendations for the standardization of in vitro stability testing of spinal implants. *Eur Spine J*. 1998;7(2):148-154.

75. Tan JS, Uppuganti S. Cumulative multiple freeze-thaw cycles and testing does not affect subsequent within-day variation in intervertebral flexibility of human cadaveric

lumbosacral spine. *Spine (Phila Pa 1976)*. 2012;37(20):E1238-E1242.

76. Analyzing a repeated measures design. Minitab 17 Support. Published 2016.

77. Using multiple comparisons to assess the practical and statistical significance of differences between means. Minitab 17 Support. Published 2016.

Appendix A: Supplemental Data and Analysis

A1: Moment Summation in Right Rod of C1PA/C2P Construct During Axial Rotation

```
%Nodal coordinates of C2 fixation locations @ t* = 70ms
P1 = [-200.233, 19.4383, -602.965];
P2 = [-199.969, 20.337, -601.842];
P3 = [-200.888, 19.8626, -600.227];
P4 = [-201.185, 19.0358, -601.397];
%
%Diagonal nodal vectors
V1 = P3 - P1;
V2 = P4 - P2;
%
%Calculation to determine intersection point of 2 vectors, moments will be
%calculated about this point
W = cross(V1,V2);
O = P1 + dot(cross(P2-P1,V2),W)/dot(W,W)*V1;
Y = P2 + dot(cross(P2-P1,V1),W)/dot(W,W)*V2;
d = norm(Y-O);
%
%C2 Node ID's from DYNA
P1Node = 2504637;
P2Node = 2504506;
P3Node = 2504499;
P4Node = 2504636;
%
%Forces about P1 node
ForceP1Node = BeamForces;
ForceP1Node = ForceP1Node(ForceP1Node(:,1)==P1Node,6:8);
ForceP1Node = [ForceP1Node]';
%
%Forces about P2 node
ForceP2Node = BeamForces;
ForceP2Node = ForceP2Node(ForceP2Node(:,1)==P2Node,6:8);
ForceP2Node = [ForceP2Node]';
%
%Forces about P3 node
ForceP3Node = BeamForces;
ForceP3Node = ForceP3Node(ForceP3Node(:,1)==P3Node,6:8);
ForceP3Node = [ForceP3Node]';
%
%Forces about P4 node
ForceP4Node = BeamForces;
ForceP4Node = ForceP4Node(ForceP4Node(:,1)==P4Node,6:8);
ForceP4Node = [ForceP4Node]';
%
%Calculations of moments about O generated by forces in beam elements
P1NodeDist = P1-O;
P1NodeDist = [P1NodeDist;P1NodeDist;P1NodeDist;P1NodeDist]';
P2NodeDist = P2-O;
P2NodeDist = [P2NodeDist;P2NodeDist;P2NodeDist;P2NodeDist]';
P3NodeDist = P3-O;
```

```
P3NodeDist = [P3NodeDist;P3NodeDist;P3NodeDist;P3NodeDist]';
P4NodeDist = P4-O;
P4NodeDist = [P4NodeDist;P4NodeDist;P4NodeDist;P4NodeDist]';
%
P1NodeMoment = cross(P1NodeDist,ForceP1Node);
P2NodeMoment = cross(P2NodeDist,ForceP2Node);
P3NodeMoment = cross(P3NodeDist,ForceP3Node);
P4NodeMoment = cross(P4NodeDist,ForceP4Node);
%
%Summation of moments
P1NodeMoment = sum(P1NodeMoment,2);
P2NodeMoment = sum(P2NodeMoment,2);
P3NodeMoment = sum(P3NodeMoment,2);
P4NodeMoment = sum(P4NodeMoment,2);
ResultantMoment = P1NodeMoment+P2NodeMoment+P3NodeMoment+P4NodeMoment
%
Mx = ResultantMoment(1,1)
My = ResultantMoment(2,1)
Mz = ResultantMoment(3,1)
```

A2: Loading Calculations for C1PA/C2P Construct During Axial Rotation

```
%Right Rod Forces [N] and Moments [Nm]
Fxr=3.91;
Fyr=3.67;
Fzr=-1.32;
%
Mxr=0.0054;
Myr=-0.0373;
Mzr=-0.0028;
%
%Left Rod Forces [N] and Moments [Nm]
Fxl=-2.71;
Fyl=3.23;
Fzl=0.612;
%
Mxl=-0.0202;
Myl=0.0023;
Mzl=-0.0098;
%
%Rod Lengths [m]
RightRodLength=0.0274;
LeftRodLength=0.0274;
%
%Rod orientation angles [Deg]
    %angle defined from ball wrt DYNA coord system
XYl=39;
XYr=39;
XZl=35.2;
XZr=35.2;
YZl=30;
YZr=30;
%
%Forces at polyaxial rod locking mechanism (right rod)
syms FRxr FRyr FRzr MRxr MRyr MRzr
eqn1 = FRxr + Fxr ==0; %sum of forces in X
eqn2 = FRyr + Fyr ==0; %sum of forces in Y
eqn3 = FRzr + Fzr ==0; %sum of forces in Z
eqn4 = MRxr + Mxr - Fyr*cos(XYr*pi()/180)*RightRodLength +
Fzr*sin(XYr*pi()/180)*RightRodLength==0; %sum of moments about x-axis
eqn5 = MRyr + Myr + Fxr*cos(XZr*pi()/180)*RightRodLength -
Fzr*sin(XZr*pi()/180)*RightRodLength==0; %sum of moments about y-axis
eqn6 = MRzr + Mzr - Fxr*cos(XYr*pi()/180)*RightRodLength +
Fyr*sin(XYr*pi()/180)*RightRodLength==0; %sum of moments about z-axis
sol=vpasolve([eqn1, eqn2, eqn3, eqn4, eqn5, eqn6],[FRxr, FRyr, FRzr, MRxr,
MRyr, MRzr]);
FRxr=sol.FRxr;
FRyr=sol.FRyr;
FRzr=sol.FRzr;
MRxr=sol.MRxr;
MRyr=sol.MRyr;
MRzr=sol.MRzr;
%
%Forces at polyaxial rod locking mechanism (left rod)
syms FRxl FRyl FRzl MRxl MRyl MRzl
eqn1 = FRxl + Fxl ==0; %sum of forces in X
eqn2 = FRyl + Fyl ==0; %sum of forces in Y
```

```matlab
eqn3 = FRzl + Fzl ==0; %sum of forces in Z
eqn4 = MRxl + Mxl - Fyl*cos(XYl*pi()/180)*LeftRodLength -
Fzl*sin(XYl*pi()/180)*LeftRodLength==0; %sum of moments about x-axis
eqn5 = MRyl + Myl + Fxl*cos(XZl*pi()/180)*LeftRodLength -
Fzl*sin(XZl*pi()/180)*LeftRodLength==0; %sum of moments about y-axis
eqn6 = MRzl + Mzl + Fxl*cos(XYl*pi()/180)*LeftRodLength +
Fyl*sin(XYl*pi()/180)*LeftRodLength==0; %sum of moments about z-axis
sol=vpasolve([eqn1, eqn2, eqn3, eqn4, eqn5, eqn6],[FRxl, FRyl, FRzl, MRxl,
MRyl, MRzl]);
FRxl=sol.FRxl;
FRyl=sol.FRyl;
FRzl=sol.FRzl;
MRxl=sol.MRxl;
MRyl=sol.MRyl;
MRzl=sol.MRzl;

%Transformation of Forces to create single loading point at center of jaws
%moment arms from end of rod to center of clamp jaws [m]
xdist=0.0056;
ydist=0.0248;
zdist=0.0223;
%
Fx =(Fxr + Fxl)
Fy =(Fyr + Fyl)
Fz =(Fzr + Fzl)
syms Mx My Mz
eqn1 = Fyr*zdistR + Fyl*zdistL + Fzr*ydistR - Fzl*ydistL + Mxl + Mxr ==Mx;
eqn2 = Fxr*zdistR + Fxl*zdistL + Fzr*xdistR + Fzl*ydistL + Myl + Myr ==My;
eqn3 = -Fxr*ydistR + Fxl*ydistL - Fyr*xdistR - Fyl*xdistL + Mzl + Mzr ==Mz;
sol=vpasolve([eqn1, eqn2, eqn3],[Mx, My, Mz]);
Mx=sol.Mx
My=sol.My
Mz=sol.Mz
```

A3: Euler Angle Calculations for Cadaveric Study Data

```matlab
function PROC_ANGLESf
% Import marker data and calculate relative angles
% C. D. McKinnon, 2016
% ~~~~~~~~~~~~~~~~~~~~~~~~~~~~~~~~~~~~~~~~~~~~~~~~~~~~~~~~~~~~~~~~~~~~~~~~~~~~~~~~~~
clc;

session = 'Jan_18';

root = 'N:\MASc\Data_Collection\';

numMarkers = 32;      % physical and virtual markers

% get trial names
[~,~,temp] = xlsread([root 'Data Collection Sheet.xlsx'],session,'C12:D35');
trials  = temp([1:6 10:15 19:24],2); % list of trials
folders = temp([1:6 10:15 19:24],1); % list of folders for each trial

fprintf('Trial: ')

sequence =
{'ZYX','YZX','ZYX','ZYX','XYZ','XYZ','YZX','YZX','ZYX','ZYX','XYZ','XYZ','YZX
','YZX','ZYX','ZYX','XYZ','XYZ'};

for H = 1%:length(trials) % by trial

    fprintf(num2str(H))

    % load marker data and calculate R
    filename = [root session '\' folders{H} '\' folders{H} '_' trials{H}]; %
define filename                                           % define filename
    [markerData,numFrames] = loadMotion(filename,numMarkers,'CSV');        %
load marker data
    markers = markers2cell(markerData,numMarkers);                        %
convert markers to cell array
    [i,j,k,o] = build_LCS(markers);                                       %
build LCS
    R = build_R(i,j,k);                                                   %
build R

    % calculate relative angles
    [fe{H}.c1_c0,ax{H}.c1_c0,lb{H}.c1_c0] =
getRelativeAngles(R.c1_c0,sequence{H});                              % RB1 about
GLOBAL Y
    [fe{H}.c2_c1,ax{H}.c2_c1,lb{H}.c2_c1] =
getRelativeAngles(R.c2_c1,sequence{H});
    [fe{H}.c3_c2,ax{H}.c3_c2,lb{H}.c3_c2] =
getRelativeAngles(R.c3_c2,sequence{H});
    [fe{H}.c2_c0,ax{H}.c2_c0,lb{H}.c2_c0] =
getRelativeAngles(R.c2_c0,sequence{H});
    [fe{H}.c3_c0,ax{H}.c3_c0,lb{H}.c3_c0] =
getRelativeAngles(R.c3_c0,sequence{H});

    outData = [fe{H}.c2_c1' ax{H}.c2_c1' lb{H}.c2_c1'];
```

```matlab
    % Save data to file
    csvwrite([root session '\' folders{H} '\' folders{H} '_' trials{H}
'_OUTPUT.csv'],outData,0,2);

    fprintf('|')

end % trials

fprintf('Complete\n')

end

%~~~~~~~~~~~~~~~~~~~~~~~~~~~~~~~~~~~~~~~~~~~~~~~~~~~~~~~~~~~~~~~~~~~~~~~~~~~~~~~~
function [markerData,numFrames] = loadMotion(filename,numMarkers,filetype)
% Author: Colin D. McKinnon
% Last Modified: August 2016
%
% Read in NDI First Principles 3D marker data as either comma-separated
% (_3d.CSV) file or binary (.N3D) file.
%
% filename      full file path and filename of input data
% numMarkers    number of markers
% markerdata    output data matrix (no index column)
%~~~~~~~~~~~~~~~~~~~~~~~~~~~~~~~~~~~~~~~~~~~~~~~~~~~~~~~~~~~~~~~~~~~~~~~~~~~~~~~~

switch filetype % ==========================================================

    case{'CSV'} % --------------------------------------------------------

        filename = [filename '_3d.csv'];
        separator = ','; % comma separated
        headerLines = 5; % standard for First Principles .csv files

        % Read in data file
        inData = importdata(filename,separator,headerLines);

        tempData = inData.data;
        tempData = tempData(:,2:end);      % trim index column

        markerData = nan(size(tempData,1),numMarkers*3);
        markerData(:,1:size(tempData,2)) = tempData;

        % Detect length of trial (frames)
        numFrames = size(markerData,1);

    case{'N3D'} % --------------------------------------------------------

        filename = [filename '.n3d'];
        numC = numMarkers*3;

        if and(ischar(filename), isnumeric(numC))
            file_id = fopen(filename);
```

```matlab
            data = fread(file_id, inf, 'float32', 0); % read in data (single
column vector)
            numR = (size(data,1) - 64)/numC;            % get number of rows

            % Remove 64-row header data
            data = data(65:end);

            % Reshape into row x col matrix (frames x channels)
            markerData = zeros(numR,numC); % pre-allocate for speed

            for A = 1:numR
                for B = 1:numC

                    markerData(A,B) = data((numC*(A-1))+B);

                end
            end

            % This function sets blank values (missing markers) as 0. This
            % converts those zeros into NaNs to match output for CSV files.
            markerData(abs(markerData) < 0.00000001) = NaN;
            markerData(abs(markerData) > 1000000) = NaN;
            % **** added this abs to handle -ve values, make sure it works...
            numFrames = numR;

            fclose(file_id);
        else

            % If not, returns an error message
            error('Error with the data: filename not a char OR numC not
numeric');
        end

end
end

%~~~~~~~~~~~~~~~~~~~~~~~~~~~~~~~~~~~~~~~~~~~~~~~~~~~~~~~~~~~~~~~~~~~~~~~~~~~~~~~~~
function markers = markers2cell(markerData,numMarkers)
% Created by: Colin McKinnon, University of Waterloo
% Last Modified: September 2016
%
% Transform a matrix of 3D marker data (XYZ) to a cell array with
% one cell for each marker.
%
% markerData      nFrames x 3*numMarkers matrix of marker data
% numMarkers      number of markers
% markers         numMarkers-element cell array of marker data
%~~~~~~~~~~~~~~~~~~~~~~~~~~~~~~~~~~~~~~~~~~~~~~~~~~~~~~~~~~~~~~~~~~~~~~~~~~~~~~~~~

for x = 1:numMarkers

    col = (x-1)*3+1;
    markers{x} = markerData(:,col:col+2);
```

131

```matlab
    end
end

%~~~~~~~~~~~~~~~~~~~~~~~~~~~~~~~~~~~~~~~~~~~~~~~~~~~~~~~~~~~~~~~~~~~~~~~~~~~~~
function [i,j,k,o] = build_LCS(data)
% Author: Colin D. McKinnon
% Last Modified: Sept 2016
%
% Build local coordinate system axes.
%
% data          marker data (cell array with one cell for each marker)
% ijko          each is a structered array of local axes and origin
%~~~~~~~~~~~~~~~~~~~~~~~~~~~~~~~~~~~~~~~~~~~~~~~~~~~~~~~~~~~~~~~~~~~~~~~~~~~~~
m = markerList; % get list of marker numbers

% [C0] (upper cup)
mid1 = (data{m.U_SW}-data{m.U_NW})/2;
mid2 = (data{m.U_SE}-data{m.U_NE})/2;
i.c0 = bsxfun(@rdivide,(mid1-mid2),normRows(mid1-mid2));
temp = bsxfun(@rdivide,(data{m.U_NE}-data{m.U_SE}),normRows(data{m.U_NE}-
data{m.U_SE}));
j.c0 = bsxfun(@rdivide,cross(temp,i.c0),normRows(cross(temp,i.c0)));
k.c0 = cross(i.c0,j.c0);
o.c0 = data{m.U_SE};

% [C1]
k.c1 = bsxfun(@rdivide,(data{m.C1_L}-data{m.C1_R}),normRows(data{m.C1_L}-
data{m.C1_R}));
temp = bsxfun(@rdivide,(data{m.C1_S}-data{m.C1_I}),normRows(data{m.C1_S}-
data{m.C1_I}));
i.c1 = bsxfun(@rdivide,cross(temp,k.c1),normRows(cross(temp,k.c1)));
j.c1 = cross(k.c1,i.c1);
o.c1 = data{m.C1_I};

% [C2]
k.c2 = bsxfun(@rdivide,(data{m.C2_L}-data{m.C2_R}),normRows(data{m.C2_L}-
data{m.C2_R}));
temp = bsxfun(@rdivide,(data{m.C2_S}-data{m.C2_I}),normRows(data{m.C2_S}-
data{m.C2_I}));
i.c2 = bsxfun(@rdivide,cross(temp,k.c2),normRows(cross(temp,k.c2)));
j.c2 = cross(k.c2,i.c2);
o.c2 = data{m.C2_I};

% [C3] (lower cup)
mid1 = (data{m.L_SW}-data{m.L_NW})/2;
mid2 = (data{m.L_SE}-data{m.L_NE})/2;
i.c3 = bsxfun(@rdivide,(mid1-mid2),normRows(mid1-mid2));
temp = bsxfun(@rdivide,(data{m.L_NE}-data{m.L_SE}),normRows(data{m.L_NE}-
data{m.L_SE}));
j.c3 = bsxfun(@rdivide,cross(temp,i.c3),normRows(cross(temp,i.c3)));
k.c3 = cross(i.c3,j.c3);
o.c3 = data{m.L_SE};
end
```

```matlab
%~~~~~~~~~~~~~~~~~~~~~~~~~~~~~~~~~~~~~~~~~~~~~~~~~~~~~~~~~~~~~~~~~~~~~~~~~~~~~~~
function m = markerList
% List of markers used - Tim Lasswell MASc Thesis Project
% Septmeber 2016

% 1-16 are rigid body markers
%~~~~~~~~~~~~~~~~~~~~~~~~~~~~~~~~~~~~~~~~~~~~~~~~~~~~~~~~~~~~~~~~~~~~~~~~~~~~~~~

% [C0] (upper cup)
m.U_NE = 25;
m.U_SE = 26;
m.U_SW = 27;
m.U_NW = 28;

% [C1]
m.C1_L = 21;
m.C1_R = 22;
m.C1_S = 23;
m.C1_I = 24;

% [C2]
m.C2_L = 17;
m.C2_R = 18;
m.C2_S = 19;
m.C2_I = 20;

% [C3] (lower cup)
m.L_NE = 29;
m.L_SE = 30;
m.L_SW = 31;
m.L_NW = 32;
end


%~~~~~~~~~~~~~~~~~~~~~~~~~~~~~~~~~~~~~~~~~~~~~~~~~~~~~~~~~~~~~~~~~~~~~~~~~~~~~~~
function result = normRows(data)
% Created by: Colin McKinnon, University of Waterloo
% Last Modified: January 2015
%
% Computes the norm for each row of a matrix, rather than for the entire
% matrix
%~~~~~~~~~~~~~~~~~~~~~~~~~~~~~~~~~~~~~~~~~~~~~~~~~~~~~~~~~~~~~~~~~~~~~~~~~~~~~~~

result = sqrt(sum(data.^2,2));
end


%~~~~~~~~~~~~~~~~~~~~~~~~~~~~~~~~~~~~~~~~~~~~~~~~~~~~~~~~~~~~~~~~~~~~~~~~~~~~~~~
function R = build_R(i,j,k)
% Author: Colin D. McKinnon
% Last Modified: June 2016
%
% Aassemble local system axes into direction cosine and rotation matrices.
%
% i,j,k    struct of local corrdinate system axis directions
% R        struct of rotation and Dc matrices
%~~~~~~~~~~~~~~~~~~~~~~~~~~~~~~~~~~~~~~~~~~~~~~~~~~~~~~~~~~~~~~~~~~~~~~~~~~~~~~~
```

```matlab
numFrames = size(i.c0,1);

for F = 1:numFrames

    %%%%%%%%%%%%%%%%%%%%%%%%%
    % DIRECTION COSINE MATRICES
    R.g_c0(:,:,F) = [i.c0(F,:)' j.c0(F,:)' k.c0(F,:)']; %3 x 3 x samples
    R.g_c1(:,:,F) = [i.c1(F,:)' j.c1(F,:)' k.c1(F,:)'];
    R.g_c2(:,:,F) = [i.c2(F,:)' j.c2(F,:)' k.c2(F,:)'];
    R.g_c3(:,:,F) = [i.c3(F,:)' j.c3(F,:)' k.c3(F,:)'];

    %%%%%%%%%%%%%%%%%%%%%%%%%
    % RELATIVE ROTATION MATRICES
    R.c1_c0(:,:,F) = R.g_c1(:,:,F)'*R.g_c0(:,:,F);      %3 x 3 x samples
    R.c2_c1(:,:,F) = R.g_c2(:,:,F)'*R.g_c1(:,:,F);      %3 x 3 x samples
    R.c3_c2(:,:,F) = R.g_c3(:,:,F)'*R.g_c2(:,:,F);      %3 x 3 x samples
    R.c2_c0(:,:,F) = R.g_c2(:,:,F)'*R.g_c0(:,:,F);      %3 x 3 x samples
    R.c3_c0(:,:,F) = R.g_c3(:,:,F)'*R.g_c0(:,:,F);      %3 x 3 x samples

end
end


%~~~~~~~~~~~~~~~~~~~~~~~~~~~~~~~~~~~~~~~~~~~~~~~~~~~~~~~~~~~~~~~~~~~~~~~~~~~~~~~
function [angle1,angle2,angle3] = getRelativeAngles(R,sequence)
% Created by: Colin McKinnon, University of Waterloo
% Last Modified: September 2016
%
% Calculate the relative angle between 2 local coordinate systems
%
% R          rotation matrix between systems (3x3 or 4x4)
% numFrames  number of frames
% sequence   string specifying rotation sequence eg. 'YXY'
%~~~~~~~~~~~~~~~~~~~~~~~~~~~~~~~~~~~~~~~~~~~~~~~~~~~~~~~~~~~~~~~~~~~~~~~~~~~~~~~
numFrames = size(R,3);

switch sequence

    case{'ZYX'} % flexion-extension trials
        for n = 1:numFrames
            % -ve angle is bird's eye clockwise
            angle1(n) = rad2deg(atan2(R(2,1,n),R(1,1,n)));  % Z (FE)
            angle2(n) = rad2deg(-asin(R(3,1,n)));           % Y (AX)
            angle3(n) = rad2deg(-atan2(R(3,2,n),R(3,3,n))); % X (LB)
        end

    case{'YZX'} % axial twist trials
        for n = 1:numFrames
            % -ve angle is bird's eye clockwise
            angle2(n) = rad2deg(-atan2(R(3,1,n),R(1,1,n))); % Y (AX)
            angle1(n) = rad2deg(asin(R(2,1,n)));            % Z (FE)
            angle3(n) = rad2deg(-atan2(R(2,3,n),R(2,2,n))); % X (LB)
        end

    case{'XYZ'} % lateral bend trials
```

134

```matlab
        for n = 1:numFrames
            % -ve angle is bird's eye clockwise
            angle3(n) = rad2deg(-atan2(R(2,3,n),R(3,3,n))); % X (LB)
            angle2(n) = rad2deg(asin(R(1,3,n)));            % Y (AX)
            angle1(n) = rad2deg(-atan2(R(1,2,n),R(1,1,n))); % Z (FE)
        end

end % switch
end
```

A4: Motion Controls for Spinal Loading Simulator

A4.1: Flexion/Extension and Lateral Bending Motion Controls

```
#MOTION
#PARAMETERS
RESTV=0.042545    ;'VOLTS
SLOPE=0.073811
YINT=0.00894
RESTMOM=((RESTV-YINT)/SLOPE) ;'Nm
TLIMIT=1.5     ;'torque limit in N.m
MAX1=30        ;'max angle in deg
SPEEDDEG=2     ;'ang vel in deg/s
CYCLES=4       ;'number of 1/2 cycles
SR=1024        ;'sample rate in Hz
N=7            ;'number of points to average
MAX2=MAX1*(140000/360)
SPEED=SPEEDDEG*(140000/360)
DA NTORQUE[0]
DM NTORQUE[1000]
AC 25600000
DC 25600000
cycleDur=MAX2/SPEED
nSamp=cycleDur*SR
SLAG=(cycleDur*1000)/nSamp
SLAG=SLAG*(1000/1024)
SLAG=2
JGX=5000
PAX=0
BG
AMX
JGX=SPEED
MG "TORQUE LIMIT: ", TLIMIT, " N.m"
```

```
MG "ANGLE LIMIT: ", MAX1, " deg"
MG "No. CYCLES: ", CYCLES
CYCLES=CYCLES+1
MG "SAMPLE RATE: ", SR, " Hz"
cCount=0.5
MG "::"
MG "BEGIN MOTION"
JP #FLEX
;'---------------------------------
#FLEX
AMX
MG "FLEXING"
PAX=0
BG
AMX            ;'MG "RETURNED TO ZERO"
DIRECT=1
cCount=cCount+0.5
JP #FINISH,(cCount=CYCLES)
MG "C:",cCount
PAX=-MAX2
BG
SC=0
JP #SAMPLE
;'---------------------------------
#EXTEND
AMX
MG "EXTENDING"
PAX=0
BG
AMX            ;'MG "RETURNED TO ZERO"
DIRECT=2
```

```
cCount=cCount+0.5 ;'MG "C:",cCount
PAX=MAX2
BG
SC=0
JP #SAMPLE
;'---------------------------------
#SAMPLE
SC=SC+1
temp=@AN[1]    ;'VOLTAGE
TORQUE=((temp-YINT)/SLOPE)
NTORQUE[SC]=TORQUE-RESTMOM
JP #AVERAGE
;'---------------------------------
#AVERAGE       ;'AVERAGE N POINTS AT A TIME
JP #SAMPLE,(SC<N)
TOTAL=0
COUNT=SC-N
COUNT2=0
JP #LOOP
#LOOP
TOTAL=NTORQUE[COUNT]+TOTAL
COUNT=COUNT+1
COUNT2=COUNT2+1
JP #EVAL,(COUNT2=N)
JP #LOOP
#EVAL
AMOM=TOTAL/N
MG "SAMPLE,AMOM:",SC,",",AMOM
IF (AMOM>TLIMIT)
MG "::EXCEEDED TORQUE LIMIT!"
ST
```

```
JP #EXTEND,(DIRECT=1)

JP #FLEX,(DIRECT=2)

ENDIF

IF (AMOM<-TLIMIT)

MG "::EXCEEDED TORQUE LIMIT!"

ST

JP #EXTEND,(DIRECT=1)

JP #FLEX,(DIRECT=2)

ENDIF

IF (SC=nSamp)        ;'MG "MAX COUNT"

JP #EXTEND,(DIRECT=1)

JP #FLEX,(DIRECT=2)

ENDIF

WT SLAG

JP #SAMPLE

;'--------------------------------

#FINISH

MG "FINISH"

ST

PAX=0

BG

MG "CYCLES COMPLETE:", (cCount-1)

ST

EN
```

A4.2 Axial Rotation Motion Controls

#MOTION

#PARAMETERS

RESTMOM=-0.46991   ;'N.m

TLIMIT=1.5   ;'NET MOMENT LIMIT (N.m)

CYCLES=4   ;'NUMBER OF CYCLES

STROKE=24000   ;'STROKE PER TWIST (counts)

SPEED=1432   ;'SPEED (counts per second)

SR=32   ;'FORCE SAMPLE RATE

N=7   ;'number of points to average

SLOPEZ=108.4571   ;'Z SLOPE

YINTZ=-2.3787   ;'Z Y-INY

SLOPEW=112.5268   ;'W SLOPE

YINTW=2.6009   ;'W Y-INT

ARMZ=-0.103   ;'MOMENT ARM (m)

ARMW=0.103   ;'MOMENT ARM (m)

DA TMOM2[0]

DM TMOM2[1000]

AC 25600000

DC 25600000

cycleDur=((STROKE*4)/SPEED)/4   ;'sec

nSamp=cycleDur*SR   ;'#

SLAG=(cycleDur*1000)/nSamp ;'msec

SLAG=2

JGZ=20000

JGW=20000

PAZ=0

PAW=0

BG

AMZ   ;'JGZ=AVELSTP

JGZ=SPEED

```
JGW=SPEED
MG "TORQUE LIMIT: ", TLIMIT, " N.m"
MG "No. CYCLES: ", CYCLES
CYCLES=CYCLES+1
MG "SAMPLE RATE: ", SR, " Hz"
cCount=0.5
MG "::"
MG "BEGIN MOTION"
JP #TWIST
;'---------------------------------
#TWIST
AMZ
MG "TWIST RIGHT"
PAZ=0
PAW=0
BG
AMZ            ;'MG "RETURNED TO ZERO"
DIRECT=1
cCount=cCount+0.5
JP #FINISH,(cCount=CYCLES)
MG "C:",cCount
PAZ=-STROKE
PAW=STROKE
BG
SC=0
JP #SAMPLE
;'---------------------------------
#UNTWIST
AMZ
MG "TWIST LEFT"
PAZ=0
```

```
PAW=0

BG

AMZ              ;'MG "RETURNED TO ZERO"

DIRECT=2

cCount=cCount+0.5 ;'MG "C:",cCount

PAZ=STROKE

PAW=-STROKE

BG

SC=0  ;'formerly sCount

JP #SAMPLE

#SAMPLE

SC=SC+1

FZ_N=(@AN[4]*SLOPEZ)+YINTZ  ;'FZ (kg)

FW_N=(@AN[5]*SLOPEW)+YINTW  ;'FW (kg)

ZMOM=-FZ_N*ARMZ

WMOM=-FW_N*ARMW

TMOM=ZMOM+WMOM

TMOM2[SC]=TMOM-RESTMOM

JP #AVERAGE

#AVERAGE       ;'AVERAGE N POINTS AT A TIME

JP #SAMPLE,(SC<N)

TOTAL=0

COUNT=SC-N

COUNT2=0

JP #LOOP

#LOOP

TOTAL=TMOM2[COUNT]+TOTAL

COUNT=COUNT+1

COUNT2=COUNT2+1

JP #EVAL,(COUNT2=N)

JP #LOOP
```

```
#EVAL
AMOM=TOTAL/N
MG "SAMPLE,AMOM:",SC,",",AMOM
IF (AMOM>TLIMIT)
MG "::EXCEEDED TORQUE LIMIT!"
ST
JP #UNTWIST,(DIRECT=1)
JP #TWIST,(DIRECT=2)
ENDIF
IF (AMOM<-TLIMIT)
MG "::EXCEEDED TORQUE LIMIT!"
ST
JP #UNTWIST,(DIRECT=1)
JP #TWIST,(DIRECT=2)
ENDIF
IF (SC=nSamp)       ;'MG "MAX COUNT"
JP #UNTWIST,(DIRECT=1)
JP #TWIST,(DIRECT=2)
ENDIF
WT SLAG
JP #SAMPLE
;'----------------------------------
#FINISH
MG "FINISH"
ST
PAZ=0
PAW=0
BG
MG "CYCLES COMPLETE:", (cCount-1)
ST
EN
```

Appendix B: Copyright Permissions

B1: License for Figure 11

License Number	4124841496921
License date	Jun 09, 2017
Licensed Content Publisher	Elsevier
Licensed Content Publication	Seminars in Spine Surgery
Licensed Content Title	Fractures of the C1 and C2 Vertebrae
Licensed Content Author	S. Babak Kalantar
Licensed Content Date	Mar 1, 2013
Licensed Content Volume	25
Licensed Content Issue	1
Licensed Content Pages	13
Start Page	23
End Page	35
Type of Use	reuse in a thesis/dissertation
Intended publisher of new work	other
Portion	figures/tables/illustrations
Number of figures/tables/illustrations	1
Format	both print and electronic
Are you the author of this Elsevier article?	No
Will you be translating?	No
Order reference number	
Original figure numbers	Figure 13
Title of your thesis/dissertation	Design and Testing of a Novel Fusion Construct for Atlantoaxial Instability
Expected completion date	Jul 2017
Estimated size (number of pages)	180
Elsevier VAT number	GB 494 6272 12
Requestor Location	University of Waterloo 200 University Ave W Waterloo, ON N2L 3G1 Canada Attn: Tim Lasswell

B2: License for Figure 12 and Figure 13

License Number	4124360262463
License date	Jun 08, 2017
Licensed Content Publisher	Elsevier
Licensed Content Publication	The Spine Journal
Licensed Content Title	Posterior atlantoaxial fixation: a review of all techniques
Licensed Content Author	Da-Geng Huang,Ding-Jun Hao,Bao-Rong He,Qi-Ning Wu,Tuan-Jiang Liu,Xiao-Dong Wang,Hua Guo,Xiang-Yi Fang
Licensed Content Date	Oct 1, 2015
Licensed Content Volume	15
Licensed Content Issue	10
Licensed Content Pages	11
Start Page	2271
End Page	2281
Type of Use	reuse in a thesis/dissertation
Portion	figures/tables/illustrations
Number of figures/tables/illustrations	3
Format	both print and electronic
Are you the author of this Elsevier article?	No
Will you be translating?	No
Order reference number	
Original figure numbers	Figure 1, Figure 4, Figure 6
Title of your thesis/dissertation	Design and Testing of a Novel Fusion Construct for Atlantoaxial Instability
Expected completion date	Jul 2017
Estimated size (number of pages)	180
Elsevier VAT number	GB 494 6272 12
Requestor Location	University of Waterloo 200 University Ave W

Waterloo, ON N2L 3G1 Canada Attn: Tim Lasswell |

B3: License for Figure 15

License Number	4124370350833
License date	Jun 08, 2017
Licensed Content Publisher	Wolters Kluwer Health, Inc.
Licensed Content Publication	Spine
Licensed Content Title	Constructs Incorporating Intralaminar C2 Screws Provide Rigid Stability for Atlantoaxial Fixation
Licensed Content Author	Joseph Gorek, Emre Acaroglu, Sigurd Berven, et al
Licensed Content Date	Jan 1, 2005
Licensed Content Volume	30
Licensed Content Issue	13
Type of Use	Dissertation/Thesis
Requestor type	Individual
Portion	Figures/table/illustration
Number of figures/tables/illustrations	1
Figures/tables/illustrations used	Figure 1
Author of this Wolters Kluwer article	No
Title of your thesis / dissertation	Design and Testing of a Novel Fusion Construct for Atlantoaxial Instability
Expected completion date	Jul 2017
Estimated size(pages)	180
Requestor Location	University of Waterloo 200 University Ave W Waterloo, ON N2L 3G1 Canada Attn: Tim Lasswell
Billing Type	Invoice
Billing Address	University of Waterloo 200 University Ave W Waterloo, ON N2L 3G1 Canada Attn: Tim Lasswell

B4: License for Figure 16

License Number	4124370685100
License date	Jun 08, 2017
Licensed Content Publisher	Wolters Kluwer Health, Inc.
Licensed Content Publication	Spine
Licensed Content Title	Biomechanical Comparison of a Novel C1 Posterior Locking Plate With the Harms Technique in A C1–C2 Fixation Model
Licensed Content Author	Brian Kelly, John Glaser, and Denis DiAngelo
Licensed Content Date	Jan 1, 2008
Licensed Content Volume	33
Licensed Content Issue	24
Type of Use	Dissertation/Thesis
Requestor type	Individual
Portion	Figures/table/illustration
Number of figures/tables/illustrations	1
Figures/tables/illustrations used	Figure 2
Author of this Wolters Kluwer article	No
Title of your thesis / dissertation	Design and Testing of a Novel Fusion Construct for Atlantoaxial Instability
Expected completion date	Jul 2017
Estimated size(pages)	180
Requestor Location	University of Waterloo 200 University Ave W Waterloo, ON N2L 3G1 Canada Attn: Tim Lasswell
Billing Type	Invoice
Billing Address	University of Waterloo 200 University Ave W Waterloo, ON N2L 3G1 Canada Attn: Tim Lasswell

B5: License for Figure 17

License Number	4124370880664
License date	Jun 08, 2017
Licensed Content Publisher	Elsevier
Licensed Content Publication	The Spine Journal
Licensed Content Title	Biomechanical investigation of a novel integrated device for intra-articular stabilization of the C1–C2 (atlantoaxial) joint
Licensed Content Author	Peter A. Robertson,Parmenion P. Tsitsopoulos,Leonard I. Voronov,Robert M. Havey,Avinash G. Patwardhan
Licensed Content Date	Feb 1, 2012
Licensed Content Volume	12
Licensed Content Issue	2
Licensed Content Pages	7
Start Page	136
End Page	142
Type of Use	reuse in a thesis/dissertation
Intended publisher of new work	other
Portion	figures/tables/illustrations
Number of figures/tables/illustrations	1
Format	both print and electronic
Are you the author of this Elsevier article?	No
Will you be translating?	No
Order reference number	
Original figure numbers	Figure 1
Title of your thesis/dissertation	Design and Testing of a Novel Fusion Construct for Atlantoaxial Instability
Expected completion date	Jul 2017
Estimated size (number of pages)	180
Elsevier VAT number	GB 494 6272 12
Requestor Location	University of Waterloo 200 University Ave W Waterloo, ON N2L 3G1 Canada Attn: Tim Lasswell

B6: License for Figure 18

License Number	4124371186297
License date	Jun 08, 2017
Licensed Content Publisher	Elsevier
Licensed Content Publication	World Neurosurgery
Licensed Content Title	Biomechanical Evaluation of a Novel Integrated C1 Laminar Hook Combined with C1–C2 Transarticular Screws for Atlantoaxial Fusion: An In Vitro Human Cadaveric Study
Licensed Content Author	Tianming Xu,Qunfeng Guo,Qi Liu,Peng Zhang,Ming Lu,Xuhua Lu,Fei Chen,Xiang Guo,Bin Ni
Licensed Content Date	Aug 1, 2016
Licensed Content Volume	92
Licensed Content Issue	n/a
Licensed Content Pages	7
Start Page	133
End Page	139
Type of Use	reuse in a thesis/dissertation
Intended publisher of new work	other
Portion	figures/tables/illustrations
Number of figures/tables/illustrations	1
Format	both print and electronic
Are you the author of this Elsevier article?	No
Will you be translating?	No
Order reference number	
Original figure numbers	Figure 2
Title of your thesis/dissertation	Design and Testing of a Novel Fusion Construct for Atlantoaxial Instability
Expected completion date	Jul 2017
Estimated size (number of pages)	180
Elsevier VAT number	GB 494 6272 12
Requestor Location	University of Waterloo 200 University Ave W Waterloo, ON N2L 3G1 Canada Attn: Tim Lasswell